RAINFALL-RUNOFF MODELLING TO ASSESS FLOOD HAZARD ON SINT EUSTATIUS, CARIBBEAN NETHERLANDS

"Op Weg naar White Wall"

MSc thesis
Earth Surface and Water
2023
Second version

Samuel R Stapel
Student ID 5977037

First supervisor Prof. dr. Steven M. de Jong
Second supervisor Dr. Wiebe Nijland

Universiteit Utrecht

ABSTRACT

The Caribbean island of Sint Eustatius experiences regular flooding during intense rainstorms. The main issues are sediment deposits and deep ponds on roads, as well as erosion on unpaved roads and in gullies. Flooding was studied on a study area on the southwestern slope of the Quill volcano, which featured urban areas, dense vegetation, active gullies and a steep rock outcrop.

To study the causes of runoff generation, rainfall-runoff models were run in the rainfall-runoff model "LISEM". LISEM is a raster based numerical model that uses rainfall rates from a design storm to compute canopy interception, infiltration and ponding for each cell. It simultaneously calculates flow between cells using differential equations and based on a digital terrain model (DTM).

A DTM with sufficiently high resolution is essential for accurate modelling of flow in urban areas. For this study, a new DTM was created using structure-from-motion, which was interpolated to resolutions of 100, 250 and 500 cm. This allowed the model to be run at a higher resolution than in previous studies, and also allowed for assessment of the effects of using different resolutions.

Rainfall data of the island from the period 2015 – 2022 was analysed to create design storms with return periods of 1, 4 and 8 years. A hurricane scenario was also defined.

Infiltration rates have been measured across the study area using a portable rainfall simulator. These experiments indicated that soil water repellency (SWR) was common in the area, and appeared to be related to soil humus content to some extent. In general, however, infiltration rates were quite high.

The cell size of 100 cm had sufficient elevation detail to model ponding and flow diversions in urban areas and across roads. This resembled field observations of flooding on many occasions. Such details were not present as clearly at the coarser resolutions, and water was allowed to run off onto permeable soils more often, causing infiltration to be overestimated. The 100 cm cell size also performed better at modelling narrow flow through gullies. At coarser resolutions, excessive spreading of the flow across a larger width caused an overestimation of infiltration, and an underestimation of flow velocity. 100 cm was however still too coarse to include all relevant obstacles to flow. Rill flow could also not be modelled, as the flow was spread excessively across the width of a cell. It is therefore likely that at a cell size of 100 cm, the model suffered from the same inaccuracies as the coarser resolutions, albeit to a lesser extent.

In the urban area, runoff was primarily generated on roads and other paved surfaces, and to a lesser extent on compacted unpaved roads. To control erosion, runoff on unpaved roads should be limited as much as possible, which can be achieved by confining runoff to paved roads, and by creating infiltration pits next to unpaved roads. Regularly spaced drains in paved roads can reduce peak discharges on the road, and prevent flooding of downslope areas. Collected runoff can be stored in infiltration basins or temporary storage facilities.

Flooding on the main road was mostly facilitated by elevated roadsides, which prevented water from running off to the sides. Ponding in these areas could be easily prevented by installing drains or breaks in the roadsides.

The active gullies were mainly fed by runoff from the impermeable rock outcrop, but peak and total discharges were also greatly affected by the presence of impermeable rock layers below a shallow topsoil, as this limited the amount of water that could infiltrate. Issues occur where gullies flow directly onto the main road, as large sediment deposits are often produced. This could be solved by installing culverts below the road, or by redirecting gullies towards an already existing culvert. When doing so, the gully dynamics should be disturbed as little as possible, to prevent severe erosion.

The amount of rain that can be stored in the canopy and in surface depressions is limited compared to the total rainfalls of the studied scenarios. The most important uncertainties are therefore related to infiltration. The field method had limitations that may have caused infiltration rates to be overestimated. Also, spatial and temporal variability of SWR and hydraulic conductivity were not taken into account for large parts of the study area. Furthermore, the subsoil was largely assumed to be excessively drained, which prevented saturation of the soil, even during the most extreme storms. Around the active gullies, it is possible that the rock layers lie at a greater depth than was assumed. Because of the importance of these factors, further fieldwork to study these properties is warranted.

The model has not been validated against real discharge records, because these did not exist for the study area. Collecting discharge data can be interesting for future research, as it will then also be possible to calibrate model parameters.

DISCLAIMER

When drawing any conclusions from the results of this study, please keep in mind that:

- Although this study aimed to meet the high scientific requirements of an MSc thesis, it does not necessarily conform to industry standards for flood hazard consultancies;
- A rainfall-runoff model is a simplified representation of many complicated hydrological processes;
- The outcome of a model is dependent on many input parameters that are challenging to determine.

The model results will inevitably deviate from real-life occurrences to varying degrees. The limitations are stated in the discussion of this report, and must be kept in mind at all times if the results of this study are used to design flood measures.

ACKNOWLEDGEMENTS

Major contributions

This MSc thesis would in many aspects not have been possible without help from others. I would like to express my sincere gratitude to the following persons:

- Steven de Jong of Universiteit Utrecht, for helping to shape this project from its initial stage and in general for guiding me through this study as first supervisor;
- Wiebe Nijland of Universiteit Utrecht, for being second supervisor, and for sharing his insights regarding GIS data analysis;
- Austin van Heiningen of the department of Economy, Nature and Infrastructure, for helping to define the study area, and for sharing his insights in local flood hazards and potential measures;
- Erik Boman of St. Eustatius National Parks and Austin van Heiningen & Anthony Reid of the department of Economy, Nature and Infrastructure, for arranging permission to fly the UAV mission;
- Philip Hahn from St. Eustatius National Parks, for preparing and piloting the UAV mission, for processing the aerial photographs, and for generating the elevation point cloud;
- Marcel van Maarseveen from Universiteit Utrecht, for preparing the rainfall simulator on a short notice;
- Johan Stapel & Gudrun Labiau, for allowing me to live in their house on Sint Eustatius for over three months, for helping me with transportation to the study area, and for joining me on a day of fieldwork as well;
- The Caribbean Netherlands Science Institute for infrastructure support and accommodation during my three months of field work on Sint Eustatius;
- George & Shelley Works from St. Eustatius Animal Welfare Foundation, for providing me with their detailed rainfall records.

Minor contributions

In addition, I have had help from:

- Bastian van den Bout of Universiteit Twente, who helped me to set the correct model parameters and deal with some errors in LISEM;
- David Rijkes & Reinout Stokking, who helped me carry the equipment halfway up the Quill on a day of fieldwork.

TABLE OF CONTENTS

APPENDICES

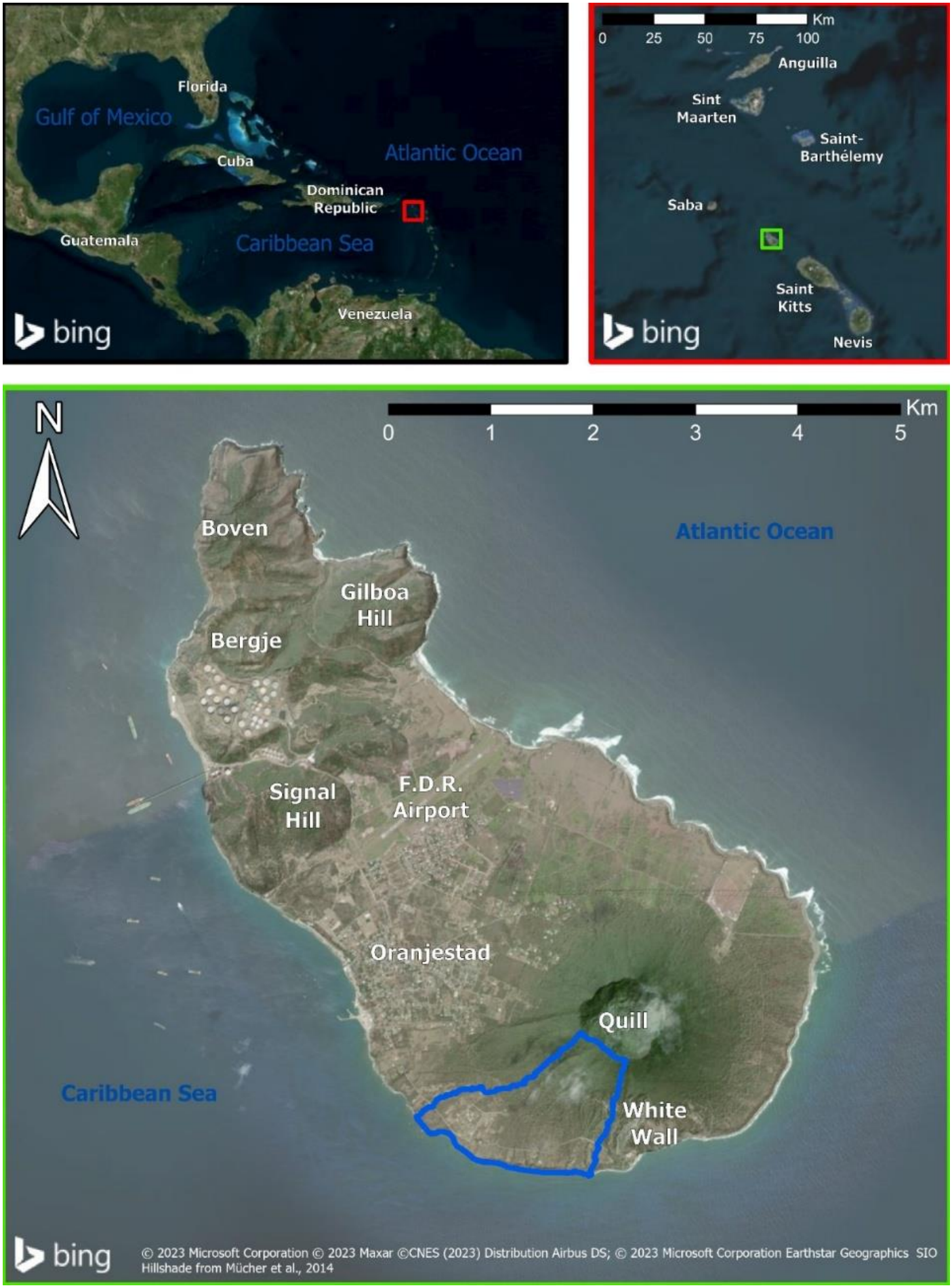

Figure 1.1: Sint Eustatius is located in the northern Leeward Caribbean, near Sint Maarten and Saint Kitts. The study area (indicated in blue) has a surface area of 1.4 km^2 and is located on the southwestern slope of the Quill, west of White Wall.

1 INTRODUCTION

1.1 Problem definition

Sint Eustatius (locally referred to as "Statia") is a small (21 km^2) volcanic island in the Caribbean (*figure 1.1*). The island frequently experiences intense rainfall that leads to widespread surface runoff and flash flooding. In urbanised areas, the runoff has a tendency to converge on roads, potentially forming powerful currents (Royal HaskoningDHV, 2018). Unpaved roads are especially vulnerable to erosion (Ramos-Scharrón & MacDonald, 2005), which can result in deep rills that make these road difficult to pass (*figure 1.2a*). Major erosion also takes place in some gullies. The sediment-laden runoff from unpaved roads and gullies sometimes flows onto level or low-lying areas. As the flow stagnates, these areas can be left inundated (*figure 1.2b*) and covered in large volumes of sediment and debris (*figure 1.2c*). In addition, a large amount of sediment is discharged into the sea, producing turbid plumes (*figure 1.2d*) that can decrease water clarity for multiple days.

Extreme rainfall is often associated tropical storms and hurricanes, which occasionally hit the island. According to Statian residents, however, the abovementioned damages are more often the result of short but intense "cloudbursts", which occur much more frequently at "around 4 to 6 times per year". Such events are not perceived as very hazardous, especially when compared to hurricanes. However, severe flash flooding after a cloudburst on the neighbouring island of Sint Maarten in 2005 (Price & Vojinovic, 2008) shows that such events can be lethally destructive. Fortunately, there are no known fatalities due to flash flooding on Sint Eustatius.

The effects of flooding are not limited to the potential loss of assets, or the hazard to personal safety. Roads that are damaged, inundated or covered with sediment hinder traffic and affect the daily lives of a large part of the population (Hammond et al. 2015). In addition, the repeated repairs to unpaved roads, and removal of sediment and debris is a

Figure 1.2: Examples of flood damage on Sint Eustatius; a. Rill erosion on an unpaved road; b. Low-lying road section that is prone to flooding; c. Massive sediment deposition from a gully onto a paved road; d. Sediment-laden discharge from gullies into the Caribbean Sea.

recurring burden on the municipal budget and the island's resources. On the longer time scale, gully erosion becomes a major contributor to soil loss (Poesen et al., 2003), while the gradual deepening and widening of the gullies (Kirby & Bracken, 2009) will destroy land area that might otherwise be used for construction or agriculture. Furthermore, excessive discharge of sediments and pollutants into the Caribbean Sea adds further stress to the already vulnerable coral reef communities in the Marine Park (Torres & Morelock, 2002). The declining health of these ecosystems will impact the island's tourism and fishing industries (MacRae & Esteban, 2007), and contribute to the worldwide loss of such ecosystems (Fabricius, 2005).

Because the consequences of repeated flooding are potentially far-reaching, it is desirable to implement measures to mitigate the negative effects of intense precipitation events. This Master's thesis aims to contribute to understanding the processes behind flooding, in addition to previous studies on (parts of) Sint Eustatius.

1.2 Previous research

Ten Harkel (2015) created a rainfall-runoff model in the opensource "LISEM" model for the central part of the island. This MSc thesis was focussed mostly on erosion, however, so flooding was not discussed in detail. At the time, LISEM only had the 1D-kinematic flow approximation. Since then, a new 2D-dynamic flow approximation was added to LISEM, which was used in the MSc thesis of De Vugt (2018) for the entire island. Flood heights were however likely underestimated in this study, because no flooding was indicated even during the more intense storms. Both models were based on a digital terrain model (DTM) by Mücher et al. (2014), which has a cell size of 5 metres. De Vugt (2018) argued that this is too coarse for detailed flood modelling, especially in urban areas. A higher quality might provide better results.

The consultancy Royal HaskoningDHV also studied rainfall-runoff in Oranjestad using propriety modelling software. In addition, a LiDAR DTM with a cell size of 0.5 x 0.5 metres was used. The severity of flooding could largely be attributed to the high density of roads and buildings (i.e. impermeable land covers), as well as a general absence of drainage infrastructure. Instead, runoff was discharged over steep roads, where the flow was confined between curbs and stone walls. Subsequently, the construction of several infiltration and retention ponds was proposed to reduce flooding.

1.3 Current research objectives

Flooding on the island was studied by researching the land surface processes regarding rainfall runoff, running high resolution runoff models of single rainfall events in LISEM, and interpreting the resulting peak and total discharges, and the maximum water heights. In consultation with the Sint Eustatius department of Economy, Nature and Infrastructure (ENI), the southwestern slope of the Quill has been proposed as the study area for this research (*figure 1.1*). The study area is discussed in detail in the next chapter. In order to better model runoff in the urban areas, a new higher resolution DTM had to be created.

The main objective of this study is to:

- assess the effects of using a higher resolution on the model's performance;
- identify the main contributing factors to flooding in the study area;
- assess the severity of flooding for different return periods and a hurricane scenario;
- propose measures to reduce the negative effects of flooding.

A major part of this study was dedicated to creating a new detailed input dataset. Raw data was acquired from a detailed record of rainfall intensities, and by conducting a fieldwork and an aerial survey. The new dataset consisted of:

- Design storms with return periods of 1, 4 and 8 years, as well as a hurricane scenario;
- Maps of the topsoil and subsoil;
- A detailed land use / land cover (LULC) map;
- Vegetation cover and leaf area index (LAI) maps;
- A new DTM for the study area.

2 STUDY AREA

Sint Eustatius is a special municipality of the Netherlands with a population of more than 3.100 (CBS Statline, 2021). Most businesses and residences, including the main village of Oranjestad, are located at the base and on the slopes of the Quill (see *figure 1.1*), a steep stratovolcano with a peak of 600 metres above sea level.

The study area has a surface area of 1.4 km^2 and is located on the southwestern slope of the Quill (*figure 1.1*). An extensive photo impression of the study area is included in **APPENDIX 1**. See also the LULC map in **APPENDIX 5**.

2.1 Urbanisation & infrastructure

The main road through the study area is the "Weg naar White Wall" (*figure 2.1; figure 2.2*), which is paved with concrete (although some sections are severely damaged). There are roadside drains. The road runs roughly parallel to the coast and the elevation contours, but has some gently sloping parts.

The largest built-up area is a subdivision in the southwest of the study area. It has roads that run roughly parallel and perpendicular to the elevation contours, with the perpendicular roads being quite steep. Most of these roads are unpaved, though Ground Dove Road, Pigeon Road and Banana Quit Road have been paved. Properties are often separated by stone walls or chain-link fences. Water that falls on the roofs of most buildings is collected in cisterns for domestic use. There are however some unfinished buildings and sheds that do not collect the water.

To the south, of the study area, there is "Statia Lodge" and some other houses, though less dense than the subdivision.

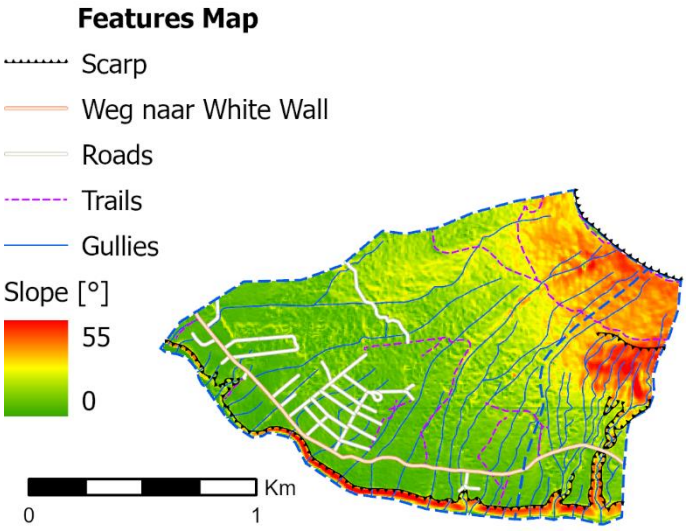

Figure 2.2: Roads and trails (source: OpenStreetMap, 2023), gullies and scarps. Slope map derived from Mücher et al., 2014. Weg naar White Wall runs across the entire study area. South of the area, there are steep coastal cliffs. The lower parts of the area have a relatively gentle slope, but the area near the crater, and also the limestone outcrop are very steep.

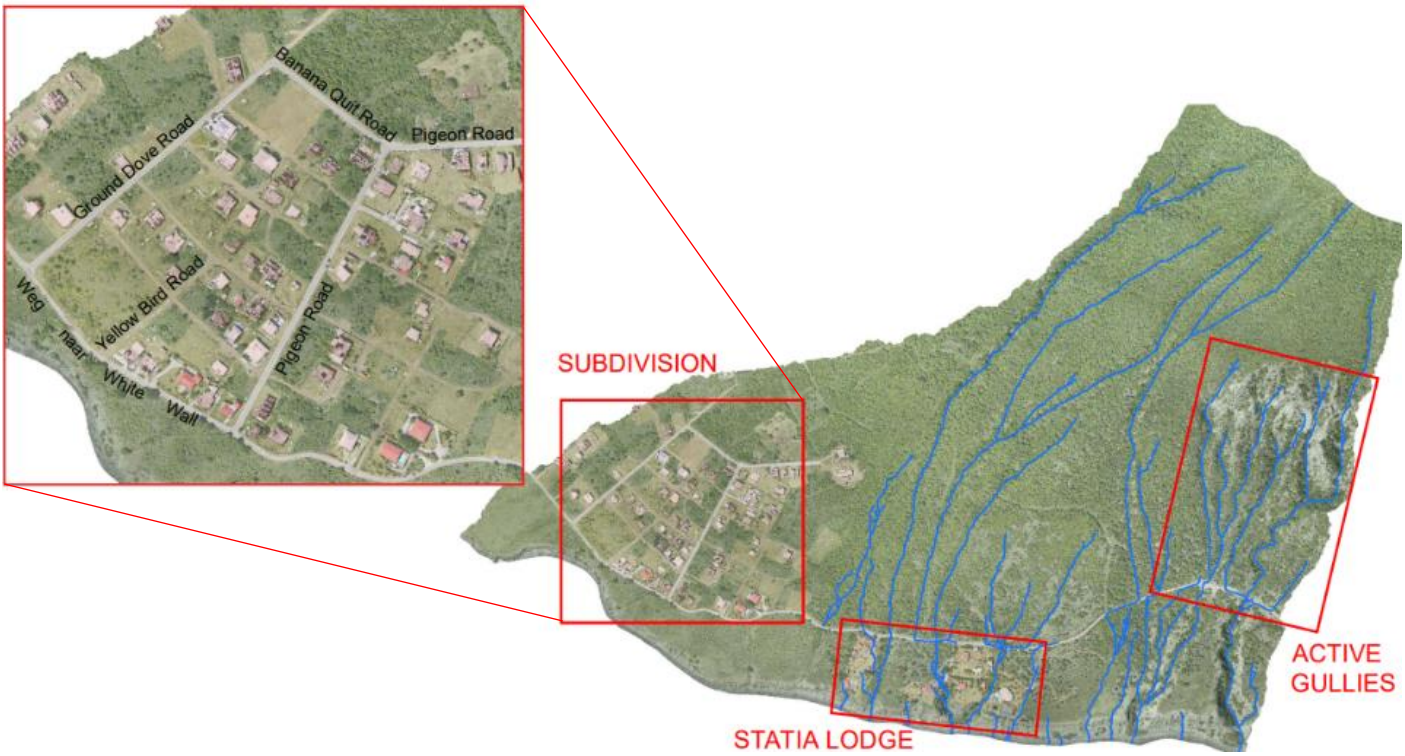

Figure 2.1: Overview of study area with specific areas of interest. The "subdivision" is most densely urbanised. Only Weg naar White Wall, Ground Dove Road, Pigeon Road and Banana Quit Road are paved. The other roads in the subdivision are unpaved. The "Statia Lodge" area has a few buildings, but a very limited amount of paved roads. The "Active gullies" originate from a steep limestone outcrop and flow south into the Caribbean Sea. The other gullies indicated on this map do not appear to have been active recently.

Densely paved areas are interesting, because they inhibit infiltration and can be major producers of runoff. Walls and other structures can be a barrier to flow, whereas paved roads can collect water that is then rapidly discharged to lower lying areas, increasing the chance of flooding. In addition, steep slopes promote water to run off more rapidly, whereas gentle slopes are more likely to develop ponds.

2.2 Geological background

The geology is dominated by pyroclastic deposits from the quill volcano (*figure 2.3*). These deposits consist of ash flows and scoria (basaltic to andesitic porous rock). The deposits appear to be sorted by size, where the coarsest material lies below the finest.

In the south of Sint Eustatius, there is an outcrop of the "White Wall – Sugar Loaf" (WW-SL) succession. It consists mainly of marine limestones and volcanic sandstones and conglomerates (Roobol & Smith, 2004). This succession is present in the east of the study area in a thin band at an elevation between 200 and 300 m (*figure 2.3*).

The WW-SL outcrop is interesting, because in contrast to the volcanic deposits, the bare rock likely has a low infiltration capacity, and therefore has a high potential for generating runoff.

2.3 Soil & geomorphology

The study area is lined by a coastal cliff, with a height of up to 30 m. Close to the coast, the terrain is relatively level, but the slope increases to around 45° near the crater rim (*figure 2.2*).

See *figure 2.4*. The soil in the study area consists largely of the "Statia loam", which has a trend of increasing stoniness and organic matter content with elevation De Freitas et al. (2012). The subsoil is very porous and provides excessive drainage of the topsoil. The area surrounding the crater rim and a large part of area B are covered by "Stony rough land". This includes the WW-SL outcrop and the slopes directly below. The south of the study area features "Terras Loam", which is characterised by a shallow clay loam layer containing gravel and cobbles. The underlying sub-soil consists of fine cemented material, providing little internal drainage of the top soil.

The description of the "Statia Loam" might suggest a high infiltration capacity, whereas the "Terras Loam" and "Stony Rough Land" might be expected to be less permeable.

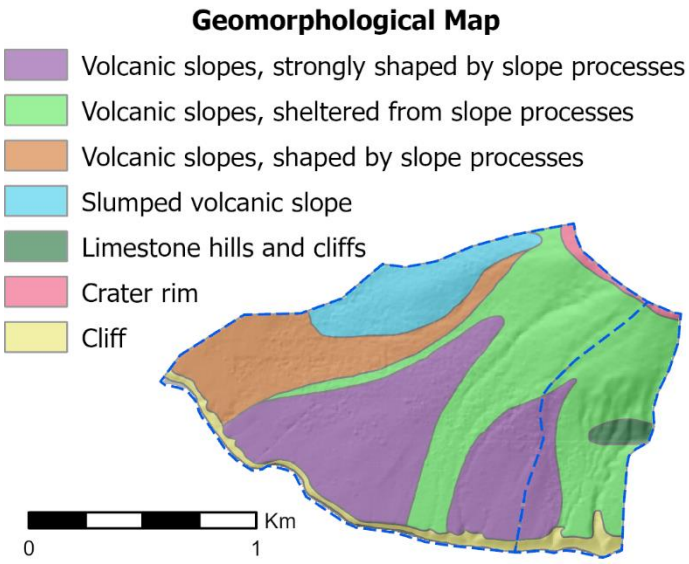

Figure 2.3: Geomorphological units (Koomen et al., 2012). The majority of the study area is covered by volcanic deposits. In the east, there is an outcrop of limestone.

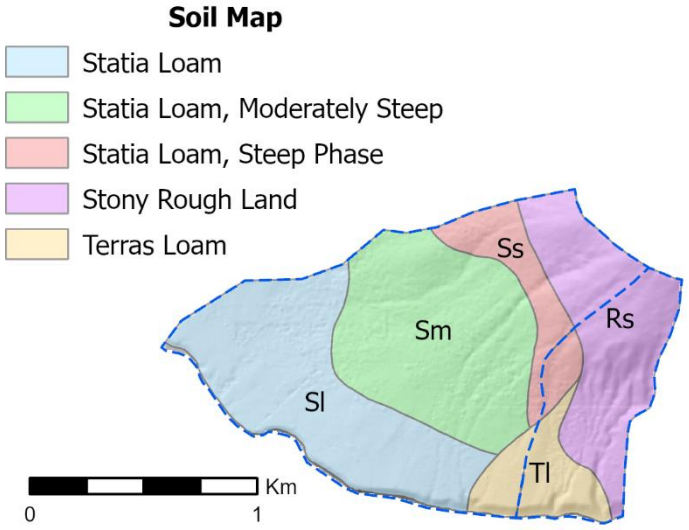

Figure 2.4: Soil map of the study area (Koomen et al., 2012). The area near the crater and around the active gullies is classified as "Stony Rough Land". South of the active gullies, "Terras Loam" may be distinguished. The rest of the study area consists of "Statia Loam".

Several gullies run down the slopes of the volcano. Some gullies appear to have been removed or interrupted by the construction of Weg naar White Wall (*figure 2.1*). The gullies in the east of the study area, which originate from the WW-SL outcrop, often produce large sediment deposits on Weg naar White Wall. Hence, they are referred to as the ***"active gullies"***, whereas the other gullies are referred to as ***"inactive gullies"***. The largest gully, "Toby Gut", passes under the road through a culvert, and is therefore not as problematic.

Because the active and inactive gullies are located in primarily undeveloped areas, the apparent difference in activity might be an indication that this is related to differences in natural factors, e.g. differences in geology, geomorphology, soil type, slope or vegetation.

2.4 Vegetation

A vegetation survey has been conducted by De Freitas et al. (2012), see *figure 2.5*. The lower elevations are mainly covered with low tree/high shrub vegetation, with many open grassy areas. The mid elevations feature mainly dense trees and shrubs, with a very open herb layer. At high elevations, there is a double layer of high and low trees, with an open herb layer and a dense litter layer. The vegetation on the WW-SL outcrop consists only of some sparse but high trees. In the slope below the outcrop, the vegetation consists mostly of open trees and shrubs.

The vegetation may be relevant, because a notable part of incoming rainwater can be intercepted by a dense vegetation canopy, therefore reducing the amount of water that reaches the ground. Dense vegetation can also add resistance to flowing water, and might promote infiltration. The possible effects of vegetation are discussed further in the next chapter.

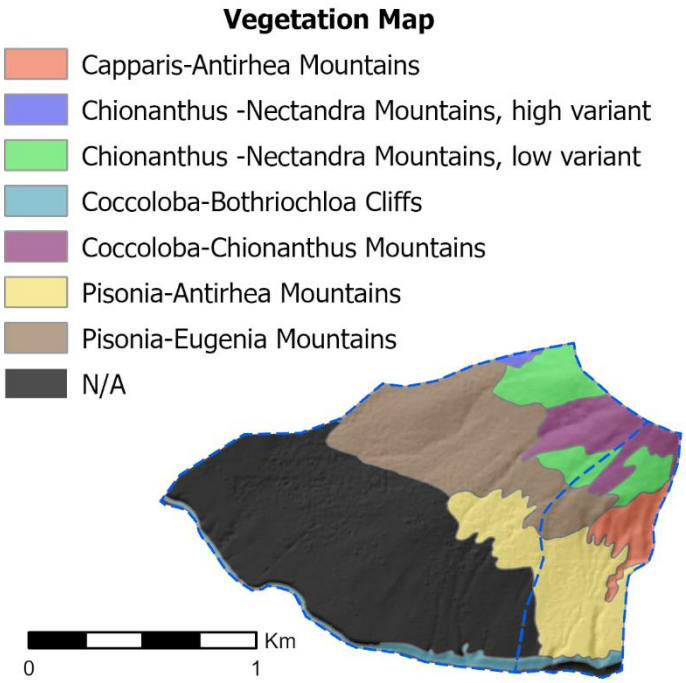

Figure 2.5: Vegetation map (De Freitas et al., 2012). The area near the crater has a multi-layered canopy (Chionanthus – Nectandra Mountains). At mid elevations, the canopy consists of dense trees and shrubs (Pisonia – Eugenia Mountains). The WW-SL outcrop is sparsely covered by high trees (Capparis – Antirhea Mountains). At lower elevations near the active gullies, the vegetation consists of open trees and shrubs (Pisonia – Antirhea Mountains). The remaining part of the study area (N/A) consists of low trees, dense shrubs or grasslands.

2.5 Precipitation

The climate is tropical, with a short to pronounced dry season (Veenenbos, 1955). Hurricanes relatively frequently pass the island within 150 kilometres: 13 in the past 30 years (NOAA, 2023). On average, almost half of the total annual precipitation (986 mm) falls in the months August to November (*figure 2.6*). Precipitation may be driven by atmospheric convection (Smith et al., 2012), or by orographic uplift. Due to this uplift, the top of the Quill can receive a considerably larger amount of rain (1500 – 2000 mm) than the lower parts of the island (MacRae & Esteban, 2007).

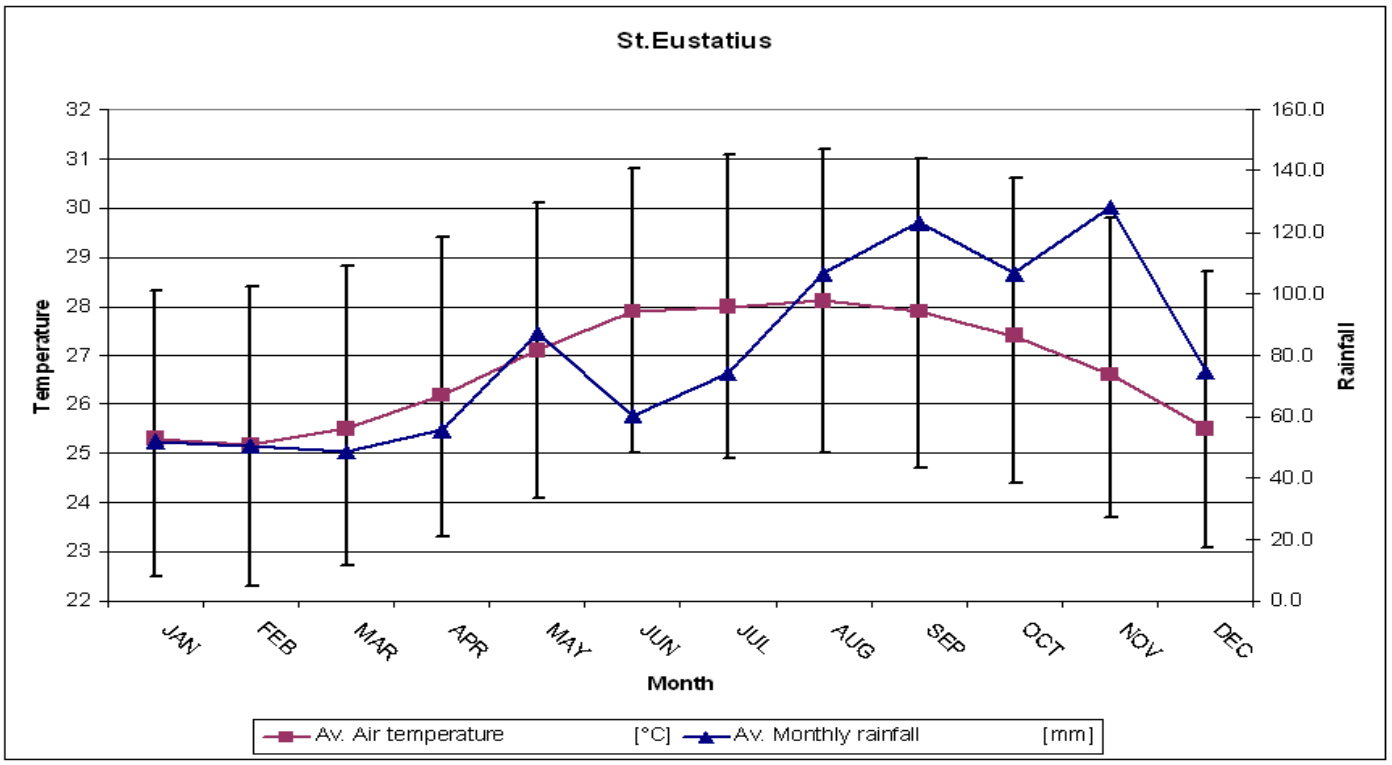

Figure 2.6: Summary of Climatological Data, Period 1971 – 2000. Supplied by Meteorological Department Curaçao. The dry season covers the months January – April. Almost half of the annual precipitation falls during the months August – November.

3 LAND SURFACE PROCESSES

This chapter discusses the hydrological processes that take place in response to rainfall P, and also how these can be numerically approximated in models such as LISEM (see also **section 4.2**). *Figure 3.1* illustrates the different mass paths that rainwater can follow. Note that evapotranspiration, interflow and baseflow are slower processes that are relatively unimportant on the short term: during and shortly after a single rainfall event. As such, they are not included in this study. The faster processes that will be discussed are canopy storage C, infiltration into the soil F, surface ponding (or depressional storage) H, and finally, runoff R. This gives the following water mass balance:

$$P = C + F + H + R_{out} - R_{in} \qquad \textbf{3.1}$$

In a spatial rainfall-runoff model, this mass balance is solved for each cell of a model grid. *Figure 3.2* shows how these storages and fluxes might act on a single cell.

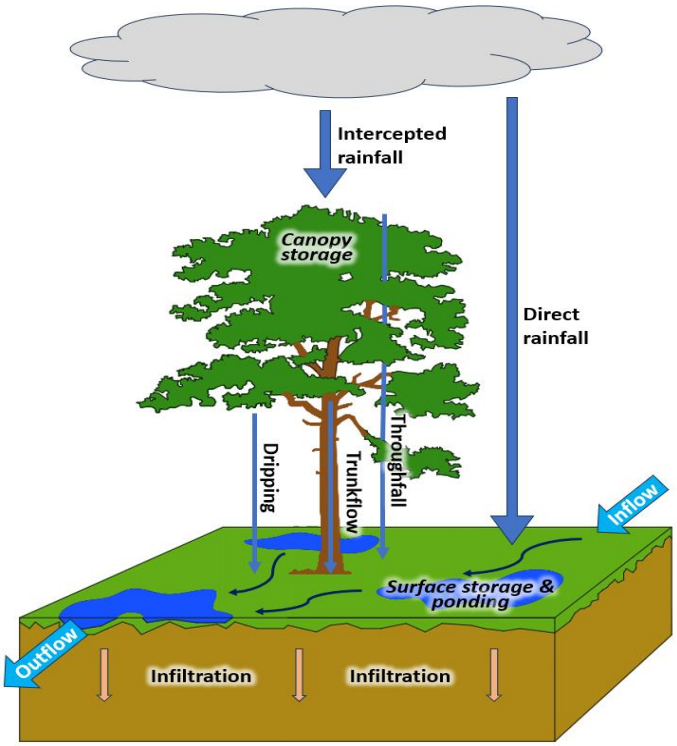

Figure 3.2: Rain can fall through or around the vegetation canopy. When rain is intercepted, a part will remain stored, while the rest may drip down from the leaves or flow along branches and the trunk. Water that reaches the ground will start to infiltrate into the soil, or it will start to pond on the surface. Any excess water leaves the area as runoff.

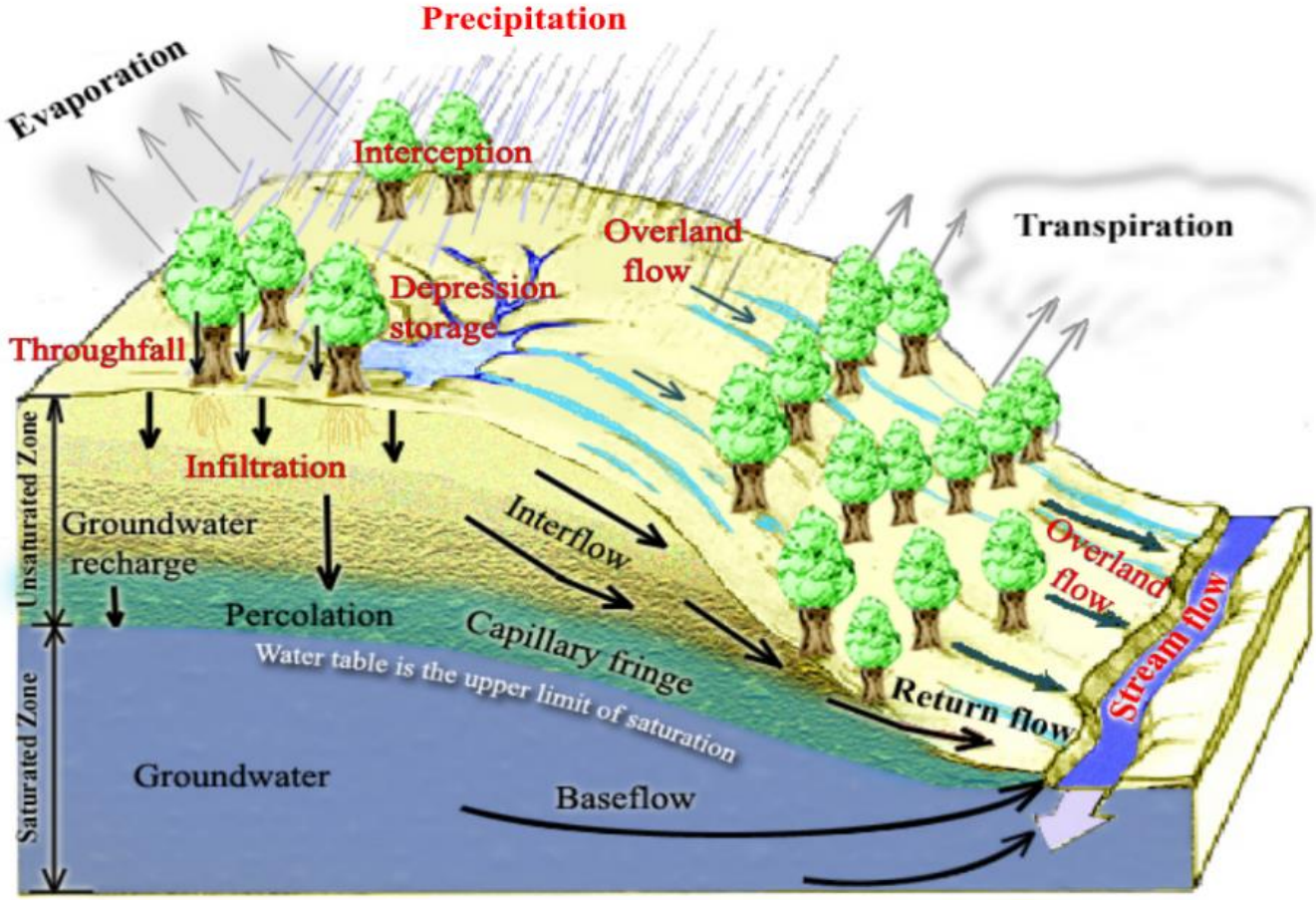

Figure 3.1: From Tarboton, 2003. Hydrological processes that take place in response to rainfall. The fast acting processes that will be discussed are shown in red. Evaporation and transpiration are quite limited during a rainfall event. Movement of water through the saturated and unsaturated zone are in general slower than surface runoff, and are thus relatively less important.

3.1 Canopy interception

When present, vegetation will be the first obstacle to raindrops on their way to the ground (*figure 3.2*). Rain may fall unhindered through gaps in the canopy as throughfall, or it may impact with the vegetation. The leaves, branches and stems of plants, shrubs and trees have the ability to store some amount of water, which can be up to 8 mm for tropical canopies (Herwitz, 1985). When the canopy nears saturation, the rate at which water drips from leaves or flows down the trunk increases. As a notable amount of rainfall is prevented from reaching the ground, the canopy is arguably important to the potential amount of runoff.

The experiments by Aston (1979) showed that the maximum storage capacity C_{max} of a plant individual can be calculated by its leaf area index (LAI), the leaf surface area per unit ground area. A model was then proposed to estimate canopy storage as a function of cumulative rainfall:

$$C = C_{max}\left[1 - e^{-k\Sigma R/C_{max}}\right] \qquad \textbf{3.2}$$

Where k is the openness factor of the canopy.

The storage capacity of a plant species is additionally dependent on the orientation and geometry of the leafs and branches (Von Hoyningen-Huene, 1983), and the roughness of tree bark (Herwitz, 1985). The relation between C_{max} and LAI thus differs across plant species, which becomes apparent when comparing different vegetation types (De Jong & Jetten, 2007). There is only a limited number of species for which the $C_{max} - LAI$ relations have been determined. Furthermore, using one specific function would not take into account a diversity of species within a vegetation canopy. This makes determining the C_{max} extremely challenging.

3.2 Infiltration

Model

The basics of flow through the unsaturated zone is explained in Dingman (2015) and Hendriks (2010). The rate of uniform downward movement of water through the unsaturated zone $\partial\theta/\partial t$ can be described by Richards equation:

$$\frac{\partial \theta}{\partial t} = \frac{\partial}{\partial z}\left(K_u(\psi)\frac{\partial \psi}{\partial z}\right) + \frac{\partial K_u(\psi)}{\partial z} \qquad \textbf{3.3}$$

Where K_u is the unsaturated conductivity, θ is the soil moisture content, ψ is the matric potential, z is the gravitational potential, and h is the total potential ($z + \psi$).

K_u is related to θ (as ψ is related to θ), because air reduces the effective porosity for the flow of water. K_u is thus always lower than the saturated conductivity, K_s. As a result, infiltrating water initially accumulates in the top soil layer, until K_u has increased sufficiently to allow further infiltration. This behaviour can be simplified by assuming that a soil layer must be completely saturated before water can start moving down, thus forming a wetting front as water moves down. This leads to the Green and Ampt equation:

$$f = K_s\left(1 + \frac{|\psi| + h_0}{L}\right) \qquad \textbf{3.4}$$

Where f is the ***potential*** infiltration rate, L is the depth of the wetting front relative to the surface, and h_0 is the height of ponded water, if any. L is in turn a function of the cumulative infiltration F:

$$L = \frac{F}{\Delta\theta} = \frac{F}{\theta - \theta_i} \qquad \textbf{3.5}$$

Where θ_i is the initial soil moisture content. According to the Green and Ampt equation, the potential infiltration rate is initially much higher than K_s, and decreases asymptotically towards K_s as L becomes larger.

Infiltration continues until it reaches an impermeable layer, such as the groundwater table, or a rock or clay layer. When this happens, the soil is saturated. Movement of water then becomes governed by groundwater flow, which is negligible within the timeframe of one rainfall event. In effect, all rainfall will contribute to ponding beyond this point: ***saturation-excess overland flow***. However, if the impermeable layer is very deep, saturation will not occur during the event.

When the supply of water is greater than the potential infiltration rate, the excess will also contribute to ponding: ***infiltration-excess overland flow*** or ***Hortonian overland flow***. This is particularly relevant during intense rainstorms.

Additional factors

Infiltration rate can show very high spatial variability (e.g. Sharma et al., 1980; Tricker, 1981). This can be linked to variations in vegetation cover, mostly because of variations in root depth and the activity of soil fauna (Tricker, 1981). Roots and soil fauna create macropores, which can drain water faster than the regular soil micropores through preferential flow (Van Schaik, 2009; *figure 3.3*)

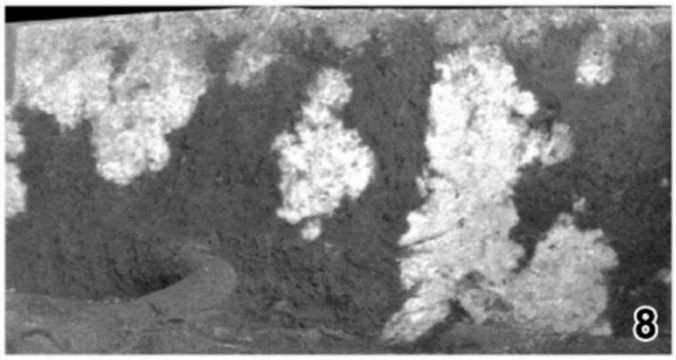

Figure 3.3: From Van Schaik, 2009. "Examples of vertical tracer-infiltration profiles, ... Light areas are dye-stained". It shows that during one rainfall event, faster infiltration occurs along clearly defined paths. Furthermore, non-preferential infiltration appears to have been very limited.

When fine grained soils (e.g. clays) dry out, they can develop cracks. This can lead to much higher infiltration rates compared to uncracked soils, at least initially (Novak et al., 2000). Crusts can also develop on coarser soils as a result of raindrop impact and infiltrating water (Valentin et al., 1992). The formation of crusts appears to be facilitated by energetic raindrops (Janeau et al., 2003).

Soil porosity can also be reduced by mechanical compaction, which is mainly caused by human activities and trampling by livestock (Batey, 2009). The most severe compaction occurs when heavy machinery is used, as is the case with agriculture, earthworks and land development. During the development of urban areas, pronounced compaction occurs, intentional or not. When compared to undisturbed soils, lower infiltration rates can be expected for soils in urban areas (Gregory et al., 2006).

Soil water repellency (SWR) occurs when soil grains are coated with amphiphillic substances. These substances can be introduced by wildfires, but also by plants or by the decomposition of plant litter (Doerr et al., 2000). SWR can dramatically reduce infiltration rates, though this effect may weaken over time, as the soil is wetted. However, SWR can be restored by severe drying of the soil.

3.3 Ponding: surface storage

A limited amount of water can be stored in microdepressions on the ground surface. When the input of water exceeds the potential infiltration rate, the excess will start filling these depressions, where a rougher soil provides greater storage capacity. Roughness is mainly created by tillage and soil aggregation, and can be reduced by raindrop impact and erosion by surface runoff (Zobeck & Onstand, 1987).

Kamphorst et al. (2000) studied the relations between maximum depressional storage (MDS) and different roughness parameters and found the highest correlation with surface random roughness (RR). The RR was defined as the standard deviation of the height readings along a transect after correction for the slope and directionality. Slope does affect MDS however: surface depressions are filled less completely on steeper slopes. The resulting difference in ponding depth can cause slightly lower infiltration rates on steep slopes, though the other factors that were discussed often better account for spatially variable infiltration (Morbidelli et al., 2018).

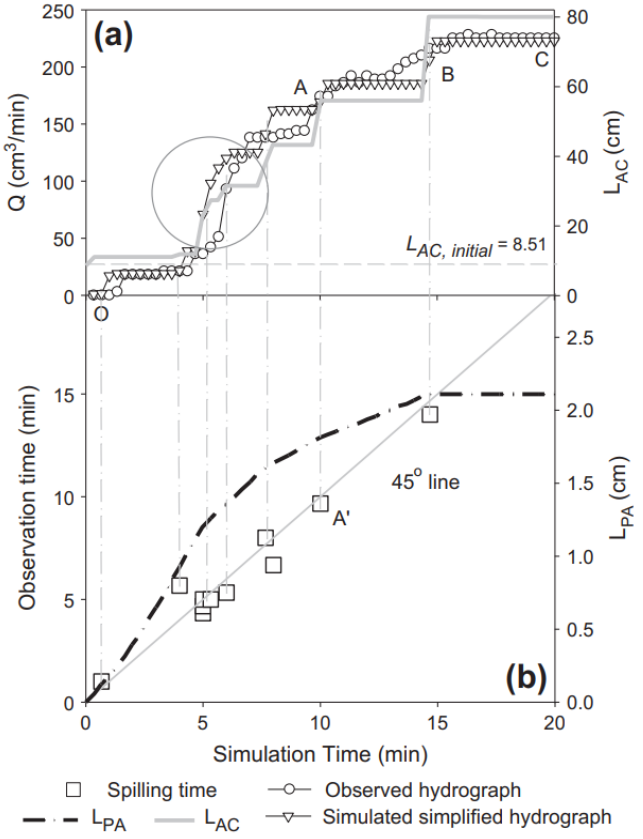

Figure 3.4: From Yang & Chu (2013). "Observed and simulated simplified hydrographs, critical times for puddle-to-puddle processes, and connectivity lengths of connected areas and ponded areas (L_{AC} and L_{PA})".

Small depressions fill up first, and start overflowing into larger ponds. The rate of overland flow therefore increases stepwise, until all depressions are filled (Yang & Chu, 2013; *figure 3.4*).

3.4 Runoff

The flow of water is primarily driven by gravity, and impeded by friction with the ground surface. The steady-state flow velocity can be calculated with Manning's equation (Chow et al., 1988):

$$\bar{v} = \frac{R_h^{2/3} S^{1/2}}{n} \qquad \textbf{3.6}$$

Where n is the Manning roughness coefficient, and S is the hydraulic gradient, which is steeper if the terrain is steeper, resulting in faster flow. R_h is the hydraulic radius:

$$R_h = \frac{A}{P_w} \quad \textbf{3.7}$$

Where A is the cross-sectional flow area, and P_w is the wetted perimeter, which is the total length of A that makes contact with the ground surface.

Manning's coefficient is an emperical constant that takes into account effects such as surface roughness, irregularities, obstacles and channel sinuousity (Acrement & Schneider, 1989). With different water heights, the flowing water may interact with different types of obstacles (Ye et al., 2018). For example, a shallow flow will be greatly affected by grass, and not at all by a tree crown. For a very deep flow on the other hand, the effect of grass would be relatively small compared to that of a tree.

3.5 Catchment response

Based on what has been discussed so far, the catchment response is affected by the vegetation canopy, spatio-temporal variations of infiltration rates, surface roughness and slope. Except for the slope and soil type, all these factors are greatly dependent on the LULC type.

Differences in LULC type will result in dramatically different responses. This can be observed when comparing two catchments that are similar in size, topography and soil type, but have different LULC (Pratomo et al., 2016), or when LULC of one catchment changes over time. For example, changing a forest to agricultural fields will reduce the canopy interception, resulting in increased total runoff (Fohrer et al., 2001). Roads, buildings and compacted soils have an even greater effect, as these also reduce infiltration over a large area.

Besides increasing total runoff, manmade surfaces induce a faster catchment response with higher peak discharges. This is because these provide less hydraulic resistance compared to natural surfaces. In addition, water is often drained from urban areas through storm sewers. Whereas a natural area would have only a few major drainage paths, dense urban areas have a much higher drainage density, and thus drain the water more rapidly (Hollis, 1975).

4 METHODS

This chapter first discusses the raw data acquisition through aerial photography and field measurements and observations. Then, a brief description of LISEM is given. Next, the processing of the raw data into the required input maps and design storms is described, as well as the anticipated model output. Finally, an overview of the executed model runs is shown.

4.1 Data acquisition

4.1.1 Aerial photography

Aerial photographs of the study area were captured at limited cloud cover between 13:45 and 14:34 on 14 February 2023. The mission was prepared and executed by Philip Hahn from STENAPA.

The mission was flown with a Quantum Systems Trinity F90+ UAV (*figure 4.1*), which was equipped with a Sony RX1 RII RGB camera (42.1 MP). The UAV was equipped with GNSS+RTK, and a reference base station with known XYZ coordinates was set up in Oranjestad.

The mission was flown at an average height of approximately 310 metres above ground level. The flight tracks were laid out roughly parallel to the elevation contour lines (*figure 4.2*). This method keeps the ground sampling distance as constant as possible across the study area (Manconi et al., 2019), and is also more energy efficient. In total, 780 photographs have been collected, which cover the study area with a side- and endlap of ~80%, and a ground sampling distance of < 4.5 cm.

Figure 4.1: Trinity F90+ performing a vertical take-off

4.1.2 Fieldwork

The study area was visited over the course of January – March. to explore the area and identify areas of interest to perform infiltration tests in. Also, the results of particularly large rainfall events were observed. Infiltration tests were conducted between 27 February and 17 March.

Figure 4.2: Flight track and locations of captured aerial photographs. The flight tracks were oriented roughly parallel to the elevation contours at a height of approximately 310 metres above ground level. The mission started near the crater and progressed downslope towards the coastline.

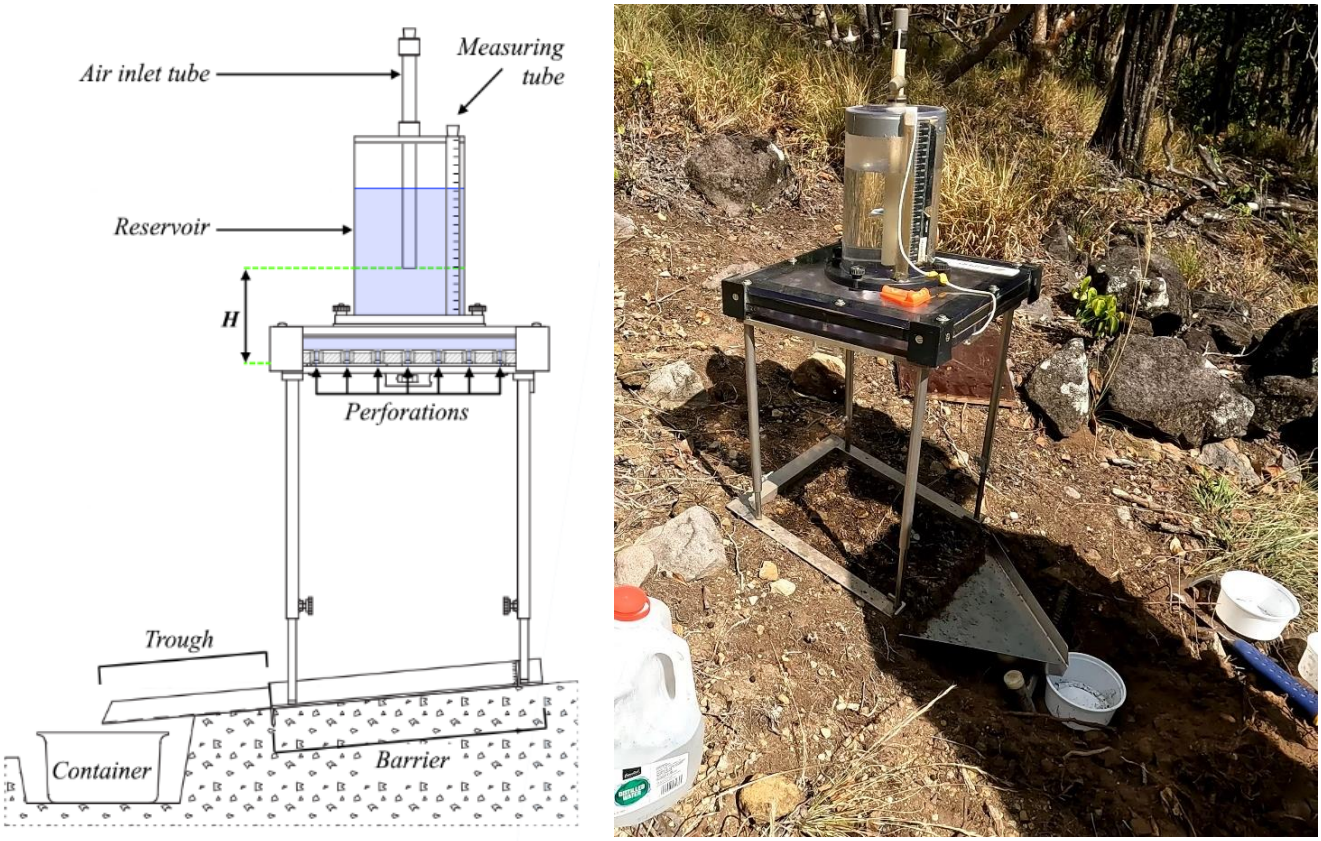

Figure 4.3: Schematic setup of the rainfall simulator, adapted from the instructions by Eijkelkamp (left); The rainfall simulator set up in the field (right). Over the course of the experiment, the hydraulic head in the reservoir remains constant, ensuring a steady input of water. Water drips through the perforations and is guided downslope via a through into a collection container. At set intervals, the discharge from the reservoir and the runoff in the container are measured.

Infiltration

Infiltration rates were measured with a small rainfall simulator (see *figure 4.3*), produced by Royal Eijkelkamp Soil & Water B.V. (Royal Eijkelkamp, 2022). Essentially, this device is a Mariotte's bottle with regularly spaced perforations at the bottom, through which water can drip down. Due to this principle, the discharge rate remains constant.

The perforated side was positioned on a stand above a small soil plot. The stand also allows for level positioning of the device, ensuring equal distribution of drops across the plot. The square plot was confined at three sides by a steel frame, with the open side pointing downslope. The frame had a size of 345 x 320 mm and was driven into the soil to a depth of 1 to 2 centimetres to seal the three sides. Runoff was collected in a trough, which funnels the runoff into a container that is placed in a dug-out pit.

A discharge rate of between 375 – 400 mL/min was used to ensure that runoff occurs within a short time. The tests were extended a few minutes beyond the time at which runoff started taking place, with a minimum of 3 minutes. During the test, the device was moved around on the stand to break up the drop impact patterns in the soil. The volume in the reservoir was measured at the measuring tube before and after a measuring period, which gives the discharge w over that period. After a measuring period has ended, the collected runoff q was measured. The infiltration f over the measuring period was then calculated as:

$$f = w - q \qquad \textbf{4.1}$$

When preparing a plot, very dense vegetation, thick roots, cobbles and very gravelly soils were avoided, as it was very difficult to properly set up the rainfall simulator here. Before setting up the rainfall simulator, the plot was cleared of any *loose* plant litter. Small vegetation, such as grass and herbs, were cut to the base. Care was taken to disturb the soil as little as possible and to prevent disturbing any soil crusts or creating cracks through which water could infiltrate.

At each infiltration test site, several other field parameters were noted:

Soil type

The soil type was assessed by hand from the soil that was dug out in the process of setting up the rainfall simulator. The soils were classified conform the NEN 5104 scheme (NEN, 1989). Note that this scheme deviates from the frequently used USDA soil texture triangle (see **APPENDIX 5**).

Preferential flow indicators

Visual observation of any influences that may induce preferential infiltration according to the theory mentioned before. These factors included mainly plant roots, soil fauna and surface crusting. Occurrence of soil water repellency has also been noted.

Note that these methods are either highly subjective and have limited precision. The results therefore indicate relative differences between test sites, rather than absolute differences.

4.2 Rainfall-runoff modelling with LISEM

As mentioned, LISEM was used to model the hydrological processes discussed in **chapter 3**. More specifically, *version 6.897* was used. In the model's documentation and user manual (Jetten, 2018), the model is described as follows:

> *"The Limburg Soil Erosion Model (LISEM) is a physically based numerical model with the purpose of event based runoff, flooding (and erosion) modelling on a catchment scale. LISEM uses a square grid to solve both cell specific processes, and the differential equations governing flow"*

This section briefly discusses LISEM, but note that the documentation provides a more detailed description.

Figure 4.4 shows the model's components that were utilised. Note that this only involves water processes. LISEM is also capable of modelling sediment transport and mass movement dynamics (see **APPENDIX 5**), which were not modelled in this study.

Cell specific processes

A sloping area has a larger surface area than the horizontal cell area. Because precipitation $R_{\perp}$ is assumed to always fall vertically, the rainfall rates are corrected for the increased surface area:

$$R_{surf} = R_{\perp} * cos(S) \qquad \textbf{(4.2)}$$

The canopy openness factor k in **equation 3.2** was calculated using:

$$k = 1 - e^{(-co \cdot LAI)} \qquad \textbf{(4.3)}$$

Where co is the vegetation cover fraction in m^2/m^2.

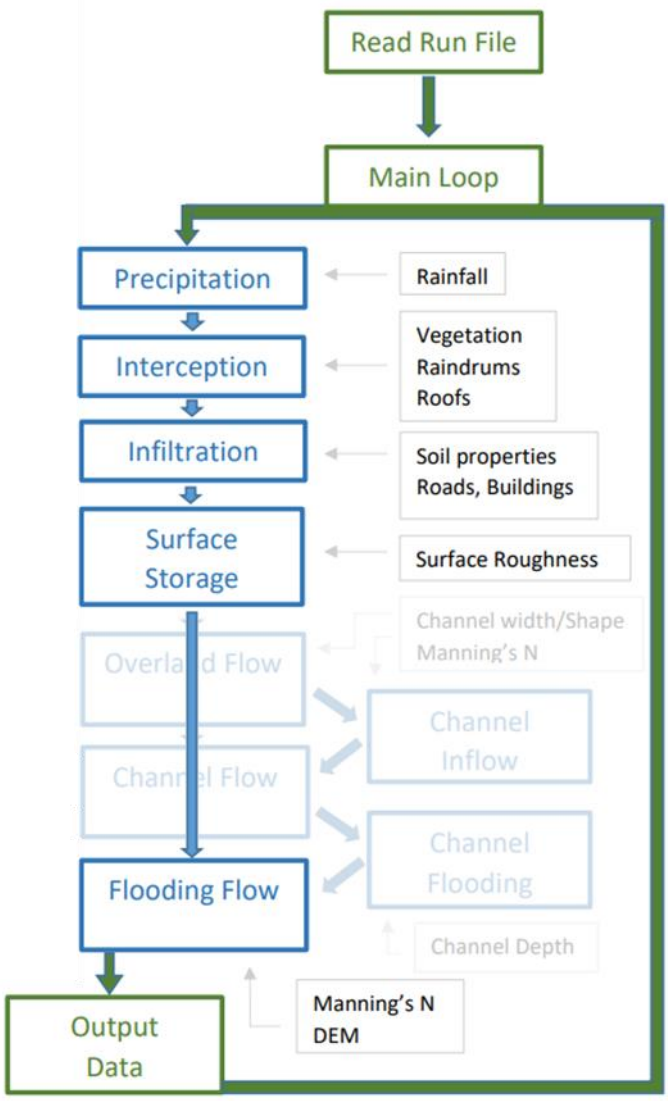

Figure 4.4: From Jetten (2018). Components of the hydrologic part of LISEM. Processes are indicated in blue boxes. Input data are indicated in grey boxes. Channel flow was not modelled in this study (faded boxes).

The C_{max} was calculated with:

$$1.036 + 0.438 \cdot LAI \qquad \textbf{(4.4)}$$

Rainfall interception by roofs and storage in drums and cisterns was also included. For this, the building cover fraction [m^2/m^2] and storage volume was specified per cell.

The cover fraction [m^2/m^2] for impermeable areas could also be specified. Depending on the degree of cover, infiltration was partly or fully inhibited. Two separate soil layers (topsoil and subsoil) were modelled using the Green and Ampt equation (**equation 3.4**). The lower boundary of the subsoil was set to free drainage. This was because the groundwater table on the island was assumed to be very deep in most areas (Bootsma, 2015), and no

impermeable layers were expected (Roobol & Smith, 2004), except around the WW-SL outcrop.

The maximum depressional storage was calculated with:

$$\mathrm{MDS} = 0.243\mathrm{RR} + 0.010\mathrm{RR}^2 + 0.012\mathrm{RR} \cdot \mathrm{S} \quad \textbf{(4.5)}$$

And the part of the ponded water *h* that can contribute to runoff was subsequently calculated with:

$$h_r = max\begin{Bmatrix} 0.0 \\ (h - 0.1MDS) * \left(1 - e^{-h\frac{h-0.1MDS}{MDS-0.1MDS}}\right) \end{Bmatrix} \quad \textbf{(4.6)}$$

Flow equations

As was mentioned in the introduction, LISEM offers two crucially different flow approximations. 1D-kinematic flow directs flow along the steepest path, which is described by a fixed local drainage direction (LDD) map. It only considers gravitational acceleration and surface friction (see **equation 3.6**). 2D-dynamic flow uses the full 2D Saint-Venant equations, and thus also considers pressure forces. This allows water to flow in any direction, rather than exclusively down the steepest path.

The performances of these approximations were compared by Van den Bout & Jetten (2018). 2D-dynamic flow was found to be more accurate in most cases, for several reasons. Most importantly, all discharge is forced over a width of a single cell with 1D-kinematic flow. Infiltration rate is therefore underestimated, while water heights are greatly overestimated. This will result in larger peak and total discharges. This problem becomes more pronounced for smaller cell sizes.

While 1D-kinematic flow may work fine on a catchment scale, the aim of this study is, among others, to model detailed flow in urban areas, which involves spreading of water in multiple directions in the case of flooding, as well as interactions with many different LULC over short distances. As such, the models were run with 2D-kinematic flow.

Spatio-temporal resolution

LISEM can be run at very high spatial resolutions. Stolte et al. (2003) for example used a cell size of 0.25 metres. With such small cell sizes, appropriately small timesteps must be used, otherwise the solutions to the 2D Saint-Venant equations become unstable, and flow will not be modelled correctly.

LISEM allows the specification of a value for the Courant number:

$$C = \frac{u\Delta t}{\Delta x} \quad \textbf{(4.7)}$$

Where u is the average flow velocity, Δt is the timestep in seconds, and Δx is the cell size in metres. During the model run, Δt is changed accordingly to keep C constant, though a minimum timestep must also be specified to prevent the model from stalling. After experimenting, a value of 0.07 was used for both the Courant number and the minimum timestep.

To analyse the effects of different model resolutions, the model was run with three cell sizes, namely 1.0 m, 2.5 m and 5.0 m.

4.3 Input maps

Table 4.1 (on the next page) gives an overview of the input raster dataset for rainfall-runoff modelling in LISEM. Note that all input maps had to be projected to the same coordinate reference system, with identical cell sizes and spatial extents. All maps were projected on WGS84 / UTM zone 20N (EPSG: 32620). The required file format of the input maps was PCRaster's **.map*. Any conversions between file formats were performed with "GDAL_translate".

The LDD and surface gradient maps served no purpose other than to verify that all maps did not have invalid cell values. Furthermore, only one rain gauge zone was used, so this map is simply a mask of the study area.

4.3.1 RGB Orthomosaic

The processing of the raw aerial photographs into a point cloud, and subsequently, an RGB orthomosaic, was performed by Philip Hahn.

The 780 aerial photographs have been georeferenced to WGS84 (Ellipsoid) using the Quantum Systems software QBase3D v2.31.33, the UAV onboard GPS, and the relative positions to the base station. The SfM-processing was performed in Agisoft Metashape. This resulted in a raw XYZ point cloud containing 3.176 billion points. This was subsequently used to generate an RGB orthomosaic with a cell size of around 4.5 cm.

4.3.2 Digital terrain model

The raw point cloud was cropped manually to only include the study area. Ground point classification was performed with the "Classify Ground Points" algorithm in Agisoft Metashape. This algorithm relies on parameters that should be adjusted for different types of terrain (i.e. the terrain slope and variability) and land cover (i.e. vegetation types and urbanised

Table 4.1: Overview of input maps that are required for rainfall-runoff modelling in LISEM

Catchment maps	Description	Type
Digital Terrain Model	Terrain height above reference level	Float [m]
Local Drainage Direction	PCRaster format for flow direction network	LDD / nominal [0 – 9]
Gradient	Sine of slope gradient in direction of flow	Float [°]
Rainfall maps		
Rain gauge zone ID	Determines input hyetograph per cell	Nominal / integer
Land use / Land cover		
Vegetation cover	Fraction of cell area covered by vegetation	Ratio [0 – 1]
Leaf Area Index	Leaf area index of the vegetation in a cell	Float [m^2 / m^2]
Roof cover	Fraction of cell area covered by collecting roof	Ratio [0 – 1]
Roof storage	Interception storage capacity of roof surface	Float [mm]
Cistern storage	Cistern storage capacity per cell	Float [m^3]
Impermeable surface	Fraction of cell area that is impermeable	Ratio [0 – 1]
Surface		
Random roughness	Standard deviation of height within a cell	Float [cm]
Manning's *n*	Hydraulic roughness of surface	Float [-]
1st and 2nd soil layer		
K_{sat}	Saturated hydraulic conductivity	Float [mm / h]
$\Delta\psi$	Matric suction differential across wetting front	Float [cm]
Soil porosity	Volumetric moisture content at saturation	Ratio [0 – 1]
Initial moisture content	Moisture content of soil layer at start of model run	Ratio [0 – 1]
Layer thickness	Depth to bottom of soil layer	Float [mm]
Hydrographs		
Reporting points	Cells for which hydrographs are reported	Nominal / integer

areas). Because the study area features different types of terrain and surface cover, the optimal parameter values also vary across the study area. For this reason, the point cloud was divided into 20 parts, based on terrain and land cover characteristics. This has the added benefit of greatly reducing the computing time. Finding the correct parameter values can be challenging, and was a matter of trial-and-error to some extent. The shorter computation time allowed for more attempts to be made within the same amount of time. After all parts were classified to a satisfactory extent, they were combined back into one point cloud again.

With the classification algorithm, the vast majority of building and vegetation points could be removed, though it did not succeed in removing all outliers and vegetation points. Many remaining non-ground points were classified by hand. Because there were no ground points below buildings and very dense vegetation, removal of non-ground points resulted in large voids. This was most notably the case in the densely vegetated areas surrounding the subdivision and higher up the volcano (*figure 4.5*). It was also problematic within the active gullies, because the exact depth of the bed could in some cases not be determined. Bare areas and areas without high vegetation were generally covered very well. The remaining ground points numbered 0.537 billion.

The classified point cloud was then exported and projected to WGS84 / UTM zone 20N. DTMs with cell sizes of 1.0 m, 2.5 m and 5.0 m were then interpolated using the ArcGIS "LAS Dataset to Raster" tool. The lowest point (minimum *Z*) in each cell was used to interpolate the DTM using the "binning" method. Voids in the point cloud were filled using linear interpolation. A low pass filter was applied once to smooth unnatural sharp edges.

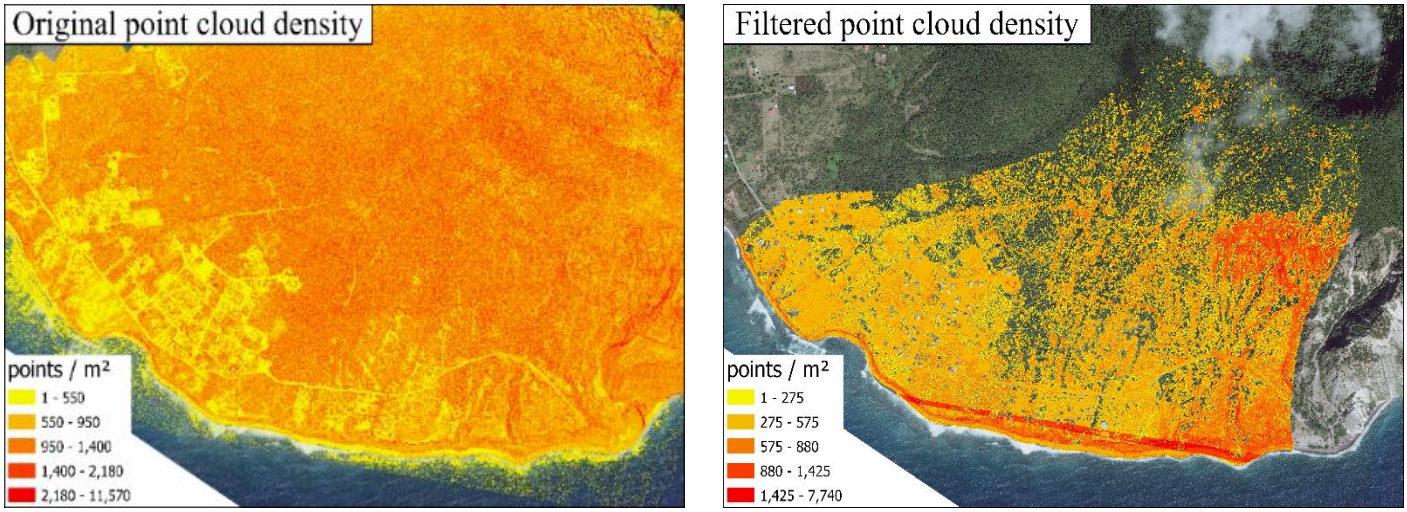

Figure 4.5: Point density per square meter for the raw point cloud (left) and the processed point cloud after clipping and classification (right). Note the large voids in the classified cloud in the densest vegetated areas. The band of high point density along the coastline in the processed cloud was the result of an error when clipping parts of the point cloud and merging them back into a single cloud.

The DTMs were analysed using the GRASS "r.watershed" tool to indicate individual watersheds. The DTMs were then clipped along the outer watershed boundaries. The culvert of Toby Gut below Weg naar White Wall was included in the DTM by manually lowering the elevation at the intersection. Next, buildings and other structures (see next paragraph) were introduced back into the DTM by increasing the elevation by an arbitrary height of 5 metres. Finally, any depressions in the DTMs were filled using the "lddcreatedem" function of PCRaster.

4.3.3 Land use / land cover

Buildings and infrastructure

A LULC-map was created by manually drawing polygons on the RGB orthomosaic in GIS. The area was classified to paved roads, unpaved roads, tracks, pavements, roofs, structures and other. The polygons were then rasterised with a cell size of 4.5 cm. The difference between unpaved roads and tracks was the degree of vegetation. "Roofs" refers specifically to main buildings that drain to cisterns. "Structures" included all other man-made objects, such as sheds, utility buildings and shipping containers.

Vegetation and LAI

The degree of vegetation cover was also estimated using the orthomosaic. Because it did not include near-infrared, the commonly used *NDVI* could not be used. Instead, the Excess Green index (*ExG*) was used (e.g. Kim et al., 2018):

$$ExG = 2G_n - R_n - B_n \qquad \textbf{(4.8)}$$

G, *R* and *B* refer to the reflection values for green, red and blue light, respectively. The reflection values were first normalised relative to the total reflection, see for example:

$$G_n = \frac{G}{R + G + B} \qquad \textbf{(4.9)}$$

The resulting map was compared to the LULC map, in order to estimate a threshold *ExG*-value for vegetation. A threshold value of 0.03 was used to classify the *ExG*-raster to a Boolean raster. This indicated vegetated and non-vegetated pixels at a cell size of 4.5 cm.

Ten Harkel (2015) determined *LAI* values for grass, shrubs, corallita and trees from representative plots and vegetation samples (unknown *N*). These values are shown in **table 4.2**. Values of the greenness *Gn* were determined for each vegetation type from single hand-picked areas. Linear regression resulted in the following relation between LAI and G_n:

$$LAI = 43 \cdot G_n + 13 \qquad \textbf{(4.10)}$$

Table 4.2: Approximate LAI values for some vegetation types (Ten Harkel, 2018), and corresponding greenness values.

Vegetation type	LAI	G_n
Grass	1	0.33
Shrubs	2	0.35
Corallita vines	3	0.37
Trees	5	0.41
Max LAI	7	0.45

Cover fractions

The cell cover fractions for impermeable surfaces, drained roofs and vegetation were generated by first creating Boolean maps at a cell size of 4.5 cm. Then, these Boolean maps were resampled to the final model cell sizes (1.0 m, 2.5 m and 5.0 m), where the average cell values of the Boolean maps were assigned to the resulting resampled cell values.

4.3.4 Surface

Values for *rr* and *n* were taken from lookup tables in the LISEM documentation & user manual (Jetten, 2018; see also **APPENDIX 5**), and applied to the LULC and soil maps (**table 4.3**).

Table 4.3: Used values for random roughness and *n* for the different LULC / soil classes. The original lookup tables are included in APPENDIX 5.

LULC / soil class	Random roughness	Manning's *n*
Structure	0.5	0.01
Pavement	0.5	0.01
Roof	0.5	0.01
Property	0.5	0.10
Unpaved road	0.5	0.01
Paved road	0.5	0.01
Track	0.5	0.10
Cleared land	0.5	0.03
Bare soil	0.5	0.03
Water	0.1	0.05
Vegetated	1.0	0.10
Limestone	0.5	0.01
Active gully bed	0.5	0.03
Inactive gully	0.5	0.05

4.3.5 Soil classes

The majority of the study area had a loamy topsoil (see chapter 5). The thalweg cells of the active gullies, the entire width of inactive gullies and also unpaved roads were defined as a separate soil type. The exposed limestone outcrop was drawn manually from the RGB orthomosaic and included in the topsoil map.

For the subsoil, the area was fully set to loam, except at the area between the limestone outcrop and the Weg naar White Wall, where the WW-SL formation may exist at a relatively shallow depth below the topsoil (see chapter 5).

4.4 Design storms

Rainfall data over the period January 2015 – December 2022 was supplied by George & Shelley Works of the St. Eustatius Animal Welfare Foundation. Rainfall was measured with a Davis Weather Vantage Plus Pro weather station, which was located on the western slope of the Quill. This weather station measured rainfall with a tipping bucket, at a minimum resolution of 0.2 millimetres rainfall depth. Rainfall was recorded per 1 minute periods. The data only included the measuring periods in which rainfall was recorded.

Separate rain showers were defined as a sequence of rainfall measurements with a dry interval of no longer than one minute. A Gumbel distribution was then created for extreme rainfall events:

$$f = \frac{1}{T} = \frac{rank}{N+1} = \frac{[1..N]}{N+1} \qquad \textbf{(4.11)}$$

This was done by identifying for each year ($N = 8$) the event with the highest cumulative rainfall, and ranking them in ascending order. From the resulting distribution, the yield of an event with a specific return period could be estimated. With this distribution, the durations and rainfall cumulatives were estimated for events with return periods of $\boldsymbol{T = 1}$, $\boldsymbol{T = 4}$ and $\boldsymbol{T = 8}$ years.

A ***hurricane scenario*** was designed with a cumulative rainfall of 450 mm and a duration of 24 hours (see for example Maass, 2016).

With the triangular hyetograph method (Chow et al., 1988), storms can be designed with a specified duration and cumulative rainfall. In this design, rainfall intensity increases and decreases at a constant rate, and peaks halfway through event. As such, this method only requires the total duration and the maximum intensity, which was be calculated with:

$$w_{max} = \frac{2 * P}{T_d} \qquad \textbf{(4.12)}$$

4.5 Model output

During the model runs, hydrographs are logged for the active gullies, specifically for single cells at the intersections with Weg naar White Wall (*figure 4.6*). Water heights are also saved at regular intervals throughout the run. At the end, LISEM outputs maps for cumulative interception and infiltration, as well as a map with the maximum water heights.

The total runoff ΔR_{AOI} from an area of interest (*figure 4.6*) was obtained by solving the mass balance (**equation 3.1**) after the run had finished.

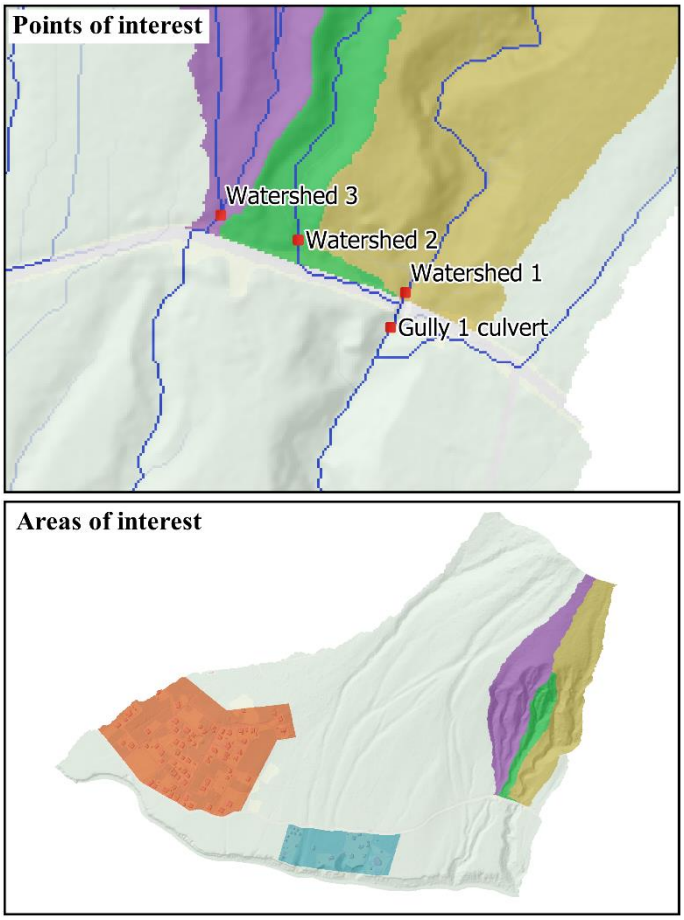

Figure 4.6: Points of interest (top) and areas of interest (bottom). The POIs were placed at the deepest cells of the channels with the largest peak discharges. The subdivision and Statia Lodge AOIs were defined by Weg naar White Wall and the borders of the properties. The gully AOIs were defined by the drainage divides until Weg naar White Wall.

Peak discharges could not be directly read from the hydrographs. This was because the flow though the gullies was sometimes wider than a single cell. Water that did not flow through the output cells would thus not be represented in the hydrographs. This problem could also not be solved by creating a row of output cells, because there might be exchange of water between output cells, which would then be represented twice in the sum of the hydrographs. Instead, the peak discharge of the hydrograph Q_{hydr} was rescaled based on the cumulative discharge ΣQ of the hydrograph, and the ΔR_{AOI} from the corresponding watershed:

$$Q_{corr} = Q_{hydr} \frac{\Sigma Q}{\Delta R_{AOI}} \qquad \textbf{(4.13)}$$

4.6 Model runs

A default set of model parameters was defined. To assess the sensitivity to different soil parameters, additional sets of parameters were created:

- Two scenarios with lower loam K_{sat} were added: ***"SWR"*** and ***"Low"***. These were included to consider respectively a scenario of widespread soil water repellency and different values found in other studies, see **section 5.1**;
- For the active gully beds, scenarios with higher and lower K_{sat} (resp. ***"K+"***, ***"K-"***), higher and lower $\Delta\theta$ (resp. ***"V+"***, ***"V-"***), and a greater soil depth (***"D+"***). These were included because the default parameters were based on some assumptions that were necessary due to the complex nature of the subsoil, see **section 5.1**.

The parameter values are shown in **section 5.2**.

The executed model runs are shown in **table 4.4**. Not all possible combinations were included. The effects of different model resolutions could be sufficiently illustrated with only the default – T = 1 yr settings. Also, the sensitivity of soil parameters could be discussed with only the T = 1 yr design storm. Besides, including more combinations with the other design storms would have greatly convoluted the overall discussion. The discussion of flood measures assumed the default soil parameters.

All models were run for one hour longer than the duration of the design storm, so that no more flow occurred at the end of the run.

Table 4.4: Executed model runs

Resolution [cm]	Soil parameters	Return period			
		1 year	4 year	8 year	Hurricane
500	Default	×			
250	Default	×			
100	Default	×	×	×	×
	SWR	×			
	Low	×			
	K+	×			
	K-	×			
	V+	×			
	V-	×			
	D+	×			

5 RESULTS

This chapter will start with discussing the field observations, including the geological and geomorphological features. Also, the soil types and their hydrological properties are discussed. Next, the resulting model input data is shown. This consists of the different sets of soil parameters and the results of the rainfall data analysis. Of the input maps, the canopy storage capacity is briefly discussed, and the different resolution terrain models are compared. Finally, the output of the various model runs is shown.

5.1 Field observations and measurements

Also, flooding in gullies and on roads has been observed on several occasions, and features that may affect the behaviour of flow have been noted as well. These observations are helpful for discussing the accuracy of modelled flooding, and are used as such later on. Also, observations have been made that pertain to geological and geomorphological features. Photographs and a map of these observations are included in **APPENDIX 1**, along with a map of the infiltration test sites and the recorded parameters.

Gullies

Intense rainstorms occurred in January 2023, and the gullies were inspected shortly afterwards. The inactive gully slopes and beds featured a well-developed layer of organic matter, which did not appear to have been disturbed by fast flowing water. The active gullies in the east of the study area did have flowing water. Moreover, they produced large sediment deposits on Weg naar White Wall, attesting to the erosive potential of the flow.

Different gully types could be distinguished based on the cross-sectional profile (*figure 5.1*). The active gullies had a very steep slopes and debris fans on one or both sides, a well-defined channel, and occasionally a floodplain. In contrast, the side walls of the inactive gullies were gentle and rounded, and had no defined channel. There were also gullies with rounded slopes, as well as an active channel. These channels were likely recently formed by debris flows. Debris end lobes were found in these gullies, and upstream, trees along the channels were damaged.

Flooding on roads

During heavy rainfall, flooding occurred on some sections of Weg naar White Wall, mostly where the road intersected with inactive gullies. In most cases, flooding appeared to have been facilitated by slightly elevated grass roadsides and curbs.

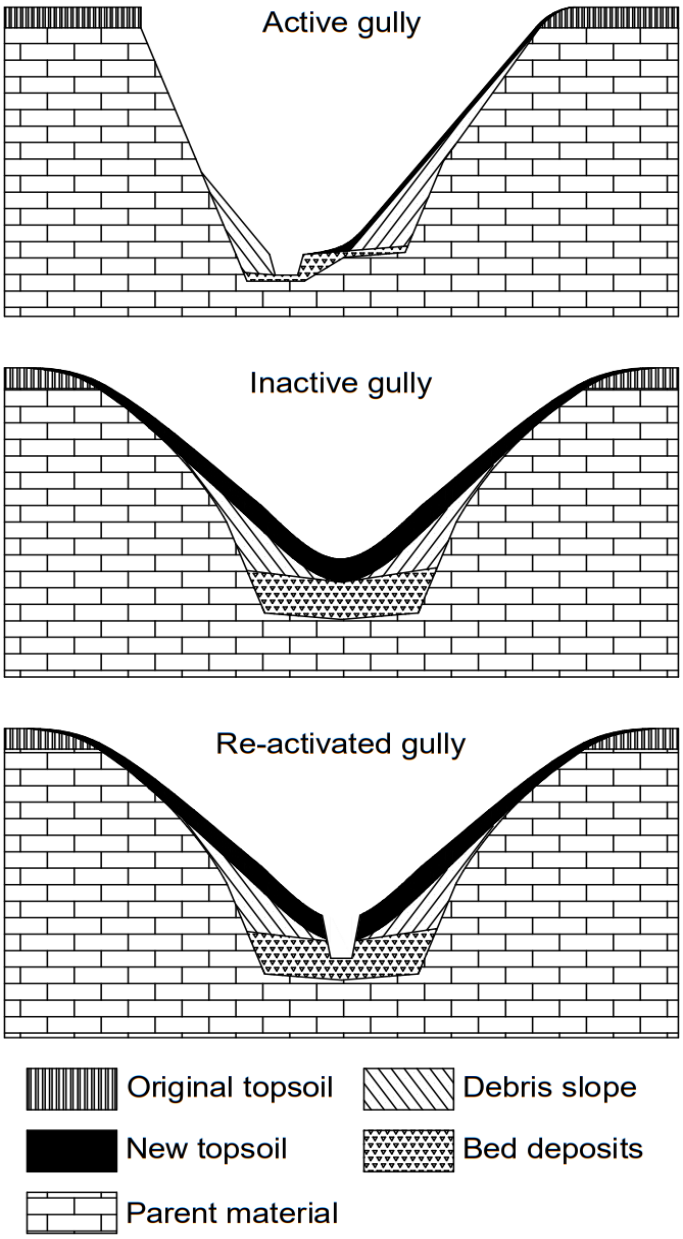

Figure 5.1: Cross sections (not to scale) of the active gullies, inactive gullies and "Re-activated" gullies. The active gullies sidewalls often consist of loose material, whereas the beds consist primarily of coarse sediments. In inactive gullies, the steep sidewalls are not maintained by erosion of the bed, allowing the gully to be reshaped and a new topsoil to develop. The Re-activated gullies may have been reshaped during a long inactive period, but recent events could have created the new channel. Photo impressions of these gully types are included in ***APPENDIX 1****.*

On the steep paved roads in the subdivision, a shallow sheet flow was observed. The flow from Ground Dove Road terminated in a pond that formed on Weg naar White Wall.

On some steep unpaved roads, runoff occurred in small rills. When the flow stagnated as it reached Weg naar White Wall, the eroded sediments formed fan-like deposits. In other cases, the flow was able to continue flowing along Weg naar White Wall, thereby spreading sediment across a longer road section.

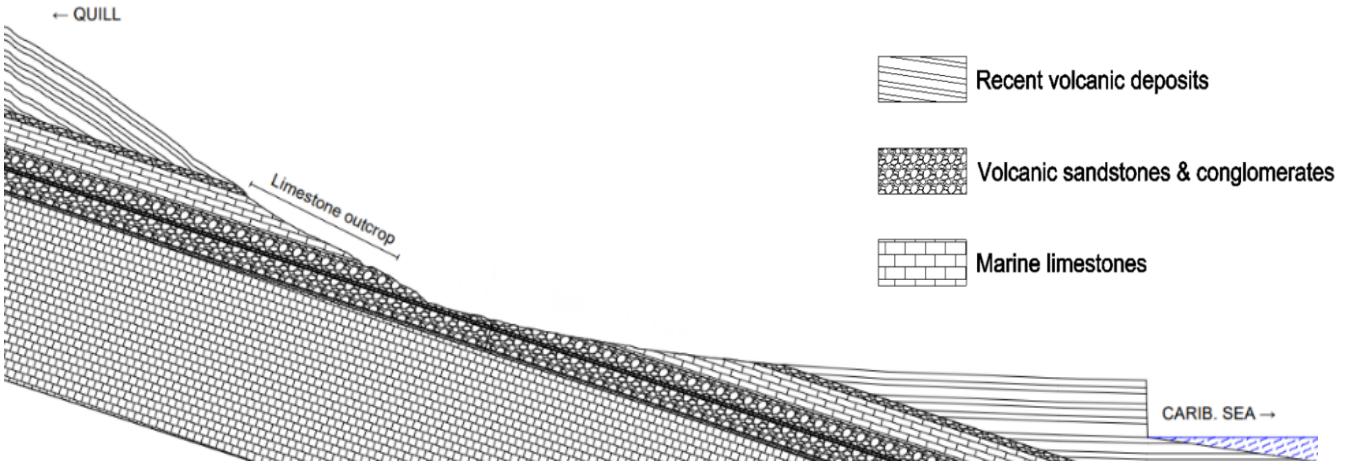

Figure 5.2: Cross-section of the White Wall – Sugar Loaf succession near the active gullies, based on the stratigraphic column of the WW-SL succession (see APPENDIX 5) and observed outcrops of limestones and (presumably) volcanic sandstones and conglomerate (see photographs in APPENDIX 1). According to this cross-section, impermeable rock may be present at a shallow depth below the gully beds.

White Wall – Sugar Loaf succession

Though the limestone outcrop was generally too steep to investigate in the field up close, some observations can be made from a distance. The aerial photographs revealed that large mounds of debris have collected within the gullies on the outcrop.

Remnants of the White Wall – Sugar Loaf succession were found in the gullies, between the outcrop and the Weg naar White Wall. These remnants mostly resemble sandstones and conglomerates, which may correspond to the volcanic deposits that underlie the top calcarenite layer of the White Wall succession (see the stratigraphic column in **APPENDIX 5**). These remnants suggest that the limestone extended further downslope in the past, and may still be present in the subsoil. The observed orientation of the layers is less steep here compared to the actual White Wall and Sugar Loaf formations to the east. In fact, the orientation appears to be somewhat similar to the slope of the ground surface. Downslope, the coastal cliffs consist of more recent volcanic deposits, which may overlie the older WW-SL strata. Based on these observations, the cross-section in *figure 5.2* was estimated. The hydrological implications of this subsoil structure are discussed in the next paragraph.

Soil types

the soil in the majority of the study area consisted of ***loam*** (USDA classes “loam”, “silt loam”, and “sandy loam” to a lesser extent), with varying amounts of gravel. A clear distinction between the different phases of the Statia Loam could not be identified in the field, as exceptionally gravelly loams have been found throughout the entire study area. An increase in organic matter content with elevation was observed. Also, the soil near the crater and in the active gullies was remarkably more stony, which is in agreement with the “Stony rough land” class. The underlying soil type could be examined at recent excavation sites, which very clearly showed the horizon sequences and underlying porous parent material, which started at a depth of around 30 cm.

The beds and side walls of the inactive gullies were often covered with a thick layer of compacted plant litter and organic matter, bound by dense plant roots. This layer mostly had a thickness between 10 to 30 cm. The organic matter content was estimated to be between 15 and 25 %. This soil should technically be referred to as “peat” within NEN 5104, but this would not appreciate the formation process of this soil type. Instead, it will be referred to as ***histosol***, despite the limited thickness. The porous Statia Loam underlays the histosols.

The beds of the active gullies consisted of silty to non-silty ***sands*** (USDA classes “sandy loam”, “loamy sand” and “sand”), as well as debris slopes and fans with very high gravel contents. Vegetated areas featured humous and littered sands and gravels. It is not clear how shallow the non-weathered White Wall – Sugar Loaf succession is present below the surface, but this can greatly influence the hydrological response of the area. Because the permeabilities of these rock layers are likely negligible compared to the Statia Loam, a shallow depth greatly limits the volume of water that can be accommodated in the soil during a rainfall event.

Infiltration

SWR was observed at a large portion of the test sites. This was clearly visible when spilled water had a high tendency to form “beads” on the ground surface, or when soil particles remained afloat on the collected runoff (*figure 5.3*). SWR was not limited to the soil

Figure 5.3: Water beading up on the soil in the runoff collection pit (left); soil particles staying afloat in a runoff collection container (right).

Figure 5.4: Preferential flow paths in a soil with low permeability (left). Besides the flow paths, infiltration in this soil was very limited; Uniform infiltration in a soil with high permeability (right).

surface, as it became apparent that when spilling water in the collection pits, it also would not infiltrate. The majority of SWR soils had a high organic matter content and litter cover. However, humous soils and soils located in densely vegetated areas did not universally feature SWR, or exceptionally low infiltration rates.

Preferential flow paths for infiltrating water have also been observed with great frequency. The water infiltrated many times deeper at these paths compared to the surrounding area (*figure 5.4*). This effect was most pronounced in soils that had a relatively low permeability, such as SWR soils. The propagation of the general wetting fronts in such soils was relatively small (~ 5 mm), and furthermore might have been driven by the impact of raindrops, rather than soil suction and gravity. Occasionally, preferential flow paths formed along the steel barrier.

Figure 5.5 shows the derived infiltration rates for each major soil class, as well as the number of tests per class. An additional distinction has been made between loam with and without SWR. According to these results, there is generally not a large difference between the median infiltration rates of sand and non-SWR loams. For SWR loams, the median value is clearly lower than for non-SWR loams. However, there is a large overlap between the ranges of these soil types. The large overlaps between the different classes are likely the result of varying degrees of preferential flow between the test sites, which can negate the effects of SWR. Most histosol test sites featured SWR. The mean values of the histosols are comparable to those of SWR loam. These results indicate that soil texture is less important than whether a soil exhibits SWR and preferential flow.

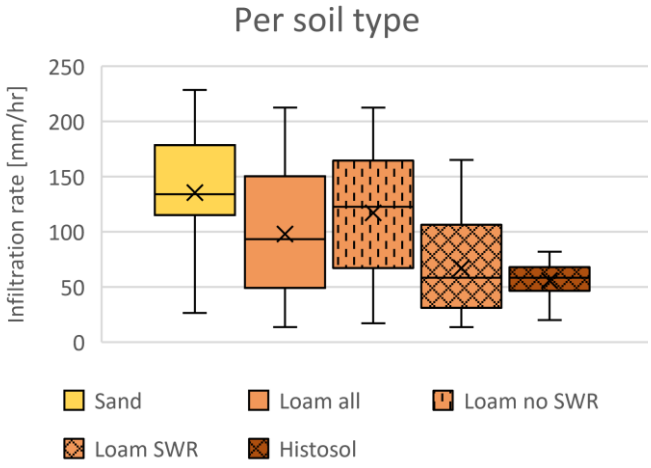

	Sand	Loam all	Loam No SWR	Loam SWR	Histosol
N	12	60	37	23	8
Max	228	212	212	165	82
Mdn	**134**	**89**	**123**	**58**	**58**
Min	26	14	17	14	20

Figure 5.5: Infiltration rates per soil texture class. The ranges of values for sand and non-SWR loam largely overlap, and the median values are similar. The median of SWR soils are clearly lower. Preferential flow likely caused the wide range for SWR loam.

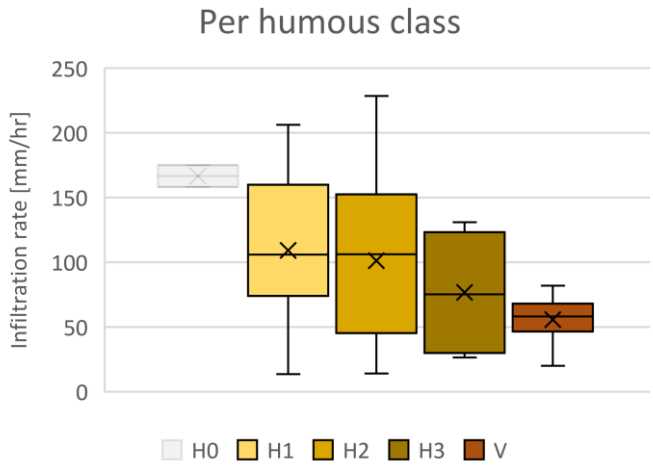

	H0	H1	H2	H3	V
N	**2**	29	35	6	8
Max	**175**	206	228	131	82
Mdn	**166**	**179**	**106**	**75**	**58**
Min	**158**	14	14	26	20

Figure 5.6: Infiltration rates per soil humous class. Infiltration rate appears to decrease with increasing organic matter content. Note that the number of tests for H0 was very limited, and the reliability is consequently low.

The infiltration rates have also been compared per soil humous class (*figure 5.6*). The mean infiltration rates decrease as the organic matter content increases to class "V" (the histosols). There is an apparent decreasing relation between infiltration rate and organic matter content.

5.2 Model input

The model input is shown in a larger size in **APPENDIX 2**.

Soil parameters

Parametrisation was based on the following sources:

- All topsoils were given a shallow depth of 30 cm, based on observations at excavated sites and around the WW-SL outcrop.
- The K_{sat} of WW-SL rock was set to (almost) impermeable.
- Default topsoil K_{sat} were based on the infiltration measurements (*figure 5.5*).
- For loams and sands, values for θ, θ_i and ψ were taken from De Vugt (2018), Ten Harkel (2015), Bootsma (2015) and the LISEM manual (Jetten, 2018).
- For unpaved roads, the *Ksat* was set to 25% of unaffected loam (Ramos-Scharrón & LaFevor, 2016).
- For very humous loams, θ and θ_i were taken from Dekker & Ritsema (2000). The same ψ as regular loam was used, as it is independent on organic matter content (Saxton and Rawls, 2006).
- The subsoil loam K_{sat} was taken from Bootsma (2015).

The soil parameters for the different scenarios are shown in **table 5.1** (on the next page).

Rainfall data

Figure 5.7 shows the number of rainfall events that fall within an interval for duration and rainfall depth. The vast majority of events have neither a long duration nor a large yield. Moreover, events with a long duration were very rare. Events exceeding 25 minutes occurred on average 3 to 4 times per year, with an anyways limited duration of 81 minutes at most. Moreover, the largest event in terms of cumulative rainfall (63,6 mm) appears to have consisted of two shorter rainstorms that took place in rapid succession (see *figure 5.8*).

While several hurricanes have closely passed the island between 2015 and 2023, exceptional rainfall has not been recorded on any of these occasions. The Works have not mentioned any failures or errors during such events. It is possible that long periods of intense rainfall have taken place in reality, but that the equipment failed to fully record these due to the extreme conditions. For example, "undercatch" of rainfall by a gauge can be caused by strong winds (Pollock et al., 2018).

Table 5.1: Default input soil parameters and adapted parameters for various scenarios.

Default	Topsoil (< 0.3 m – GL)				Subsoil (> 0.3 m – GL)			
Soil type	**K_{sat} [mm/h]**	**θ [-]**	**$θ_i$ [-]**	**ψ [cm]**	**K_{sat} [mm/h]**	**θ [-]**	**$θ_i$ [-]**	**ψ [cm]**
Loam	89	0.50	0.35	11	343	0.41	0.25	11
Sand	134	0.50	0.30	20	N/A			
Histosol	58	0.70	0.35	11	N/A			
Compacted	22	0.35	0.10	11	N/A			
WW-SL	0.1	0.10	0.05	40	0.1	0.10	0.05	40
SWR								
Loam	***58***	0.50	0.35	11	343	0.41	0.25	11
Histosol	***58***	0.70	0.35	11	N/A			
Low								
Loam	***30***	0.50	0.35	11	343	0.41	0.25	11
Histosol	***30***	0.70	0.35	11	N/A			
K+								
Sand	***343***	0.50	0.30	20	N/A			
K-								
Sand	***89***	0.50	0.30	20	N/A			
V+								
Sand	134	0.50	***0.20***	20	N/A			
V-								
Sand	134	0.50	***0.40***	20	N/A			
D+	Topsoil (< *1.0 m – GL*)							
Sand	134	0.50	0.30	20	N/A			

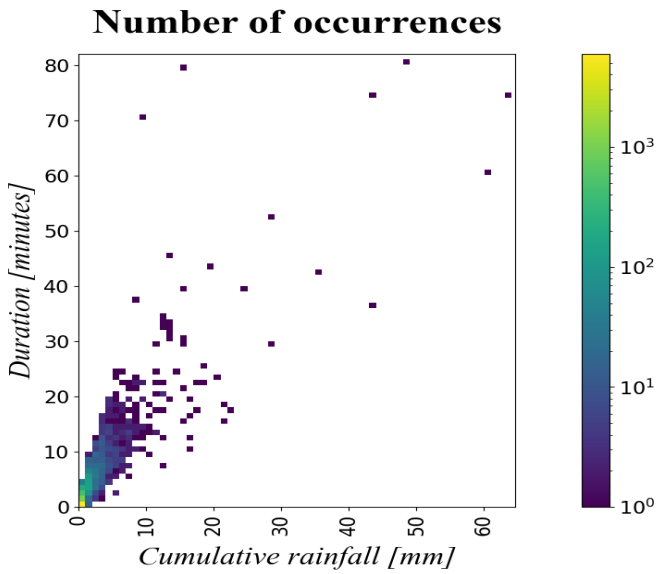

Figure 5.7: Number of events per duration and depth interval, amounting to a total of 8861 isolated events. Duration and depth intervals are 1 minute and 1 millimetre wide.

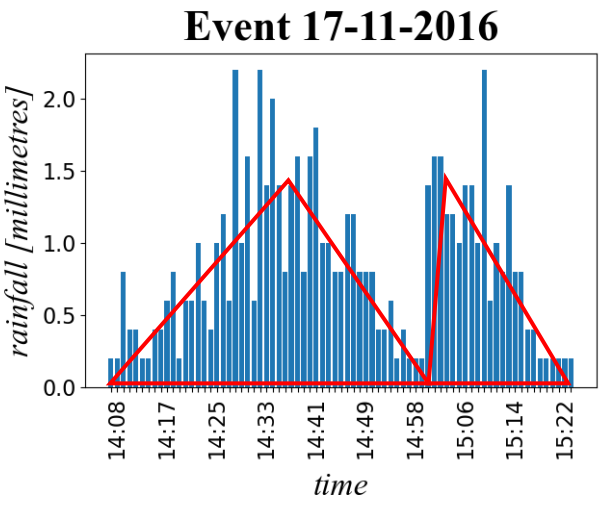

Figure 5.8: The largest event in the dataset in terms of yield, 63.6 mm. The event appears to consist of two heavy rainstorms that occurred in short succession.

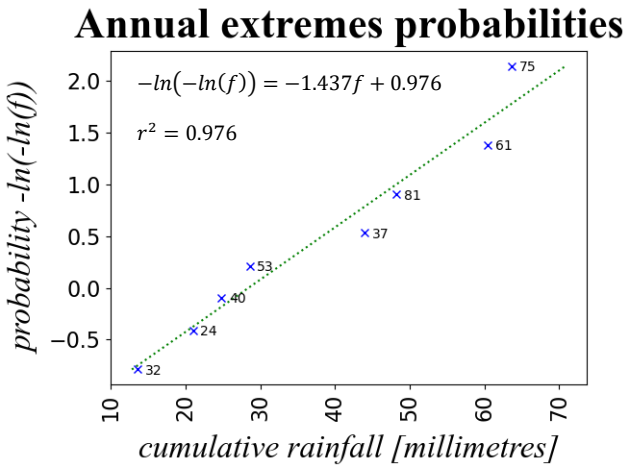

Figure 5.9: The ranked annual largest events in terms of cumulative rainfall, plotted against the logarithmic probability. The labels at each point show the duration (in minutes) of the event. The green line shows the relationship between cumulative rainfall and return period.

Table 5.2: Design storm properties.

Return period	Cumulative rainfall [mm]	Duration	h_{max} [mm/h]
T = 1 yr	30 mm	45 min	80.0
T = 4 yr	53 mm	60 min	104.2
T = 8 yr	68 mm	75 min	108.8
Hurricane	450 mm	24 hr	37.5

Figure 5.9 shows the annual extremes probability distribution. From this relationship, the rainfall cumulatives were estimated for the return periods of 1, 4 and 8 years, which are shown in **table 5.2**. The durations of the design storms were approximated from the durations of the nearest events in *figure 5.9*. The corresponding hyetographs are shown in **APPENDIX 2**.

Digital terrain models

Figure 5.10 compares the DTMs with different resolutions, as well as the DTM by Mücher et al. (2014). The Mücher DTM manages to present the major gullies, but there is a lot of noise halfway up the volcano slope. In comparison, the new Δx = 500 cm DTM has less noise, so that the gullies are presented more clearly. With higher resolution, features such as roads and even rock walls become more clearly visible. Also, the steep slopes of the coastal cliff and the active gullies suffered less from smoothing effects. However, the effects of linear interpolation of large voids in the point cloud (see *figure 4.5*) also become more pronounced, and are most obvious for Δx = 100 cm. The resulting artefacts

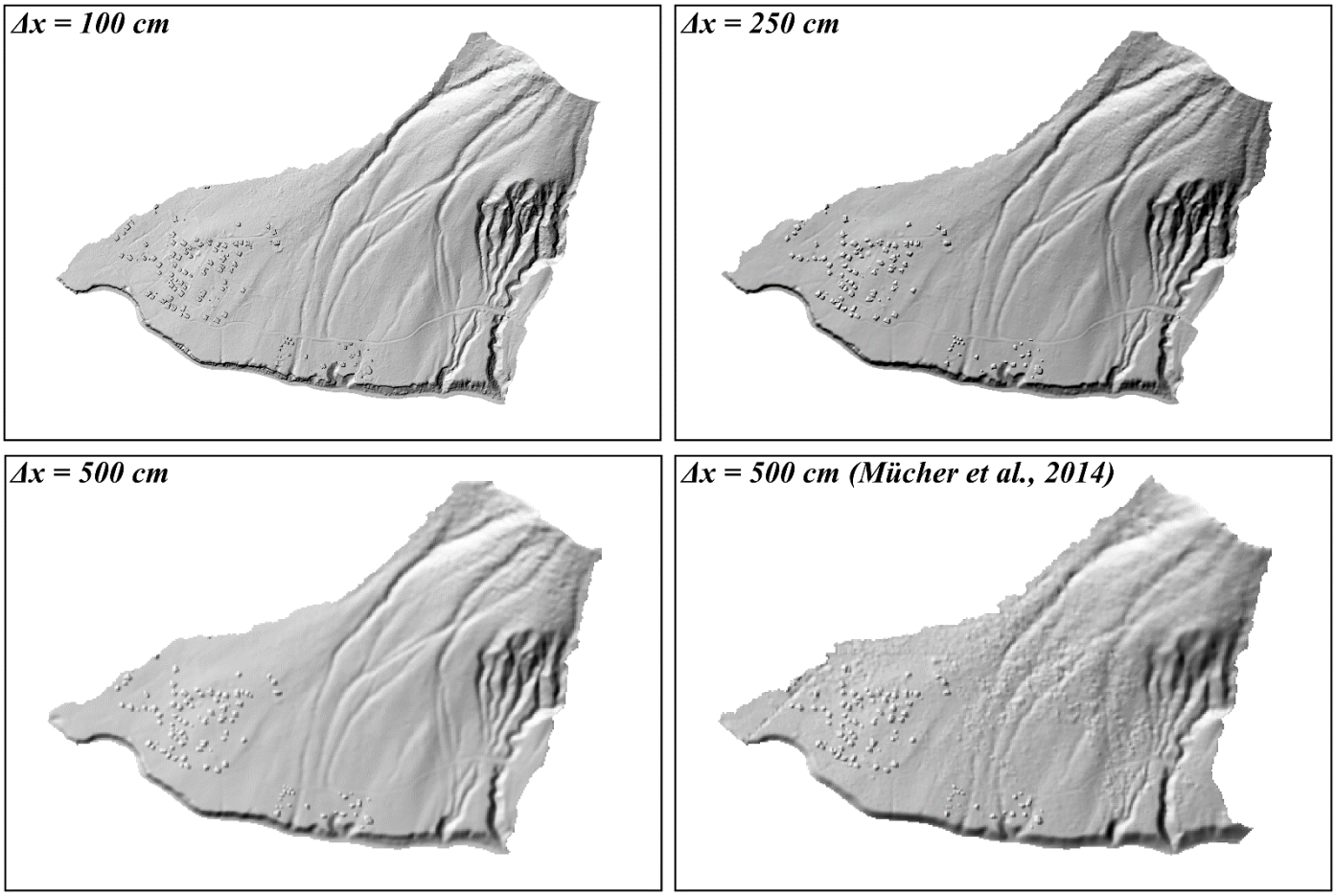

*Figure 5.10: Hillshades of different resolution DTMs. See **APPENDIX 2** for more detailed maps. Compared to the Mücher et al. (2014) DTM, the new Δx = 500 cm DTM has less noise at mid elevations, and the gullies are generally better defined. The finer resolution DTMs suffer less from smoothing effects than the coarser DTMs, thereby allowing for even more detail for gullies and smaller features, such as roads. On the other hand, the finer resolutions relied more heavily on interpolation to close voids in the point cloud, resulting in polygonal artefacts around the crater rim.*

are visible as polygonal planes with alternating uniform slopes. They are primarily present around the crater rim, and to a lesser extent to the north and northeast of the subdivision. This may be better visible on the maps in **APPENDIX 2**.

Canopy storage capacity

The majority of C_{max}-values of the entire study area lie between 1.5 and 3.5 mm, with a mean value of 2.2 mm. As expected, canopy storage capacity is low around built-up areas and the WW-SL outcrop (*figure 5.11*). The limestone outcrop and the area below Weg naar White Wall in general also have less dense vegetation and thus lower interception capacities. The remaining area with dense forests and shrubs has a larger storage capacity, with a mean of 2.5 mm.

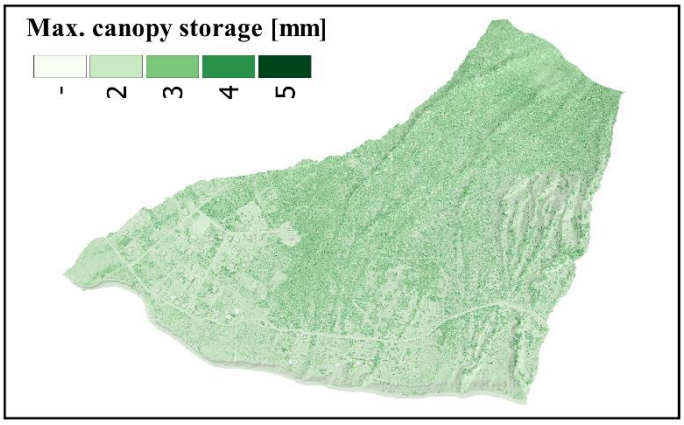

Figure 5.11: Estimated values for C_{max}. Built up areas, the limestone outcrop, and the area below Weg naar White Wall have less canopy storage, as they are mostly covered with grass and sparse shrubs. The rest of the study area is covered by a dense forest canopy.

5.3 Model output

The severity of flooding can be expressed by its spatial extent and the water height, which can be displayed using maps of the maximum water height per cell. These maps are effective for identifying inundated areas, flow patterns and types of flow. They also allow for easy comparison between model runs. The model output is included on a larger size in **APPENDIX 3**.

5.3.1 Effects of model resolution

The differences caused by model resolution are most obvious at the subdivision (*figure 5.12a*) and the active gullies (*figure 5.12b*). In addition, the gully flood waves responded differently, which is illustrated for the culvert of gully 1 (*figure 5.13*). The main features of the default Δx = 100 cm run is discussed first, and are then compared to the coarser resolutions.

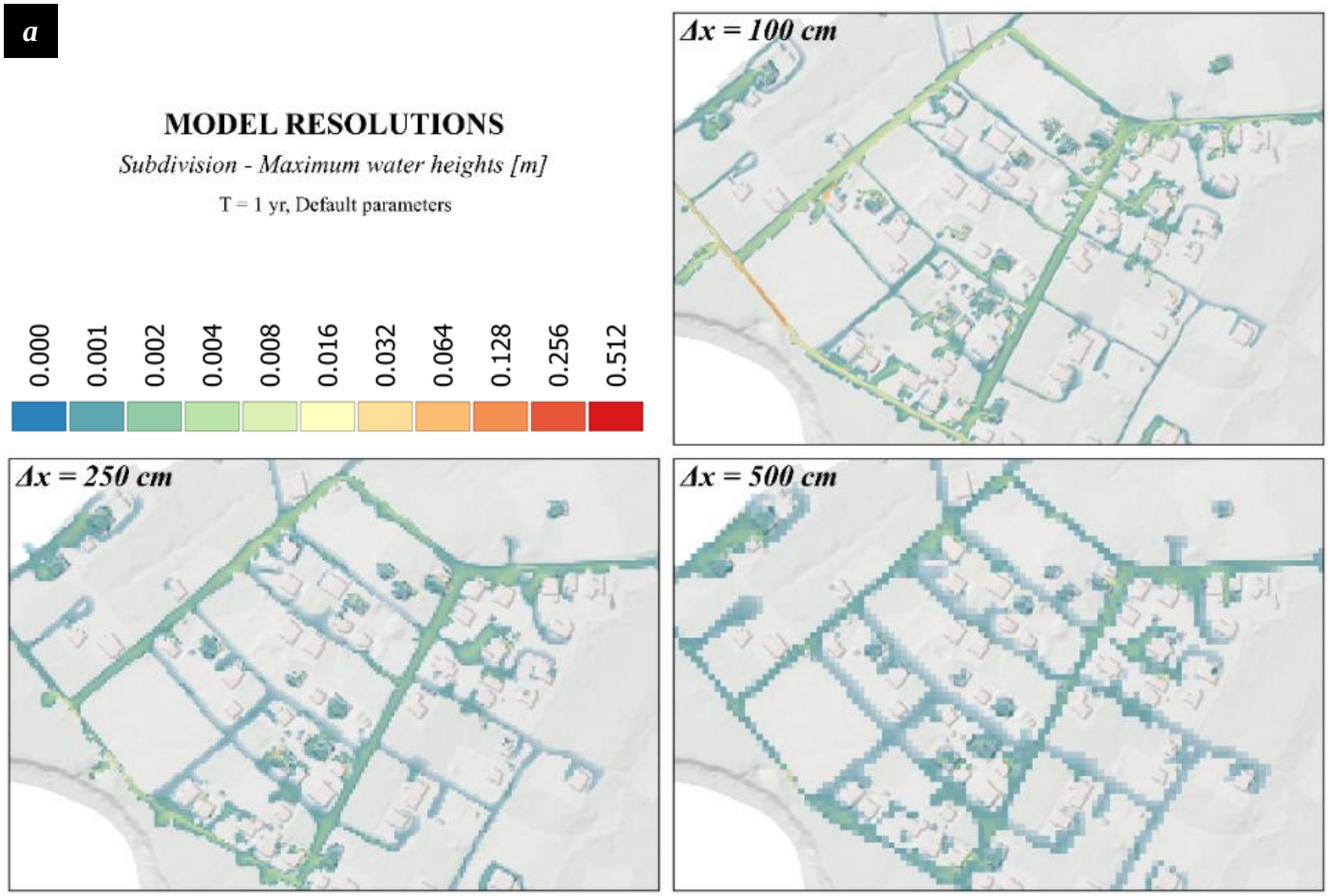

Figure 5.12a: Effects of model resolution. At Δx = 100 cm, there is a shallow sheet flow on Ground Dove Road and Pigeon road, and there is clear ponding on Weg naar White Wall. At Δx = 250 cm, there sheet flow was shallower, but still present, but ponding on Weg naar White Wall was smaller and shallower. At Δx = 500 cm, almost no ponding occurred, and water heights were small in general.

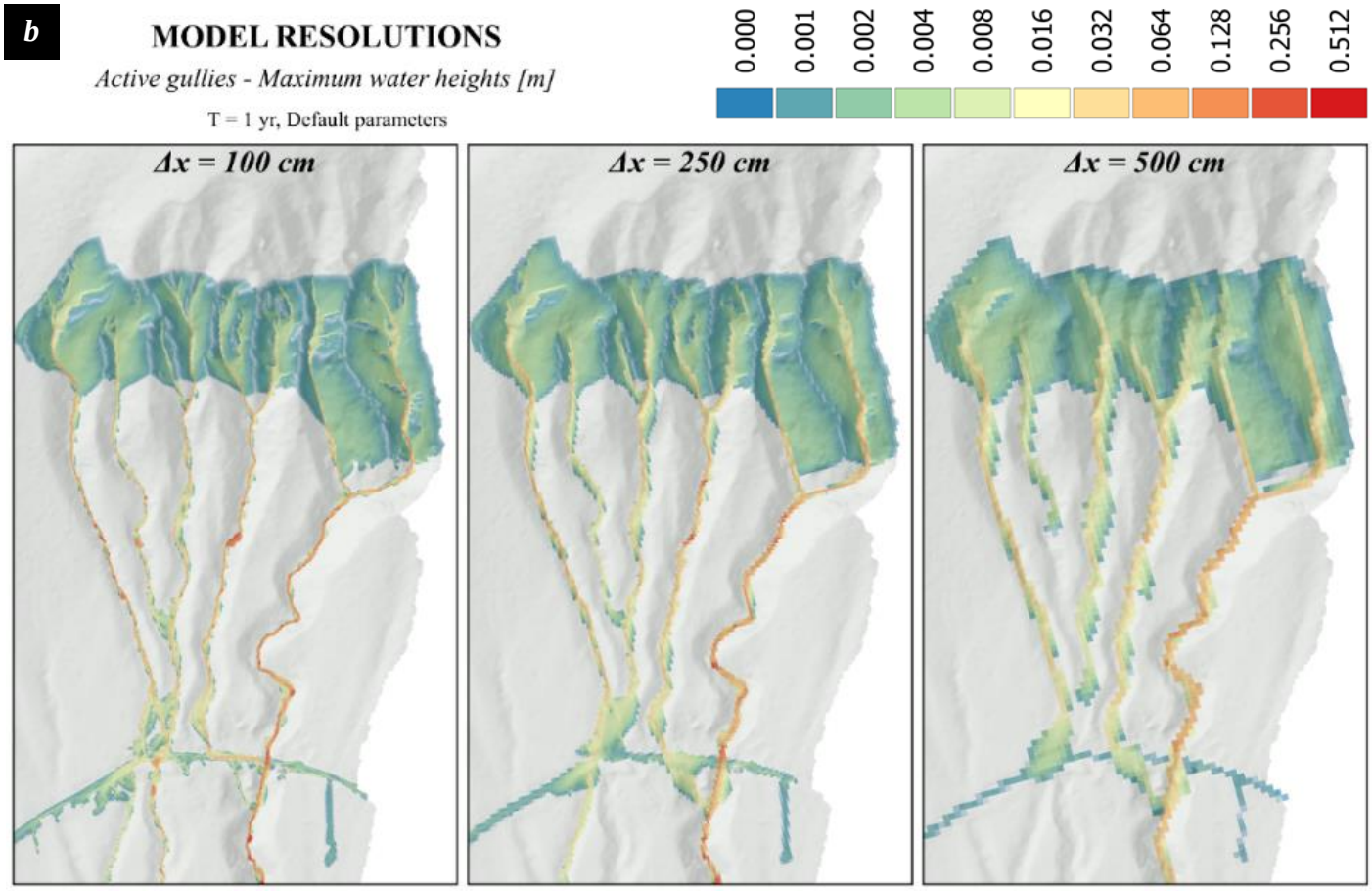

Figure 5.12b: Effects of model resolution. At Δx = 100 cm, the flow through the gullies was quite narrow, except at flat spots in the DTM. At the confluence of gullies, water was allowed to diffuse somewhat. At the intersection between gully 2 and Weg naar White Wall, the runoff is rerouted almost completely towards gully 1. At Δx = 250 cm, the flow in the gullies was slightly wider. The runoff from gully 2 mostly crosses Weg naar White Wall, and very little water is rerouted towards gully 1. At Δx = 500 cm, the flow in the gullies is notably wider. Runoff from some gullies in watershed 3 does not appear to reach Weg naar White Wall at all. Also, water from gully 2 is not rerouted towards gully 1 at all.

Δx = 100 cm

On Ground Dove Road, a relatively deep sheet flow formed, with a depth up to 1.5 cm. This flow was partly contained on the road, but and partly ran over the side. Some of this water appeared to have flowed onto unpaved roads. A large amount of runoff also emerged from unfinished buildings and other structures, and contributed to runoff on unpaved roads. Besides these areas, water heights were generally low on unpaved roads.

At the subdivision, water started ponding between the sides of Weg naar White Wall. Water heights reached up to 10 cm, after which the water spilled over the downslope roadside. Ponding also occurred along other low lying sections (e.g. figure 5.14b).

Flow in the active gullies was for the most part very concentrated and continuous, but there were some flat areas where large volumes of water could accumulate, reaching water heights up to 20 cm. In other flat areas, the concentrated flow was allowed to spread out, as can be seen at the confluences of gullies in watershed 3. The runoff from gully 2 was redirected almost completely over Weg naar White

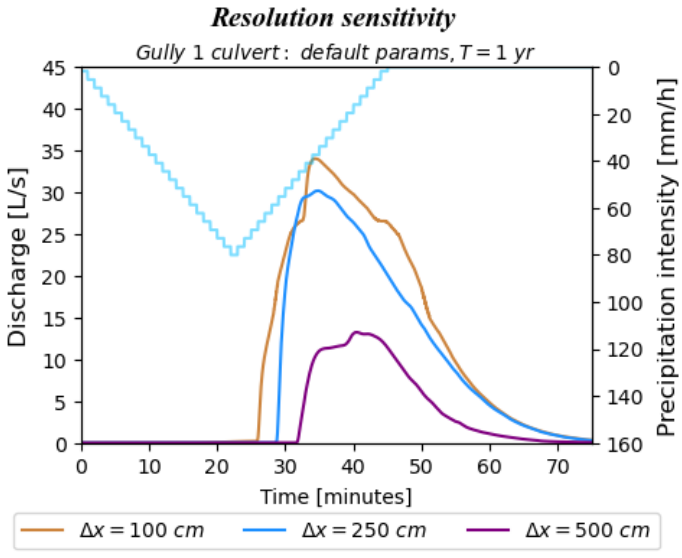

Figure 5.13: Effects of model resolution. For Δx = 100 cm, the initial rise was caused by the flood wave from gully 1, after which the rerouted water from gully 2 arrived and was superimposed on the flood wave of gully 1. The flood wave of Δx = 250 cm was retarded slightly, and there is no visible influence of gully 2. Nevertheless, the peak and total discharge are relatively similar. The flood wave of Δx 500 cm arrived much later, and the peak and total discharge are clearly lower.

Wall towards gully 1. From watershed 3, a small part of the runoff was routed to the west over Weg naar White Wall, but the majority continued downslope, spread over two gullies.

The hydrograph at the gully 1 culvert shows two stages. The first stage was caused by runoff from the upstream area of gully 1. The second stage was caused by runoff from gully 2, that was routed over Weg naar White Wall to gully 1.

Δx = 250 cm

The ponding on Weg naar White Wall covered a much smaller area and had a maximum depth of only 5 cm. Where the water could overtop the roadside, the water spread out much more. The flow over Ground Dove Road was more diffuse, and was generally less deep. The same was true for the runoff from the undrained structures and unpaved roads.

Flow in the gullies appeared comparable in terms of concentration and accumulation in flat areas. However, the spreading between the gullies in watershed 3 was diffuse, and the water was directed towards only one of the two gullies. Also, most runoff from gully 2 crossed Weg naar White Wall, with only a small portion being redirected towards the culvert.

The flood wave arrived more than two minutes later, but reached a similar peak discharge. The lack of a second peak reflects the different flow pattern from gully 2.

Δx = 500 cm

Almost no ponding occurred on Weg naar White Wall, with depths of 2 cm at most. There also were no meaningful water heights on Ground Dove Road or any of the unpaved roads in the subdivision.

The flow in gully 1 was clearly wider, and the water heights were much shallower in general. Runoff from gully 2 and many streams in watershed 3 did not reach Weg naar White Wall at all. Furthermore, the runoff emerging from watershed 3 diffused completely nearing Weg naar White Wall.

The flood wave arrived almost four minutes later compared to Δx = 100 cm, and the peak discharge was remarkably lower than for the other resolutions. The total runoff volume generated from watershed 1 appears to be much lower as well.

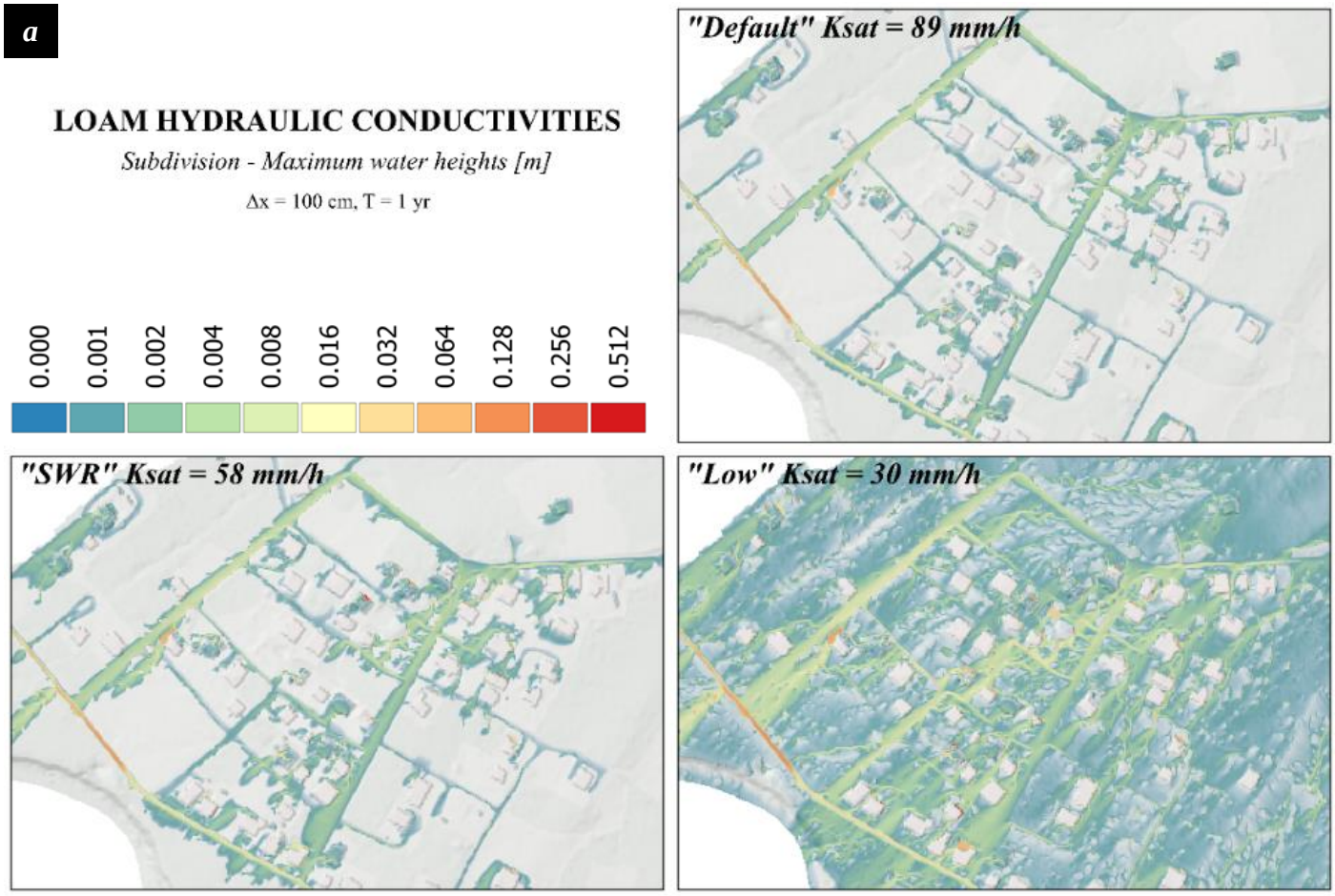

Figure 5.14a: Effects of loam K_{sat}. For "SWR", runoff from roads was able to flow overland slightly further before infiltrating completely. With "Low", small amounts of runoff could be generated well outside the subdivision, and runoff from paved surfaces did not appear to infiltrate much.

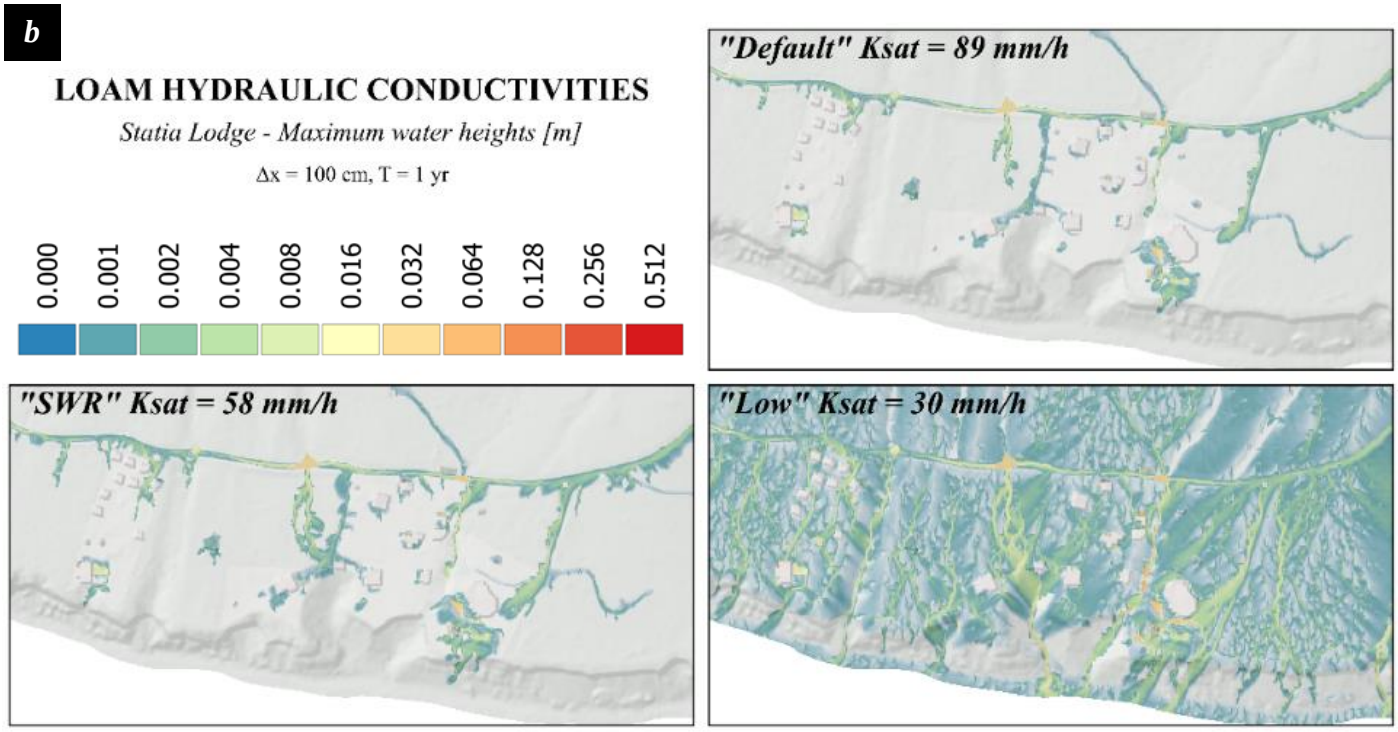

Figure 5.14b: Effects of loam K_{sat}. Between "Default" and "SWR", the difference is again limited. For "SWR", runoff from Weg naar White Wall penetrated downslope areas slightly further. For "Low", runoff was generated on the regular loam topsoil, and runoff from paved surfaces did not infiltrate much.

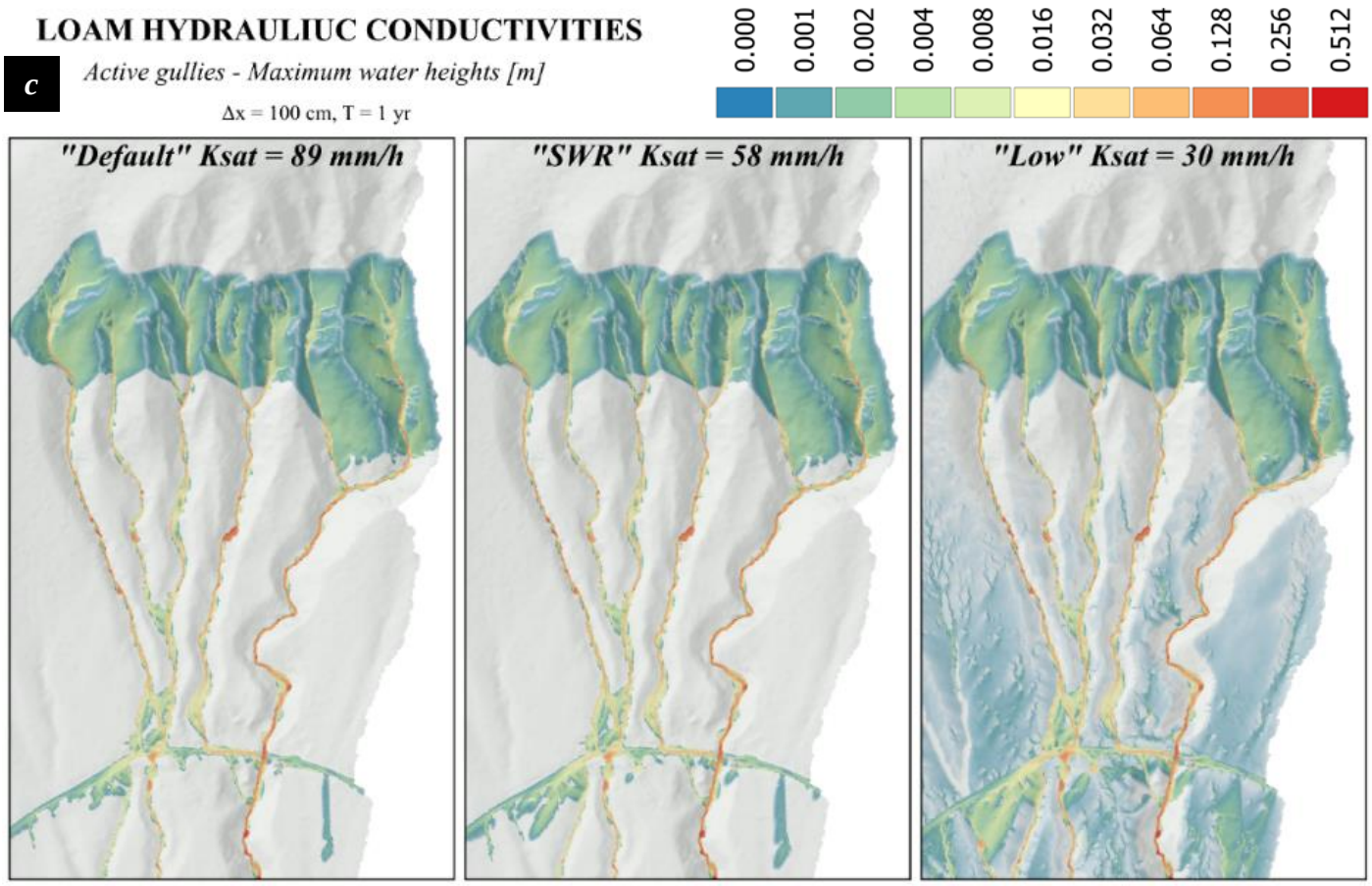

Figure 5.14c: Effects of loam K_{sat}. Between "Default" and "SWR", the difference is again limited. For "SWR", runoff from Weg naar White Wall penetrated downslope areas slightly further. For "Low", runoff could be generated on the less steep areas. Runoff from roads did not infiltrate much.

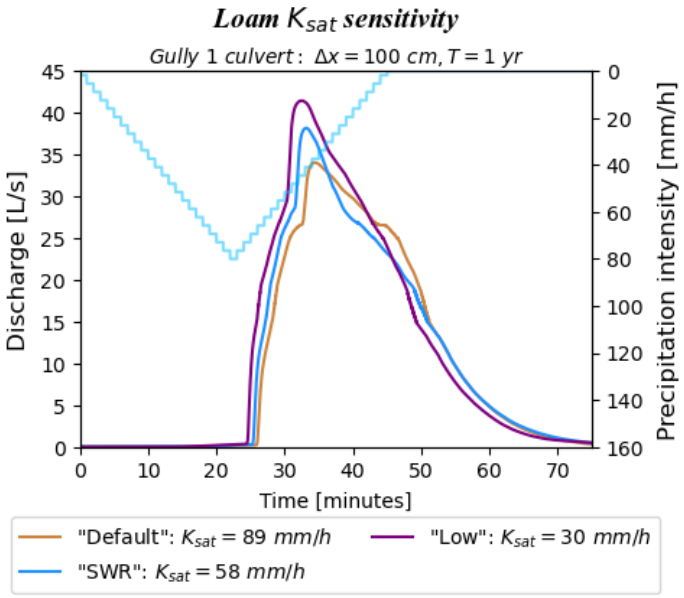

Figure 5.15: Effects of loam K_{sat}. With decreasing loam K_{sat}, the flood wave arrived and peaked slightly earlier, and peak discharge also became higher.

5.3.2 Soil parameter sensitivity

The effects of using different soil parameters is assessed by comparing the results from the model runs with varied soil parameters, but with otherwise the default parameters and design storm (T = 1 yr).

Loam K_{sat}

The effects of different loam K_{sat}-values in the subdivision are again illustrated best by the maximum water heights. The most obvious difference between these scenarios is the widespread runoff generation on the loam topsoil in the "Low" scenario. This did not occur on steep slopes, such as gully sidewalls and at higher elevations. Also, no flooding occurred in the inactive gullies (*figure 5.14b*). Important to note is that the topsoil had not become saturated.

Flooding in the subdivision and around Statia Lodge was much more severe in the "Low" scenario, where the runoff mostly followed the road network (*figure 5.14a*; *figure 5.14b*). The difference between the "Default" and "SWR" scenarios is limited in comparison. Flooding was only slightly more extensive in "SWR".

Runoff that flowed down from the limestone outcrop infiltrated into the loam topsoil, limiting the extent to which it could flow downslope. This flow could extend slightly further with lower K_{sat}-values (*figure 5.14c*). Also, a larger amount of water was drained over Weg naar White Wall towards the west.

The different K_{sat}-values resulted in slight differences in catchment response of the active gullies. *Figure 5.15* shows the hydrographs at the culvert of gully 1. The peak and total discharge increased slightly with a lower K_{sat}, and the flood wave also arrived slightly earlier.

Gully bed sand

The sensitivity of the active gullies' response to the channel sand properties are compared for gully 1 in *figure 5.16*. Despite the large differences in K_{sat}, the effect on the catchment response was quite limited, both in terms of peak and total discharges. Different initial moisture contents had much larger effects on peak discharge. In the first half of the hydrograph, the difference between "V –" and "D +" was minimal, but after the peak, discharge rates decreased much faster for "D +".

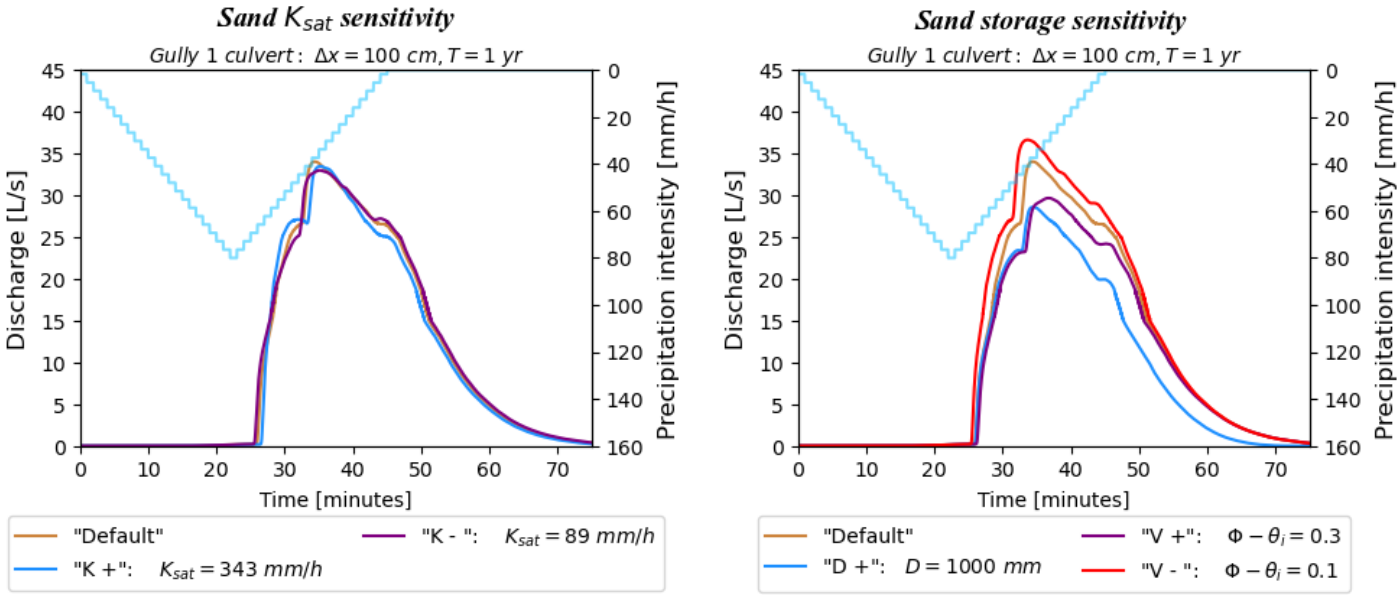

Figure 5.16: Effects of sand soil parameters. Hydrographs at the culvert of gully 1, for model runs with different channel sand hydraulic conductivities (left) and different storage capacities (right). The effects of the different hydraulic conductivities were very limited. In comparison, small changes in initial soil moisture had a much larger effect on peak and total discharge. Initially, the difference between "V-" and "D+" was small, but after the peak, the discharge rate decreased faster for "D+".

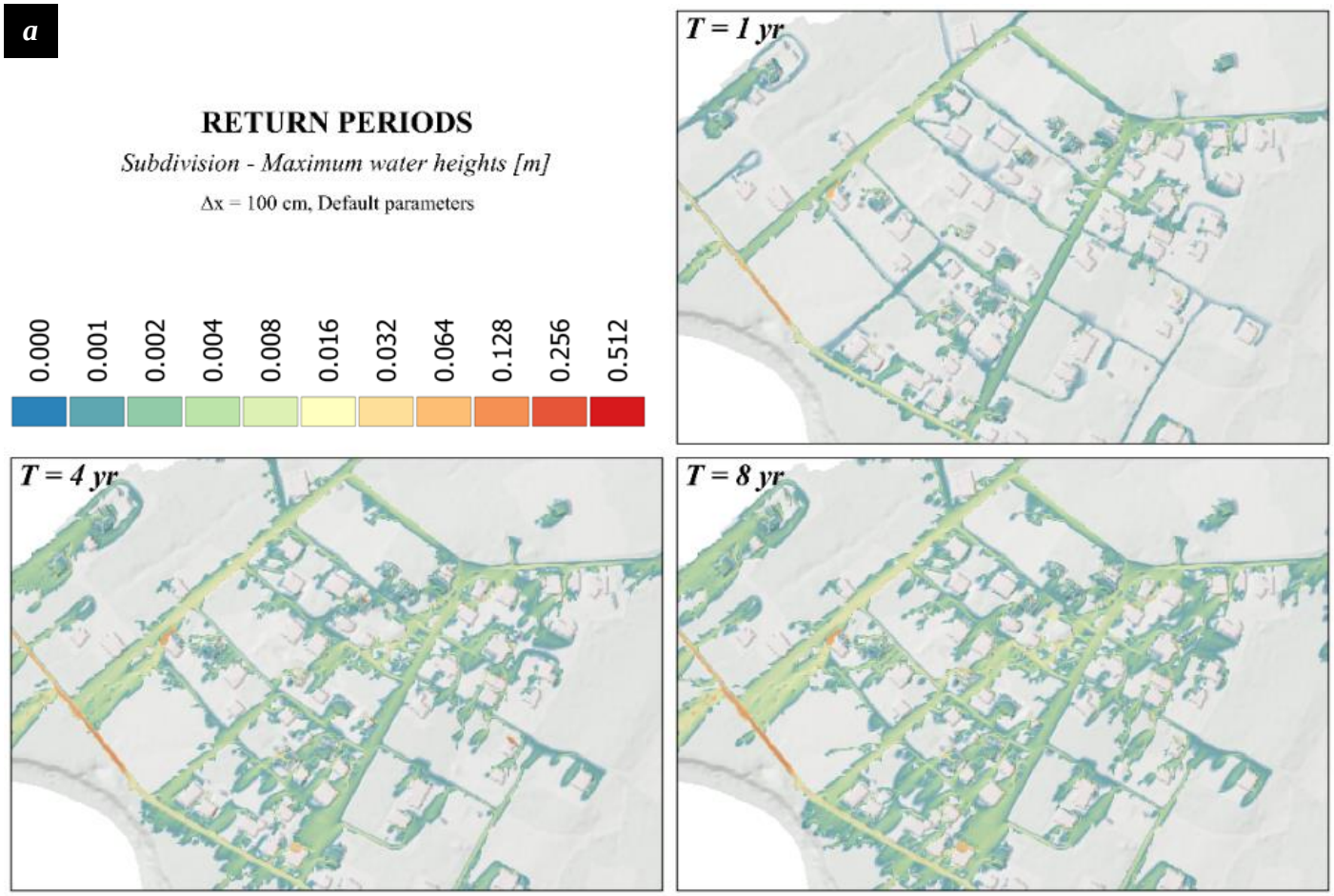

Figure 5.17a: Effects of storm intensity. At T = 4 yr, runoff from paved surfaces could flow further across loam soils before completely infiltrating. Also, more runoff was generated on unpaved roads. For T = 8 yr, this became even more pronounced, to the point that runoff could flow completely across the subdivision. Ponding on Weg naar White Wall did not increase much in depth or extent.

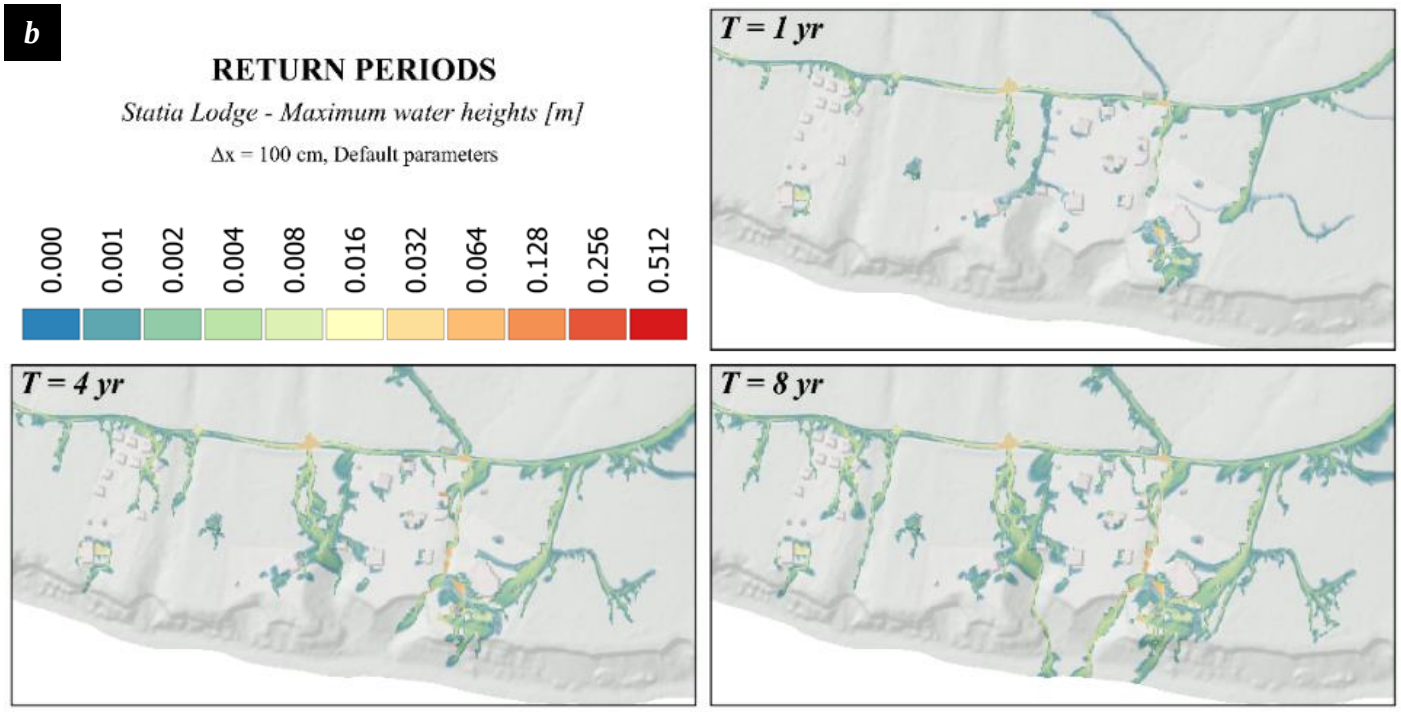

Figure 5.17b: Effects of storm intensity. At T = 4 yr, runoff from Weg naar White Wall was able to flow further across the soil before completely infiltrating. At T = 8 yr, the runoff reached the coast. Ponding on the road did not increase much in depth or extent.

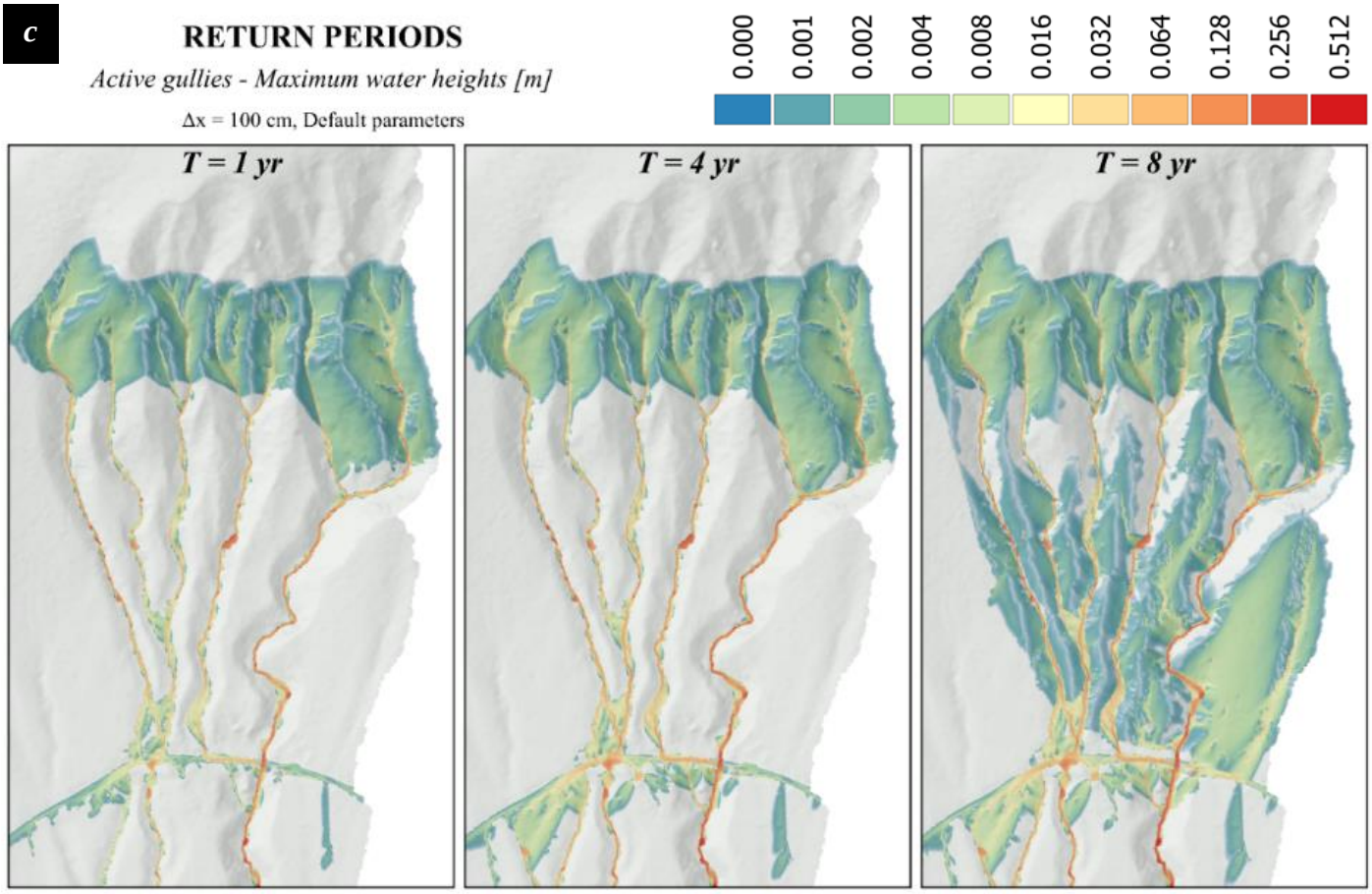

Figure 5.17c: Effects of storm intensity. For T = 4 yr, runoff from Weg naar White Wall could flow further downslope into gullies. For T = 8 yr, runoff was generated on the area around the active gullies when the topsoil became saturated.

5.3.3 Extreme storms

Rainstorms

With more intense rainfall events, flooding became more widespread within the subdivision. Appreciably more runoff was generated on the unpaved roads, to the point that it started to flow in between buildings (*figure 5.17a*). In T = 8 yr, the extent of flooding became comparable to the "Low" K_{sat}-scenario (*figure 5.14a*), but a notable difference is the lack of runoff generation outside of the subdivision.

Around Statia Lodge (*figure 5.17b*), the flooding on Weg naar White Wall did not become much deeper during the more extreme events. Any excess water was drained downslope, with the majority of the water being routed through shallow gullies between properties.

At the active gullies (*figure 5.17c*), the loam topsoil became saturated in the T = 8 yr run. After that, runoff was generated. This is reflected by the second peak in the hydrograph (*figure 5.18*). For more intense storms, greater water heights developed on Weg naar White Wall.

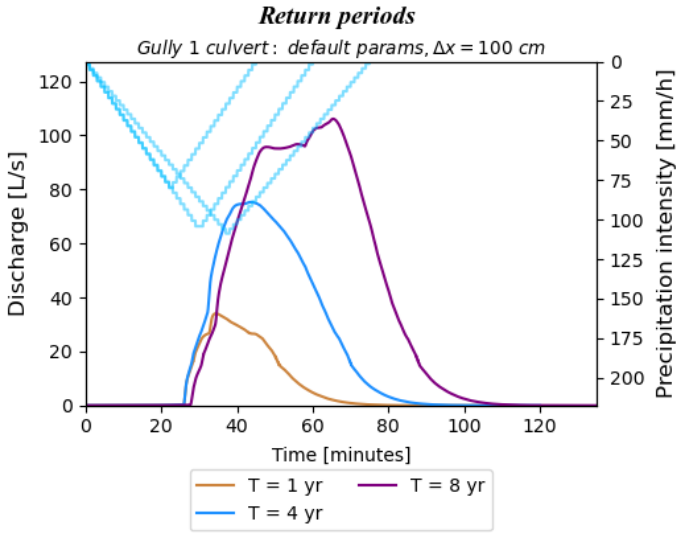

Figure 5.18: Effects of storm intensity. As could be expected, the peak and total discharge increase with storm intensity and duration. For T = 8 yr, a second peak occurred after the loam topsoil became saturated and started to contribute runoff.

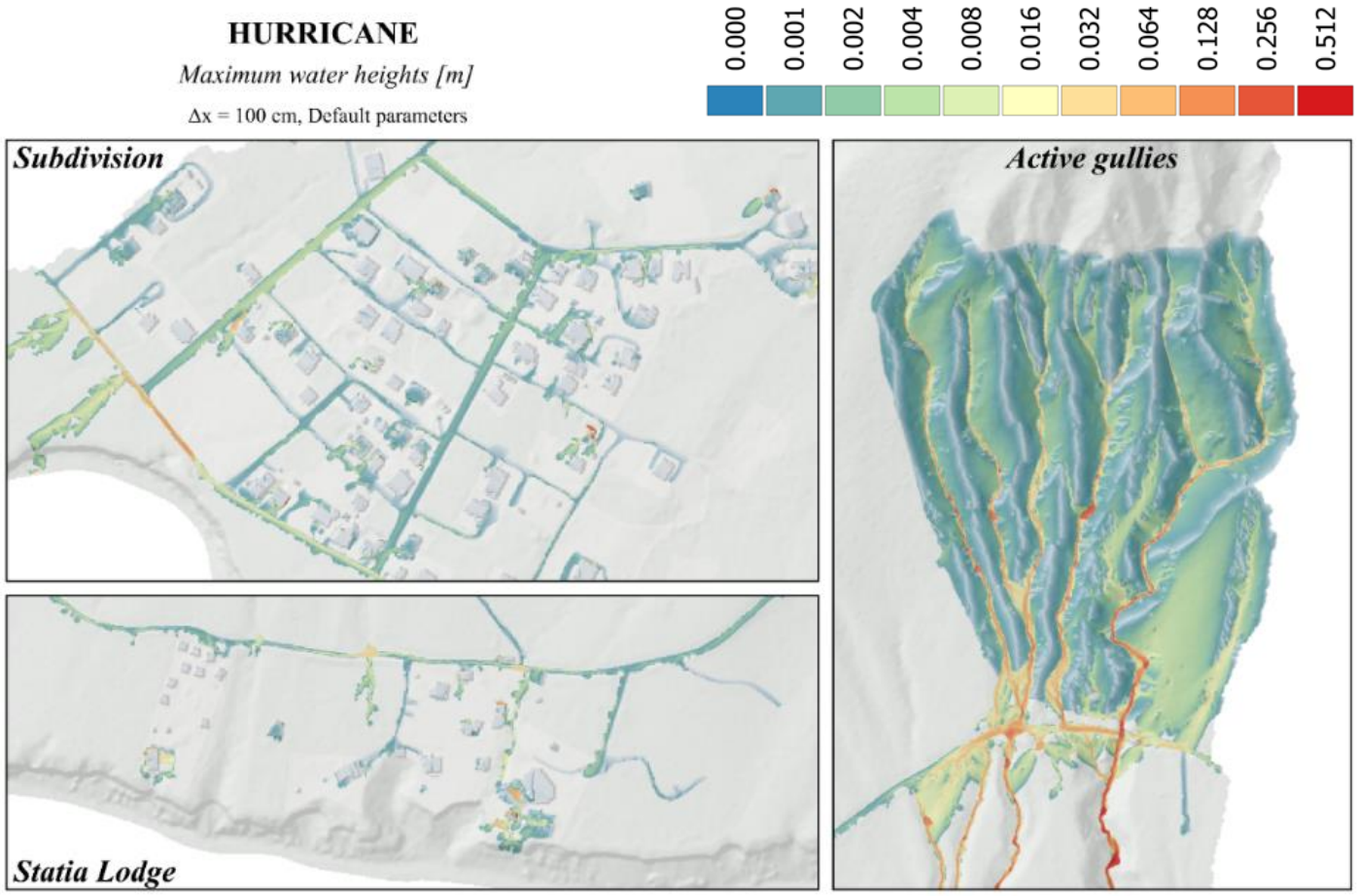

Figure 5.19: Maximum water heights as a result of the "Hurricane" scenario. Around the subdivision and Statia Lodge, the amount of flooding is very similar to T = 1 yr. Around the active gullies, the topsoil became even more saturated that for T = 8 yr.

Hurricane

See *figure 5.19*. In terms of water heights in the subdivision and around Statia Lodge, the hurricane scenario is comparable to the T = 1 yr storm. Evidently, no saturation-excess overland flow had occurred. In contrast, the soil did become saturated around the active gullies. Similar to the T = 8 yr event, the larger area contributed to runoff.

5.3.4 Peak and total discharge

The corrected peak discharges from the active gully watersheds are shown in **table 5.3**. The calculated precipitation excesses for the areas of interest are shown in **table 5.4**.

Table 5.3: Scaled peak discharges at the intersections between the gullies and Weg naar White Wall

Watershed / area	Peak discharge [L/s] at active gully × Weg naar White Wall intersection			
	T = 1 yr	T = 4 yr	T = 8 yr	Hurricane
Watershed 1	259	367	409	386
Watershed 2	91	159	172	170
Watershed 3	132	294	329	388

Table 5.4: Precipitation excesses at areas of interest

Area of interest	Precipitation excess [m³] in area of interest: $P - C - F = H + \Delta Q$			
	T = 1 yr	T = 4 yr	T = 8 yr	Hurricane
Watershed 1	366	751	1 089	13 177
Watershed 2	118	290	417	5 870
Watershed 3	155	468	723	12 439
Subdivision	28	37	78	-1 410
Statia Lodge	-39	-98	-114	-1 627

6 DISCUSSION

6.1 DTM & model resolution

The resolution of the model was in this study limited by the resolution of the DTM. The new Δx = 100 cm DTM was a great improvement over the existing model by Mücher et al. (2014) (*figure 5.10*). There appear to be less artefacts in general. The large voids in the point clouds also did not appear to have had negative effects. This section discusses the effects of the finer resolution on runoff modelling, as well as the remaining limitations.

DTM quality

In real-life, flow paths and ponding are often incidentally or deliberately affected by small surface features. In urban areas, the microtopography can greatly affect flow routing and ponding. For example, curbs and road cross-profiles can cause flow to become concentrated on a part of the road, and can also prevent water from running off to the side. Ozdemir et al. (2013) compared DTMs of different sub-metre resolutions, and found that with increasing cell size, small-scale depressions and flow paths became less pronounced and therefore contained shallower water heights. De Almeida et al. (2018) subsequently found that introducing small changes to the microtopography on roads could drastically alter flow paths, and whether or not ponding occurred in specific areas. The accuracy of modelled interactions between the microtopography and runoff is clearly dependent on DTM resolution.

It is interesting to see that in the Δx = 100 cm models, ponding and flow paths in many cases reflected the field observations, especially when considering that these occurrences were dependent on sub-metre-scale features (elevated roadsides, curbs). *Figure 5.12* shows that larger cell sizes indeed resulted in overall shallower water heights, which suggests that coarser resolutions can lead to an underestimation of flooding. Different resolutions also produced different flow paths. A clear example is where the active gullies intersect with Weg naar White Wall (*figure 5.12b*), which can be linked to the extent to which the curb is represented in the DTMs. This demonstrates in a similar way to De Almeida et al. (2018) that a small difference in terrain height can dictate which area in the model receives runoff and becomes flooded.

The effect of such details also allowed runoff to flow over the roadside more often, where it could infiltrate rapidly into the loams. In reality, runoff would be confined on (un)paved roads by tracks, curbs and walls. This can be seen in the subdivision already for Δx = 100 cm, but was more pronounced for coarser resolutions (*figure 5.12a*). Because most of these roads should drain onto Ground Dove Road and Pigeon Road, these inaccuracies accumulate at the downslope sections of these roads. The severity of flooding in these areas is then underestimated more with increasing cell size.

The differences in DTM resolution have also affected the response of the active gullies. The flow width for Δx = 100 cm and Δx = 250 cm were mostly comparable, while the flow was much wider for Δx = 500 cm (*figure 5.12b*). Evidently, the gully channel is much less clearly defined at this coarse resolution. The rate at which infiltration takes place is not only limited by $K_{sat,}$ but also by the surface area across which it takes place (Van den Bout & Jetten, 2018). Because at Δx = 500 cm the flow was spread over a wider area, it was allowed to infiltrate faster. The peak and total discharges were therefore much lower compared to the smaller cell sizes (*figure 5.13*).

Note that LISEM uses the cell-average water height to calculate flow, and that flow velocities are dependent on water height (**equation 3.6**). As such, the lower water heights caused by excessive spreading of the flow can slow down the propagation of the flood wave (Ozdemir et al., 2013). This most likely caused the delayed arrival of Δx = 500 cm compared to Δx = 100 cm (*figure 5.13*). The delay of Δx = 250 cm is more nuanced. At Δx = 250 cm, the gully bed was relatively flat, whereas the better resolved Δx = 100 cm had a narrow “channel”. In the initial stage of the flood wave, the water height could increase faster within this channel, leading to higher flow velocities compared to the Δx = 250 cm model.

Model resolution

While the accuracy of the modelled flow paths are largely dependent on the quality of the DTM, inaccuracies can also arise from the spatial resolution at which flow is calculated. This is the case when the scale of a flow process is much smaller than the model cell size. This causes the modelled flow to cover a much larger area, which again results in overestimated infiltration. Also, because the cell-averaged water height is lower than in real-life, flow velocities are again underestimated as well. A good example of this is the rill flow on unpaved roads, which typically had a width of decimetres. Even Δx = 100 cm would therefore not have been able to properly represent rill flow, and as such, the severity

of flooding on unpaved roads may have been underestimated. These inaccuracies become more prominent at larger cell sizes, because the flow is spread out even further. The water heights shown in the results chapter should thus be interpreted with care, because a wide and shallow sheet flow in the model might in reality be a concentrated and fast flowing current.

Based on the above, a higher DTM and model resolution would be expected to produce more accurate results in urban areas and narrow gullies, as it is important that the cell size matches the scale of hydrologically relevant features. However, the resolution is often restricted by the limits of the DTM acquisition method, which was in this study the dense vegetation. Also, one should consider that with smaller cell sizes, the vertical accuracy of the DTM becomes critical. For example, De Almeida et al. (2018) argued that systematic errors in the order of centimetres, which can occur even in aerial LiDAR, will unpredictably affect the model outcome.

With regards to the accuracy of the DTM, it is important to note that the new model has not been validated, because no discharge records were available. In addition, many relevant surface features may have been removed because the DTM cell values were based on the lowest cloud points. Using the average height of the cloud points might include the effects of a barrier to the extent that flow is routed accurately. This would however require vegetation to be filtered out to the highest degree, which could not be achieved within a reasonable amount of effort.

Within the limited resolution of the DTM, the inaccuracies imposed on the modelled infiltration and flow velocities could (to some extent) be remedied by calibrating the K_{sat} and manning's n, respectively (Van den Bout & Jetten, 2018; Ozdemir et al., 2013). For future research, it may therefore be interesting to collect discharge data and perform a validation.

6.2 Model performance

Infiltration in freely drained loam

Figure 5.14 showed that for T = 1 yr, runoff could only be generated in the "Low" scenario, at least according to the Green and Ampt model (**equation 3.4**). It appears that a value of 30 mm/h is on the tipping point, beyond which Hortonian overland flow could occur. This is shown by the lack of runoff on steeper terrain, such as gully sidewalls and at higher elevation (*figure 5.14c*). This is because steeper terrain received less rainfall per surface area.

In the active gullies, the "SWR" and "Low" scenarios resulted in higher peak discharges (*figure 5.15*). This was because infiltration in the loam downslope of the outcrop and in the floodplains was initially lower compared to the default. As a result, the loams around the outcrop became saturated faster in the default. When the peak of the storm had passed, "Default" infiltration rates around the outcrop were smaller, which is why the discharge rate decreased less rapidly compared to the other two scenarios.

Assessing the validity of the topsoil loam K_{sat}-values is difficult, because only a T ≈ 1 yr event was witnessed on 9 January 2023, and surveys of the wider area were only conducted after the event. In addition, no traces were found that water flowed from upslope onto Banana Quit Road and Pigeon Road. These observations are in disagreement with the "Low" scenario (*figure 5.14a*). A K_{sat} of 30 mm/h may thus be too low for the majority of the study area. However, such low K_{sat} may be present locally.

Further statements about whether the "SWR" or the "Default" scenario is more valid, cannot be made, but should be subject to further study. Which value is used, appears to have little effect on the subdivision in the case of a T = 1 yr storm. For a more intense storm, the difference may greatly increase if the "SWR" scenario also reaches the tipping point for Hortonian overland flow. The loam K_{sat} also slightly affects peak discharges from the active gullies (*figure 5.15*).

Infiltration in channel sand

The effects of different sand K_{sat} values is relatively limited (*figure 5.16*). With a higher K_{sat}, the propagation of the flood wave was slightly slower, but the sand also became saturated faster. This caused the wave front to become steeper, which is why the discharge of "K+" was highest for a brief period. After the peak of the peak of the hydrograph, infiltration again affected runoff volumes. This occurred at a higher rate for higher K_{sat} values, which is why discharge rates decreased faster. The peak and total discharge do not appear to differ much.

The storage capacity of the sand is much more important (*figure 5.16*). When the sand was almost saturated ("V–"), the flood wave was allowed to propagate much faster, and with a smaller loss of runoff volume. This caused a higher peak discharge. The opposite was true when the sand was drier ("V+"). The increased depth of the sand had the largest effect, which became most apparent after the peak of the hydrograph. The storage capacity in the "D+" scenario was much larger than in the "V+"

scenario (200 mm compared to 90 mm). The deeper sand could therefore cause a much larger reduction in total discharge.

The used values for K_{sat} and θ_i represent the possible range of values quite well, so larger differences than shown in *figure 5.16* are not expected. The soil depth may however be deeper than 1 metre. Because the catchments are so sensitive to soil depth, this can be a major source of uncertainty

Interception & surface storage sensitivity

In LISEM, canopy interception is a function of cumulative rainfall (**equation 3.2**). It reduces the amount of rainwater that reaches the soil only in the initial stage of an extreme rainfall event, but it does not affect the peak intensities. The effect on Hortonian overland flow will therefore be limited. In case the main cause of runoff is Dunian overland flow, interception could theoretically affect total runoff. Saturation could however only occur at the active gullies, and only after an extreme amount of rainfall (T = 8 yr or hurricane). Moreover, the vegetation cover in this area was relatively limited.

Finally, the events that lead to problematic runoff are quite extreme. The volume of water that can be stored by the canopy and on the surface are limited compared to the cumulative rainfall of these events. When assuming the mean C_{max} of the dense vegetation (2.5 mm), this only accounts for 8.3%, 4.7%, 3.7% and 0.6% for the 1 yr, 4 yr, 8 yr and hurricane scenarios. It can therefore be argued that the accuracy of vegetation cover, *LAI* and *rr*, as well as the validity of the interception and surface storage models, were of limited importance to the performance of the model.

6.3 Flood propagation and hazards

Subdivision

The models indicate that runoff in the subdivision (*figure 5.17a*) originated readily on the impermeable surfaces. The relative importance of unpaved roads became larger with more intense storms, as peak intensities further exceeded potential infiltration rates. For none of the design storms did runoff occur on the loam topsoils around the subdivision. Because only a limited amount of water entered the subdivision from outside, it can be concluded that the vast majority of the runoff is generated locally.

An important part of overland flow was captured by roads parallel to the elevation contours. Subsequently, the runoff was mostly conducted out of the subdivision over perpendicular roads. It can be concluded that the road network increased the drainage density, which is a known phenomenon in urban areas (Hollis, 1975). The flow concentration seems to have resulted in more discharge over Yellow Bird Road in particular. The rapid runoff led to deep ponding on Weg naar White Wall. This was further facilitated by the shallow gradient, the elevated grass verges and a lack of outlet points.

While the models indicate abundant flow through the subdivision, water heights remained low for all return periods. The buildings are thus at little risk to flooding. However, runoff concentration and rill erosion can cause major damage to unpaved roads (Ramos-Scharrón & MacDonald, 2007). Risk factors for erosion are a large catchment area and a steep road gradient (Zhang et al., 2019). Yellow Bird Road may therefore be especially at risk. More severe damage can be expected as a result of more intense storms.

As discussed in previous sections, infiltration within the subdivision may have been overestimated. The precipitation excesses shown in **table 5.4** may thus be an underestimation.

Statia Lodge

Runoff in this area was generated primarily on Weg naar White Wall, with little runoff originating from the properties themselves (*figure 5.17b*). This can be attributed to the general absence of impervious pavements. In addition, almost all structures had drained roofs, and the terrain had no steep slopes. Again, no runoff originated from the loam topsoils, but rather allowed for infiltration. The infiltration of water from Weg naar White Wall explains the overall negative precipitation excesses in this area (**table 5.4**). The remaining runoff mostly flowed into shallow gullies, thus posing little hazard to buildings.

Active gullies

The impermeable limestone outcrop showed immediate response in the beginning of rainfall events. In the initial phase of a storm, water could only infiltrate in the area below the outcrop. Infiltration decreased as the gully channels gradually became saturated. For the T = 1 yr and T = 4 yr design storms, the outcrop remained the only source of runoff. During the T = 8 yr and the hurricane scenarios, runoff was generated on the loam topsoil at some point (*figure 5.17c*; *figure 5.18*)

Flooding of the gullies occurs on average *at least* once a year (T = 1 yr), so the sediment deposits will also occur at least once a year. For more intense storms, the sediment will spread out further along the road. Other damages to the road will likely be limited.

6.4 Measures

Weg naar White Wall

In the short term, ponding on Weg naar White Wall can be easily reduced by lowering the roadsides along the downslope side. This will allow water to run off the road along its entire length. Outlets can also be dug in the roadside along sections that frequently experience flooding, though the outflow should be managed properly. Because the road collects runoff from large areas, most notably the subdivision, the concentrated discharge from these outlets can cause erosion if not properly managed (Nyssen et al., 2002). The water from these outlets can be collected in roadside infiltration pits (e.g. *figure 6.1c*).

Figure 6.1: Some existing water management applications on Sint Eustatius. a. Infiltration pit at the side of an unpaved road; b. A linear drain followed by a speed bump. It discharges directly into an infiltration basin; c. A roadside storm drain; d. Large infiltration basin; e. Runoff storage facility; f. Small bioswale / infiltration basin. These photos are also included in ***APPENDIX 4****.*

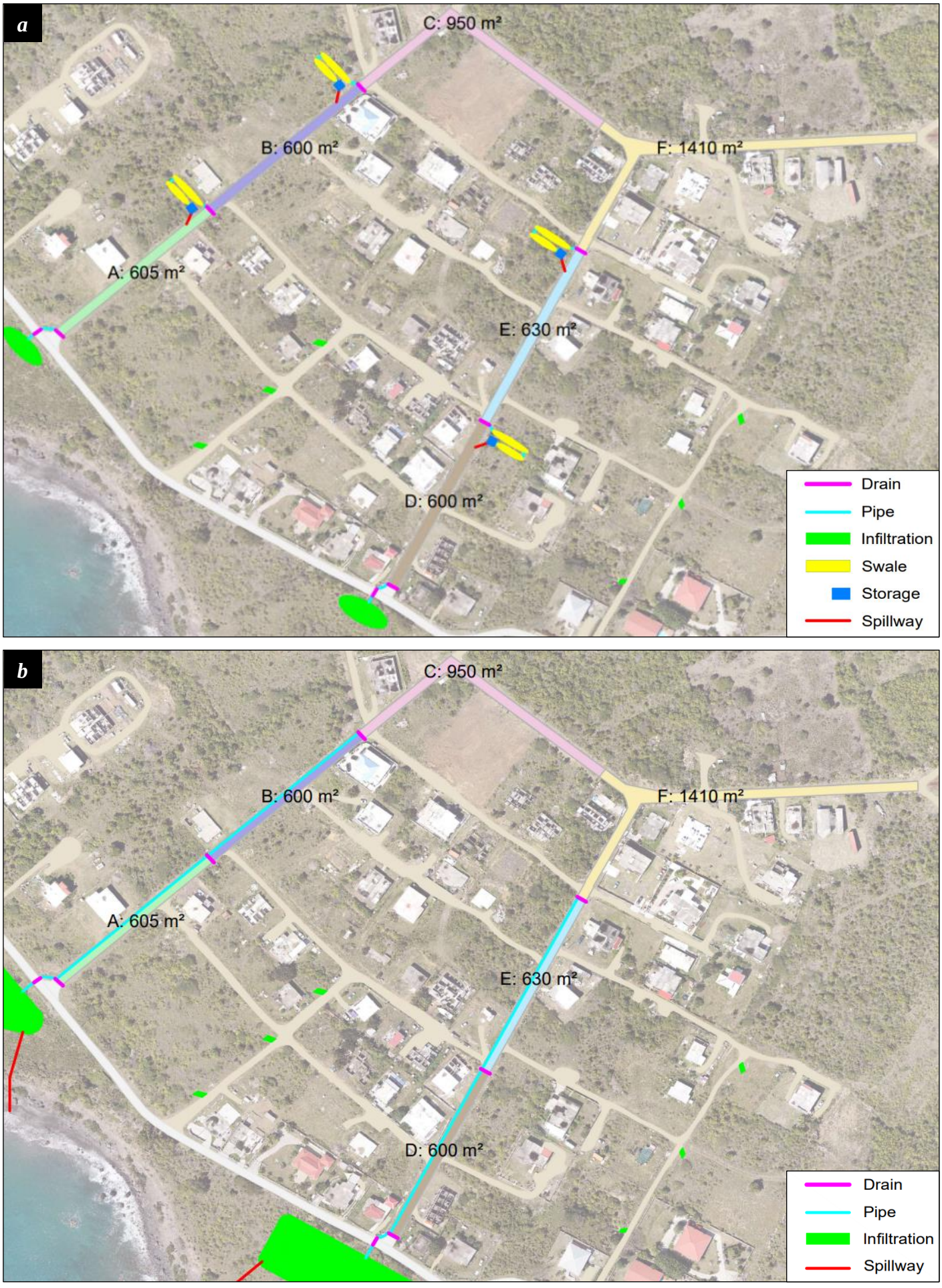

Figure 6.2: Paved roads of the subdivision, divided with several sections. Surface areas are indicated per section. a. Layout with several storages throughout the area; b. Drainage layout with two large infiltration basins at the base of the slope. These maps are included on a larger size in ***APPENDIX 4****.*

Subdivision

Measures should be aimed at managing runoff on the roads. An obvious approach would be to install drains. These can again be roadside infiltration pits (e.g. *figure 6.1a*), drains at the side of the road (e.g. *figure 6.1b*), or linear drains that span the entire width of the road (e.g. *figure 6.1c*), which could furthermore be combined with speed bumps to increase its effectiveness. Discharge from paved roads onto unpaved roads should be prevented. This can be done by lining the paved roads with (mountable) curbs. However, runoff and sediment will still be allowed to flow from unpaved roads onto the paved roads.

Table 6.1: Required storage capacity per section for T = 1 yr (30 mm total rainfall).

Section	m^3
A	18
B	18
C	29
Sum	65

Section	m^3
D	18
E	19
F	42
Sum	79

These measures will effectively divide the catchments in several subcatchments. Peak discharge and flow velocity will then be lower, resulting in less erosion and sediment nuisance from unpaved roads, and it will also alleviate flooding on Weg naar White Wall.

It makes sense to direct the water to infiltration basins (e.g. *figure 6.1d*) spread throughout the subdivision. At the time of the fieldwork, there were numerous empty lots that could be used for this (though it is unknown if these were already assigned for housing). This would negate the need for an extensive drainage system. However, the steep slopes make the area unsuitable for constructing very large basins without using reinforced embankments (Woods-Ballard et al., 2007). More advanced constructions, such as large dry wells or storage facilities could be considered (*figure 6.1e*; *figure 6.2a*). These can be constructed to allow a greater water depth, thus providing more storage within a smaller footprint. They can be emptied gradually through infiltration or pumping.

If runoff is collected from unpaved roads, the basins should be preceded by some form of pre-treatment structure that will reduce the inflow of sediment. Pre-treatment can for example be achieved with swales (e.g. *figure 6.1f*), which receives the raw stormwater from the drainage system, and passes it to the storage facility. When oriented parallel to elevation contours, the gradient will be shallow, resulting in lower flow velocities. On the same lot, multiple adjacent swales can be connected in series (*figure 6.2a*), similar to some proposed measures in Royal HaskoningDHV (2018).

An alternative to local basins would be to construct a larger drainage system, consisting of trenches and/or pipes next to or below Ground Dove Road and Pigeon Road. The water can then be channelled to a large infiltration basins (e.g. *figure 6.1d*) that can be constructed on fields with a gentler slope (*figure 6.2b*). This approach would however require more substantial earth- and roadworks.

With these measures, the runoff will be contained on the paved roads. Moreover, the runoff received from other areas will be limited, at least for T = 1 yr events. The total runoff that will be generated is proportional to the surface area A_{road} of the pavement:

$$R = P \cdot A_{road} \qquad \textbf{(6.1)}$$

For the road sections, the required storage space for one single T = 1 yr event would for example be:
Note that for more intense storms, the required capacity will not increase linearly with total rainfall if widespread Hortonian overland flow starts to occur.

Active gullies

The current sediment nuisance that is experienced on Weg naar White Wall are caused by the uncontrolled discharge from gullies 2 and 3. It is evident from gully 1 that a culvert will prevent sediment from accumulating on the road. Culverts can also be considered for watersheds 2 and 3 (*figure 6.3*; *figure 6.4a*). This would respect the natural gully courses that existed prior to the construction of Weg naar White Wall. Alternatively, gullies 2 and 3 can be diverted towards gully 1, prior to the intersection with Weg naar White Wall (*figure 6.4b*).

Modifying the courses of the gullies should be done with caution. Changes to the water budget or gradient of a gully can cause an increase in its erosive activity (Kirby & Bracken, 2009). At the intersection with Weg naar White Wall, the beds of gullies 2 and 3 lie around 1 metre higher than the road surface. In the field, it was already apparent that the gullies had been incising towards road level to some extent. If the gullies are to pass through culverts under the road, the height difference will become even greater. If no further measures are taken at the upstream end, this can give rise to major incision of the gullies. In the long term, this will result in increased side- and headwall erosion in the entire upstream sections of the gullies.

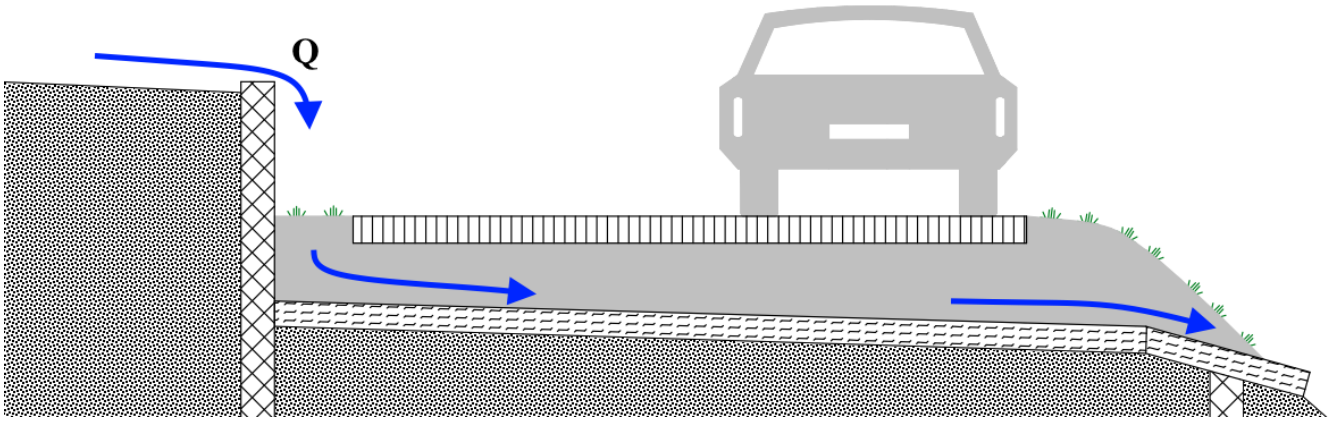

Figure 6.3: Cross-section of a culvert under Weg naar White Wall for gully 2 or 3. The culvert can be a covered design, such as the already existing culvert in gully 1. Alternatively, the watercourse can be covered with a removable grate (see figure 6.1b) that allows for road drainage, as well as easy inspection and maintenance. A retaining wall will prevent the water from cutting into the soil as it flows towards road level. This allows the current gully profile to be conserved. The outlet should be protected against undercutting.

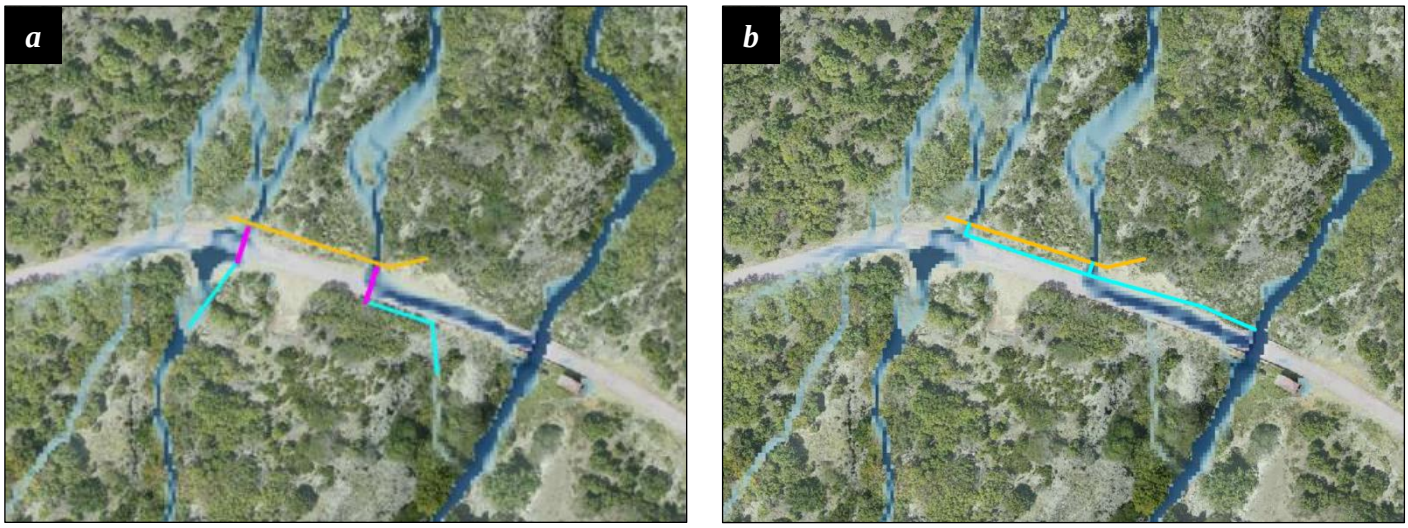

*Figure 6.4: Possible drainage layouts fort the active gullies. a. Two new culverts below Weg naar White Wall for gully 2 and gully 3. A retaining wall at the upstream side should prevent runoff from circumventing the culvert. Protected outlets guide the runoff towards the downslope gully sections; b. Rerouting towards gully 1. A retaining wall concentrates the runoff towards channels that guide the water to the culvert of gully 1. These maps are included on a larger size in **APPENDIX 4**.*

Diverting both gullies through the same culvert as gully 1 is also not without risk, because this will increase the peak discharges in the downstream end of gully 1. This can also cause further incision and activation of the sidewalls. In any case, one must be aware that discharge from culverts is strongly concentrated, and if not controlled properly, it may over time undercut the road at the downstream end.

Gully erosion can be prevented to a large extent with check dams (Frankl et al., 2021). This is especially necessary where gullies 2 and 3 will enter their culverts / channels, and can be achieved with retaining walls (*figure 6.3*). In the downstream sections of a gully, a large infiltration basin can be created using a single dam. This will ultimately prevent the majority of sediment from reaching the marina park, and has already been done in other gullies on the island (e.g. *figure 6.5*).

The required dimensions of the culverts must be appropriate for the peak discharges (**table 5.3**).

*Figure 6.5: Large infiltration basin created inside a gully. Erosion by inflowing water is controlled with a geotextile. A spillway is installed in the dam at the downstream end of the basin. This photo is included in **APPENDIX 4***

The required storage volumes for infiltration basins are shown in **table 5.4**. The performance of any of these proposed measures can only be guaranteed with proper maintenance (clearing of vegetation, debris and sediments).

It may not be possible to create enough storage capacity to process the most extreme storms, nor is it reasonable to expect this (see hurricane). Besides extreme storms, the possibility of multiple large storms occurring in rapid succession should also be considered. If this happens, the storages may not have been emptied sufficiently to process the following storm. Finally, it should be noted that the peak and total discharges in **table 5.3**, **table 5.4** or **table 6.1** are subject to some uncertainties and considerations, which are discussed in the next section. In any case, it is justified to use a generous factor of safety when specifying the required discharge and storage capacities. In addition, any storages should be fitted with emergency spillways in case of overloading (*figure 6.2*).

6.5 Uncertainties

Infiltration

Infiltration is the most important sink in the water balance (**Table 5.4**). The most important shortcoming with regards to K_{sat} is the lack of spatial variability, especially when considering how common SWR was. In addition, SWR can also vary throughout the year, depending on the soil moisture levels (Doerr et al., 2000). After all, the infiltration measurements were conducted during the dry season (see Meteorological Department Curaçao, 2023).

While lower K_{sat} were used for unpaved roads, no actual measurements have been done. Also, no measurements have been done on private properties in the subdivision. As such, the effects of soil compaction are not known. Because these LULC types cover the majority of the subdivision, this introduces major uncertainty at what point overland flow will occur.

The infiltration capacity of the topsoil should be further assessed, especially within the subdivision. When infiltration basins are to be installed, the infiltration capacity of the subsoil should be further assessed as well. In this study, the subsoil was assumed to have exceptional drainage properties. While this may be true for the majority of the volcanic deposits, a small confining layer could affect percolation rates through the entire column by creating a perched groundwater table. This might especially be relevant for events with a large total rainfall, such as a hurricane, as it increases the chance of saturation-excess overland flow. On a smaller scale, more accurate methods can be used, such as the double ring infiltrometer or the inverse auger-hole method.

Active gullies

The WW-SL outcrop was the most important source of runoff, and the volume will be directly related to the impermeable surface area. In this model, the outcrop was defined by the easily visible limestone area. However, the succession also consists of dark sandstones and conglomerates (Roobol & Smith, 2004). The impermeable area is likely larger, thus the peak.

On the other hand, the soil depth was also estimated, but a topsoil depth of 30 cm is likely a minimum. The sensitivity analysis showed that a larger storage capacity of the sand will decrease peak and total discharge to some extent. Also, a larger depth of the loam will delay or prevent saturation-excess runoff in this area. Literature regarding the WW-SL succession is focussed mostly on the actual White Wall and Sugar Loaf formations. The cross-section in *figure 5.2* was based on a more or less constant inclination of the rock layers. It is however likely that the strata are deformed to some extent. To more accurately model runoff in this area, the geology of the WW-SL should be researched further, and actual topsoil depths should be measured.

Rainfall

The triangular hyetographs do not include the very high peak intensities that have been recorded in real storms (e.g. *figure 5.8*). The model also did not take any spatial variability into account. For example, more rain likely falls at higher elevations (MacRae & Esteban, 2007). The amount of Hortonian overland flow may thus have been underestimated.

With a changing climate, very intense rainstorms may be expected to become more frequent, although climate models so far are undecided about the effects on small Caribbean islands (Avila-Diaz, 2022).

7 CONCLUSIONS

The Caribbean island of Sint Eustatius ("Statia") frequently experiences extreme rainfall. The resulting flash flooding disrupts daily life, damages infrastructure, and may be a long-term hazard to the island's economy and ecology (*figure 1.2*). To study flooding, rainfall-runoff models were run using the numerical model "LISEM" for a study area on the southwestern slope of the Quill volcano (*figure 1.1*). The main objectives were to:

- assess the effects of using a higher resolution on the model's performance;
- identify the main contributing factors to flooding in the study area;
- assess the severity of flooding for different return periods and a hurricane scenario;
- propose measures to reduce the negative effects of flooding.

A major effort was put into creating a new input dataset, which consisted of:

- A new DTM with a cell size of 100 cm. In terms of resolution, this was an improvement compared to the previously available DTM;
- A soil map with the major classes "Statia loam", "channel sand" and "histosol". Their hydraulic conductivities were determined to be 89, 134 and 58 mm/h, respectively. Compacted soils and rock outcrops were included as well.
- LULC and vegetation cover maps. The canopy storage capacity ranged mostly between 1.5 and 3.5 mm, and had an overall mean of 2.2 mm.
- Design storms for return periods of 1, 4 and 8 years, as well as a hurricane, which had total rainfalls of 30, 53, 68 and 450 mm, respectively;

Effects of resolution

The effects of using different resolutions was assessed by comparing model runs with cell sizes of 100 cm, 250 cm and 500 cm.

The higher resolution DTM provided greater detail of the gullies, and also better represented the effects of small-scale features, such as roadsides and walls (*figure 5.10*). These features sometimes redirected modelled flows (*figure 5.12*), which could dictate if runoff would largely infiltrate into the soil, or if it would contribute to inundation of sensitive areas. However, the 100 cm cell size was still too coarse to reliably resolve many small-scale features, so the accuracy of flow patterns in urban areas in particular would benefit from even smaller cell sizes.

The cell size also affected the width of flows. This was in part because a higher resolution DTM could better represent small channels, but also because the minimum flow width in LISEM is limited to the width of one cell. The spreading of flow over a wider area decreased water heights and flow velocities, and increased infiltration. For larger cell sizes, this resulted in slower propagation of flood waves, as well as lower peak and total discharges (*figure 5.13*). Excessive spreading was also relevant for the 100 cm cell size, as this was too coarse to model flow through narrow rills in unpaved roads.

Contributing factors

In the subdivision, the most important source areas were ***impervious roads*** and ***pavements***, and to a lesser extent, the unpaved roads with compacted soils. Most structures did not produce any runoff, because rainwater from roofs was stored in cisterns. The majority of the runoff was subsequently guided along the road network towards Weg naar White Wall (*figure 5.17a*). There, ponding occurred because the roadsides were higher than the road surface, and there were few outlet points.

The ***impermeable limestone outcrop*** was the largest source of runoff to the active gullies. The topsoil in the area is possibly shallow and poorly drained due to ***underlying rock layers*** (*figure 5.2*). However, only during the T = 8 yr and hurricane scenarios did the loam saturate and contribute to runoff (*figure 5.17c*; *figure 5.19*). Infiltration in the sandy beds of the gullies reduced the peak and total discharges to some extent before the water reached Weg naar White Wall. A sensitivity analysis showed that this was mostly affected by the soil depth, and to a lesser extent by the initial soil moisture content (*figure 5.16*). Flooding and sedimentation on Weg naar White Wall were caused by the fact that gullies 2 and 3 discharge directly onto the road surface. Gully 1 flowed through a culvert, and thus caused no issues.

Much less runoff was generated in the Statia Lodge area, which can be attributed to the lesser cover by pavements, compared to the subdivision. Most runoff in this area was derived from Weg naar White Wall (*figure 5.17b*).

In the remaining part of the study area was for the most part densely vegetated. It was however concluded that for these extreme storms, interception by the canopy did could not decrease runoff by an important amount. Large-scale runoff generation did not occur in these areas, because the loam topsoil had

on average a high infiltration capacity. This was despite the widespread occurrence of SWR. In addition, the deep loam subsoil provided excessive drainage, thereby preventing the soil from becoming saturated during even the most extreme events.

Severity

Flooding depths in the subdivision and around Statia Lodge were not high enough that it could be a hazard to people and buildings. The roads mostly featured sheet flows, with a depth up to 1.5 cm. However, for more intense storms, runoff could penetrate further into these areas. Flow over the unpaved roads also became more prevalent, with greater water heights as well. As such, more severe erosion could be expected.

Ponding depths on Weg naar White Wall ranged from 3 to 15 cm, and were caused by raised road sides without drains. The height of the roadsides limited ponding depth, and therefore, more extreme storms did not necessarily cause deeper ponding.

Peak and total discharges in the active gullies increased with more intense storms, as more runoff was generated on the outcrop. For the largest gully, gully 1, peak discharges were 259, 367, 409 and 386 L/s. Total discharges of the T = 8 yr and hurricane events were especially high, not only due to the large cumulative rainfalls, but also because saturation-excess overland flow became prevalent on the loam topsoil.

Measures

Ponding on Weg naar White Wall could be easily reduced by lowering the roadsides and allowing water to run off the pavement at regular intervals.

The severity of flooding and subsequent erosion of unpaved roads within the subdivision could be reduced by containing the flow on the paved roads, and by preventing water from flowing onto unpaved roads. Runoff that is generated on unpaved roads should be allowed to run off to the side into infiltration pits. The urban watershed could furthermore be divided into smaller areas using drains in the paved roads, in order to limit peak discharges over the road surface, and also to prevent flooding in downslope areas. The collected water could be temporarily stored inside several small infiltration basins and/or storage facilities spread throughout the area, or inside a fewer large units downslope of the area (*figure 6.2*).

Flooding by the active gullies could be addressed by rerouting the flow towards the existing culvert, or by installing new culverts where the water is currently discharged onto the road (*figure 6.4*).

Uncertainties of soil properties

Field measurements showed great variation of infiltration rates of the loam topsoil, which could be linked to different degrees of SWR and preferential flow. These spatial variations have not been taken into account in the models. Furthermore, the mean K_{sat} that was determined for the loam may have been overestimated, due to limitations of the field measurements. The K_{sat} may in reality be lower, which could be particularly relevant for flooding in the subdivision.

The loam subsoil was assumed to be deep and highly permeable. This largely prevented saturation-excess overland flow, even for the T = 8 yr and hurricane scenarios. It is possible that small confining layers are present, which in reality may decrease percolation rates through the entire soil column, and increase the amount of runoff.

The peak and total discharges from the active gullies were greatly affected by the depths of the loam topsoil and channel sands, and the presence of underlying impermeable rock layers. However, the soil depths have not actually been measured, and the presence of the rock layers has not been verified throughout this area.

Further research

The model has not been validated, because there were no records of discharge rates in the study area. Otherwise, parameters such as K_{sat} and Manning's n could be calibrated. This could partly solve inaccuracies caused by the mismatch between cell size and flow width.

The spatial variability of K_{sat} should be further measured. In addition, there may be seasonal patterns in the degree of SWR, due to changes in soil moisture. Also, infiltration rates of unpaved roads be measured extensively.

For modelling percolation, but also for calculating the required size of infiltration basins, the hydrologic properties of the loam subsoil should be measured thoroughly. For runoff in the active gullies, it is also essential to study the underlying geology of the White Wall – Sugar Loaf succession, and to measure topsoil depths.

REFERENCES

Arcement, G. J., & Schneider, V. R. (1989). Guide for selecting Manning's roughness coefficients for natural channels and flood plains.

Aston, A. R. (1979). Rainfall interception by eight small trees. Journal of hydrology, 42(3-4), 383-396.

Avila-Diaz, A., Torres, R. R., Zuluaga, C. F., Cerón, W. L., Oliveira, L., Benezoli, V., ... & Medeiros, F. (2022). Current and Future Climate Extremes Over Latin America and Caribbean: Assessing Earth System Models from High Resolution Model Intercomparison Project (HighResMIP). Earth Systems and Environment, 1-32.

Batey, T. (2009). Soil compaction and soil management–a review. Soil use and management, 25(4), 335-345.

Bootsma, H. (2015). Groundwater Recharge on the Cultuurvlakte of St. Eustatius.

CBS Statline (Visited on 18 January 2023). Caribisch Nederland; bevolkingsontwikkeling, geboorte, sterfte en migratie. https://opendata.cbs.nl/statline/#/CBS/nl/dataset/83774NED/table?ts=1663134216890

Chow V. T., Maidment D. R., Mays L. W. (1988). Applied Hydrology. McGraw-Hill: New York

De Almeida, G. A., Bates, P., & Ozdemir, H. (2018). Modelling urban floods at submetre resolution: challenges or opportunities for flood risk management?. Journal of Flood Risk Management, 11, S855-S865.

De Freitas, J. A., Rojer, A. C., Nijhof, B. S. J., & Debrot, A. O. (2012). A landscape ecological vegetation map of Sint Eustatius (Lesser Antilles) (No. C053/12). IMARES.

De Jong, S. M., & Jetten, V. G. (2007). Estimating spatial patterns of rainfall interception from remotely sensed vegetation indices and spectral mixture analysis. International Journal of Geographical Information Science, 21(5), 529-545.

Dekker, L. W., & Ritsema, C. J. (2000). Wetting patterns and moisture variability in water repellent Dutch soils. Journal of Hydrology, 231, 148-164.

De Vugt, L. C. (2018). Mapping and modelling of landslide and flood hazards on St. Eustatius with openLISEM. MSc thesis.

Dingman, S. L. (2015). Physical hydrology. Waveland press.

Doerr, S. H., Shakesby, R. A., & Walsh, R. (2000). Soil water repellency: its causes, characteristics and hydro-geomorphological significance. Earth-Science Reviews, 51(1-4), 33-65.

Fabricius, K. E. (2005). Effects of terrestrial runoff on the ecology of corals and coral reefs: review and synthesis. Marine pollution bulletin, 50(2), 125-146.

Frankl, A., Nyssen, J., Vanmaercke, M., & Poesen, J. (2021). Gully prevention and control: Techniques, failures and effectiveness. Earth Surface Processes and Landforms, 46(1), 220-238.

Fohrer, N., Haverkamp, S., Eckhardt, K., & Frede, H. G. (2001). Hydrologic response to land use changes on the catchment scale. Physics and Chemistry of the Earth, Part B: Hydrology, Oceans and Atmosphere, 26(7-8), 577-582.

Gregory, J. H., Dukes, M. D., Jones, P. H., & Miller, G. L. (2006). Effect of urban soil compaction on infiltration rate. Journal of soil and water conservation, 61(3), 117-124.

Hammond, M. J., Chen, A. S., Djordjević, S., Butler, D., & Mark, O. (2015). Urban flood impact assessment: A state-of-the-art review. Urban Water Journal, 12(1), 14-29.

Hendriks, M. (2010). Introduction to physical hydrology. Oxford University Press.

Herwitz, S. R. (1985). Interception storage capacities of tropical rainforest canopy trees. Journal of Hydrology, 77(1-4), 237-252.

Hollis, G. E. (1975). The effect of urbanization on floods of different recurrence interval. Water resources research, 11(3), 431-435.

Janeau, J. L., Bricquet, J. P., Planchon, O., & Valentin, C. (2003). Soil crusting and infiltration on steep slopes in northern Thailand. European Journal of Soil Science, 54(3), 543-554.

Jetten, V. (2018). OpenLISEM–Multi-Hazard Land Surface Process Model–Documentation & User Manual. University of Twente.

Kamphorst, E. C., Jetten, V., Guerif, J., Pitk a¨ nen, J., Iversen, B. V., Douglas, J. T., & Paz, A. (2000). Predicting depressional storage from soil surface roughness. Soil Science Society of America Journal, 64(5), 1749-1758.

Kim, D. W., Yun, H. S., Jeong, S. J., Kwon, Y. S., Kim, S. G., Lee, W. S., & Kim, H. J. (2018). Modeling and testing of growth status for Chinese cabbage and white radish with UAV-based RGB imagery. Remote Sensing, 10(4), 563.

Kirkby, M. J., & Bracken, L. J. (2009). Gully processes and gully dynamics. Earth Surface Processes and Landforms: The Journal of the British Geomorphological Research Group, 34(14), 1841-1851.

Koomen, A., Dorland, G. and Van Malaske, B. (2012). Soil map of St. Eustatius (GIS) based on historical paper maps, updated from field surveys.

Maass, C. (2016). Flash floods modeling in the south coast of Haiti. Study case: Côtes de Fer watershed.

MacRae, D. R. & Esteban, N. (2007). St Eustatius Marine Park Management Plan. Coastal Zone Management (UK) and St Eustatius National Parks Foundation (STENAPA).

Manconi, A., Ziegler, M., Blöchliger, T., & Wolter, A. (2019). Optimization of unmanned aerial vehicles flight planning in steep terrains. International Journal of Remote Sensing, 40(7), 2483-2492.

Meteorological Department Curaçao (Visited on 18 January 2023). Oranjestad, St. Eustatius (17°29'N, 62°59'W) Summary of Climatological Data, Period 1971 – 2000.
https://www.meteo.cw/climate.php?Lang=Eng&St=TNCC&Sws=R11

Morbidelli, R., Saltalippi, C., Flammini, A., & Govindaraju, R. S. (2018). Role of slope on infiltration: a Review. Journal of hydrology, 557, 878-886

Mücher, C. A., Jonker, D., Stuiver, H. J., Kramer, H., & Meesters, H. W. G. (2014). Production of digital terrain models for the Dutch Caribbean: implication for Saba & St. Eustatius (No. 2569). Wageningen UR Alterra.

NOAA (Visited on 9 February 2023). Historical Hurricane Tracks.
https://coast.noaa.gov/hurricanes/

Novak, V., Šimůnek, J., & Genuchten, M. T. V. (2000). Infiltration of water into soil with cracks. Journal of irrigation and Drainage Engineering, 126(1), 41-47.

Nederlands normalisatie-instituut (NEN). (1989). Nederlandse Norm NEN 5104, Classificatie van onverharde grondmonsters. Nederlands Normalisatie-instituut, Delft.

Nyssen, J., Poesen, J., Moeyersons, J., Luyten, E., Veyret-Picot, M., Deckers, J., ... & Govers, G. (2002). Impact of road building on gully erosion risk: a case study from the northern Ethiopian highlands. Earth Surface Processes and Landforms: The Journal of the British Geomorphological Research Group, 27(12), 1267-1283.

OpenStreetMap contributors (2023).
https://www.openstreetmap.org/

Ozdemir, H., Sampson, C. C., de Almeida, G. A., & Bates, P. D. (2013). Evaluating scale and roughness effects in urban flood modelling using terrestrial LIDAR data. Hydrology and Earth System Sciences, 17(10), 4015-4030.

Poesen, J., Nachtergaele, J., Verstraeten, G., & Valentin, C. (2003). Gully erosion and environmental change: importance and research needs. Catena, 50(2-4), 91-133.

Pollock, M. D., O'donnell, G., Quinn, P., Dutton, M., Black, A., Wilkinson, M. E., ... & O'Connell, P. E. (2018). Quantifying and mitigating wind-induced undercatch in rainfall measurements. Water Resources Research, 54(6), 3863-3875.

Pratomo, R. A., Jetten, V., & Alkema, D. (2016). A comparison of flash flood response at two different watersheds in Grenada, Caribbean Islands. In IOP conference series: Earth and environmental science (Vol. 29, No. 1, p. 012004). IOP Publishing.

Price, R. K., & Vojinovic, Z. (2008). Urban flood disaster management. Urban water journal, 5(3), 259-276.

Ramos-Scharrón, C. E., & LaFevor, M. C. (2016). The role of unpaved roads as active source areas of precipitation excess in small watersheds drained by ephemeral streams in the Northeastern Caribbean. Journal of Hydrology, 533, 168-179.

Ramos-Scharrón, C. E., & MacDonald, L. H. (2005). Measurement and prediction of sediment production from unpaved roads, St John, US Virgin Islands. Earth Surface Processes and Landforms: The Journal of the British Geomorphological Research Group, 30(10), 1283-1304.

Roobol, M. J., & Smith, A. L. (2004). Volcanology of Saba and St. Eustatius, Northern Lesser Antilles. Koninklijke nederlandse Akademie van wetenschappen.

Royal Eijkelkamp (2022). Rainfall simulator Operating instructions.

Royal HaskoningDHV (2018). Masterplan Drainage Oranjestad Sint-Eustatius. Conceptrapport Fase 1.

Saxton, K. E., & Rawls, W. J. (2006). Soil water characteristic estimates by texture and organic matter for hydrologic solutions. Soil science society of America Journal, 70(5), 1569-1578.

Sharma, M. L., Gander, G. A., & Hunt, C. G. (1980). Spatial variability of infiltration in a watershed. Journal of Hydrology, 45(1-2), 101-122.

Smith, R. B., Minder, J. R., Nugent, A. D., Storelvmo, T., Kirshbaum, D. J., Warren, R., ... & French, J. (2012). Orographic precipitation in the tropics: The Dominica Experiment. Bulletin of the American Meteorological Society, 93(10), 1567-1579.

Stolte, J., Liu, B., Ritsema, C. J., Van Den Elsen, H. G. M., & Hessel, R. (2003). Modelling water flow and sediment processes in a small gully system on the Loess Plateau in China. Catena, 54(1-2), 117-130.

Tarboton, D. G. (2003). Rainfall-runoff processes. Utah State University, 1(2).

Torres, J. L., & Morelock, J. A. C. K. (2002). Effect of terrigenous sediment influx on coral cover and linear extension rates of three Caribbean massive coral species. Caribbean Journal of Science, 38(3/4), 222-229.

Ten Harkel, W. (2015). Runoff and erosion on the Cultuurvlakte of St. Eustatius. MSc thesis.

Tricker, A. S. (1981). Spatial and temporal patterns of infiltration. Journal of Hydrology, 49(3-4), 261-277.

Valentin, C., & Bresson, L. M. (1992). Morphology, genesis and classification of surface crusts in loamy and sandy soils. Geoderma, 55(3-4), 225-245.

Van den Bout, B., & Jetten, V. G. (2018). The validity of flow approximations when simulating catchment-integrated flash floods. Journal of hydrology, 556, 674-688.

Van Schaik, N. L. M. B. (2009). Spatial variability of infiltration patterns related to site characteristics in a semi-arid watershed. Catena, 78(1), 36-47.

Veenenbos, J. S. (1955). A soil and land capability survey of St. Maarten, St Eustatius, and Saba: Netherlands Antilles.

Von Hoyningen-Huene, J. (1983). Die interzeption des Niederschlages in landwirtschaftlichen Pflanzenbeständen.

Woods-Ballard, B., Kellagher, R., Martin, P., Jefferies, C., Bray, R., & Shaffer, P. (2007). The SUDS manual (Vol. 697). London: Ciria.

Yang, J., & Chu, X. (2013). Quantification of the spatio-temporal variations in hydrologic connectivity of small-scale topographic surfaces under various rainfall conditions. Journal of Hydrology, 505, 65-77.

Ye, A., Zhou, Z., You, J., Ma, F., & Duan, Q. (2018). Dynamic Manning's roughness coefficients for hydrological modelling in basins. Hydrology Research, 49(5), 1379-1395.

Zhang, Y., Zhao, Y., Liu, B., Wang, Z., & Zhang, S. (2019). Rill and gully erosion on unpaved roads under heavy rainfall in agricultural watersheds on China's Loess Plateau. Agriculture, Ecosystems & Environment, 284, 106580.

Zobeck, T. M., & Onstad, C. A. (1987). Tillage and rainfall effects on random roughness: A review. Soil and Tillage Research, 9(1), 1-20.